1-1-2014

Effects Of Altering The Peroxisomal Redox State In Models Of Degenerative Disease

Courtney Rose Giordano
Wayne State University,

EFFECTS OF ALTERING THE PEROXISOMAL REDOX STATE IN MODELS OF DEGENERATIVE DISEASE

by

COURTNEY R. GIORDANO

DISSERTATION

Submitted to the Graduate School

of Wayne State University,

Detroit, Michigan

in partial fulfillment of the requirements

for the degree of

DOCTOR OF PHILOSOPY

2014

PHARMACOLOGY

Approved By:

_____

Advisor Date

_____

_____

_____

_____

DEDICATION

I would like to dedicate my dissertation to my parents, Gregory and Gabriele Baracy. You have both supported me 110% throughout my life and have always instilled the importance of education. I appreciate your helpful advice and constant inspiration through all of my endeavors.

Lastly to my husband, Paul Giordano - your endless love, understanding, and encouragement allowed me to stay confident and successful throughout this experience.

ACKNOWLEDGMENTS

First, I would like to thank my advisor, Dr. Stanley R. Terlecky. I am forever thankful for your guidance and careful mentorship that I believe has made me a better scientist, critical thinker, and overall efficient individual. You have taught me not only the technicalities and scientific expertise needed to become a successful individual but also various important life lessons along the way. I am truly grateful and very appreciative of all the time you have provided to mentor me.

I would also like to thank Laura Terlecky for your time and effort training me in the laboratory setting. Your expertise helped support and guide me through many of my experiments.

Next, I would like to thank my committee members – Drs. Boerner, McCauley, Rempel and Walton. Your guidance throughout my graduate career was very much appreciated. Your input has been integral in the development of an exciting and important dissertation project.

Lastly, I would like to acknowledge the Department of Pharmacology and Wayne State University School of Medicine for additional support throughout my graduate career.

TABLE OF CONTENTS

LIST OF FIGURES

LIST OF ABBREVIATIONS

Ac1	**Glycated hemoglobin**
AD	**Alzheimer's disease**
ADDLs	**Amyloid β-derived diffusible ligands**
Aβ	**Amyloid-beta**
BSA	**Bovine serum albumin**
CAT-SKL	**(His_6)-tagged polyarginine-containing catalase with SKL peroxisomal targeting signal**
DAPI	**4',6-diamidino-2-phenylindole**
DCF	**Dichlorofluorescein**
DCF-DA	**2',7'-dichlorofluorescin diacetate**
DMEM	**Dulbecco's modified eagle medium**
DMEM:F12	**Dulbecco's modified eagle medium: Nutrient mixture F-12**
DNA	**Deoxyribonucleic acid**
ECL	**Enhanced chemiluminescence**
EDTA	**Ethylenediaminetetraacetic acid**
EGF	**Epidermal growth factor**
EGFR	**Epidermal growth factor receptor**
ErbB	**Epidermal growth factor family**
FBS	**Fetal bovine serum**
GST	**Glutathione S-transferase**
H2O2	**Hydrogen peroxide**

HER2	**Human epidermal growth factor receptor 2**
HFIP	**1,1,1,3,3,3-hexafluoror-2-propanol**
HG	**High glucose**
HMOX1	**Heme oxygenase-1**
HRP	**Horseradish peroxidase**
IC50	**Half maximal inhibitor concentration**
IGF-1R	**Insulin like growth factor receptor**
Ig-G	**Immunoglobulin G**
JC-1	**5,5',6,6'-tetrachloro-1,1',3,3'-tetraethylbenzimidazolylcarbocyanine iodide**
kDa	**Kilodalton**
MAP-2	**Microtubule-associated protein 2**
MAPK	**Mitogen-activated protein kinase**
MEMRI	**Manganese-enhanced magnetic resonance imaging**
MIO-M1	**Müller cells**
Mn2+	**Manganese ion**
mRNA	**Messenger ribonucleic acid**
MTT	**3-(4,5-dimethylthiazol-2-yl)-2,5-diphenyltetrazolium bromide**
NAC	**N-acetyl cysteine**
NBT/BCIP	**Nitro-blue tetrazolium chloride/5-bromo-4-chloro-3'-indolyphosphate p-toluidine salt**
NFE2L2	**Nuclear factor (erythroid-derived 2)-like 2**
NG	**Normal glucose**

Nqo1	**NAD(P)H quinone oxidoreductase 1**
PBS	**Phosphate buffered saline**
PMP70	**70-kDa peroxisomal membrane protein**
PTP	**Protein tyrosine phosphatase**
RNA	**Ribonucleic acid**
ROS	**Reactive oxygen species**
RPE	**Retinal pigment epithelial cells**
SDS-PAGE	**Sodium dodecyl sulfate-polyacrylamide gel electrophoresis**
SEM	**Standard error of the mean**
STZ	**Streptozotocin**
TKI	**Tyrosine kinase inhibitor**
TNF-α	**Tumor necrosis factor-alpha**
UGT1A6	**UDP-glucuronosyltransferase**
VEGFR	**Vascular endothelial growth factor**
WST-1	**Water soluble tetrazolium**
3-AT	**3-amino-1,2,4-triazole**

CHAPTER 1: Introduction: Peroxisomes, cell senescence, rates of aging, and age related disease

Published: **Giordano CR** and Terlecky SR (2012) Peroxisomes, cell senescence, and rates of aging *Biochim Biophys Acta* **1822**:1358-62.

1.1 Abstract

The peroxisome is functionally integrated into an exquisitely complex network of communicating endomembranes that is only beginning to be appreciated. Despite great advances in identifying essential components and characterizing molecular mechanisms associated with the organelle's biogenesis and function, there is a large gap in our understanding of how peroxisomes are incorporated into metabolic pathways and subcellular communication networks, how they contribute to cellular aging, and where their influence is manifest on the initiation and progression of degenerative disease. In this introduction, we summarize recent evidence pointing to the organelle as an important regulator of cellular redox balance with potentially far-reaching effects on cell aging and the genesis of human disease.

1.2 Cellular senescence and organismal aging

The role of cellular senescence in organismal aging burst into our collective consciousness with the publication of a paper by Dr. Jan Van Deursen and colleagues at the Mayo Clinic College of Medicine in Rochester, Minnesota. In their landmark work, the team showed that eliminating senescent cells in a mouse model delayed appearance of age-related disorders (Baker et al., 2011). Importantly, the strategy was effective both when clearance was started from birth, as well as when initiated later in

life. However, in the latter case, already existing pathologies were not reversed, rather their progression was thwarted. In many ways, this research serves as the ultimate confirmation of what many had long speculated – that senescent cells amass in tissues and organs of aging animals and contribute to their physiological decline. What a long way the field had come from days when cellular senescence was considered an *in vitro* phenomenon, not applicable to the whole animal. In fact, it is only some eight years since Dr. John Sedivy and colleagues at Brown University in Providence, Rhode Island, confirmed the existence of senescent cells in the tissue of aging primates (Herbig et al., 2006).

A considerable literature exists concerning exactly what cellular senescence is (for example, see (Kuilman et al., 2010) for a detailed overview); therefore, the phenomena will only be briefly described here. Senescent cells have lost their ability to replicate, yet remain metabolically active. The cells are enlarged and express so-called senescence markers, including an alkaline β-galactosidase activity, heterochromatin and/or DNA damage foci, and the cyclin-dependent kinase inhibitor/tumor suppressor, $p16^{Ink4a}$. (Eradication of (senescent) cells expressing the latter biomarker was the mechanism employed by the Van Deursen group to largely eliminate diseases of aging in mice.) Senescent cells are resistant to apoptosis and exhibit a distinct "secretory phenotype" (reviewed in (Coppe et al., 2010)). They secrete a number of bioactive molecules, including cytokines, growth factors, inflammatory mediators, and various proteases. Secretion of these molecules undoubtedly alter the cell and tissue microenvironments with potentially important implications on aging and disease phenomena. Indeed, there is an emergent consensus view, articulated by Dr. Manuel

Collado and co-authors (Collado et al., 2007) among others, that tissue aging results from the combined effects of an accumulation of senescent cells and accompanying secretions, and the loss of stem cell renewal capacities.[1]

Triggers of replicative senescence include telomere shortening, accumulation of reactive oxygen species (ROS) and associated damage to cellular macromolecules, DNA alterations and accompanying responses, a loss of cell cycle checkpoint regulation, and the effects of environmental or intrinsic stressors including oncogenes. Importantly, these activators do not necessarily act alone; rather, they may cooperate to elicit the growth stasis and accompanying cellular changes associated with the senescent phenotype.

Is there a reason senescence happens? A widely supported view is that senescence exists to suppress tumor formation; cells that are incapable of dividing cannot contribute to cancer – at least not directly. But as Dr. Judith Campisi (Campisi, 2005) and others argue, senescence may be antagonistically pleiotropic – beneficial in early life to thwart cancer, but permissive of an environment later in life which potentiates transformation. Consider the senescent cell's tissue milieu; rich in growth-promoting secreted biomolecules, rich in oxidants, and rich in functionally compromised stem cells. This is an environment ripe for cancerous transformation. Thus, the thought is cancer is held in check early, but may thrive later. Consistent with this notion is the fact that cancer is a disease of aging – the older the individual, the more likely is tumorigenesis.

[1] The extent to which stem cells actually senesce is not clear; regardless, their diminished function certainly compromises tissue integrity.

1.3 Peroxisomes

1.3.1 Overview of biogenesis

To be able to position peroxisomes as players in cellular aging processes and degenerative disease, an overview of their assembly and function is warranted.

Peroxisome biogenesis is brought about by a series of proteins termed peroxins (see (Ma et al., 2011; Rucktaschel et al., 2011) for recent analyses). The organelle's membrane is derived by growth and division of pre-existing peroxisomes (Lazarow and Fujiki, 1985), as well as by recruitment from certain endoplasmic reticulum subdomains (Geuze et al., 2003). Peroxisomal enzymes, synthesized on cytoplasmic ribosomes and containing specific targeting signals, are recognized post-translationally and directed to the organelle's membrane. A surface-associated docking complex then engages the to-be-imported enzyme and its cognate receptor, and channels the complex to a still rather enigmatic translocation machinery. Mechanisms exist to recycle components of the import apparatus as well as to regulate luminal enzyme levels, and organelle number.

1.3.2 Overview of biological functions

Peroxisomes are critical contributors to cell metabolism, tissue and organ function, and organismal well-being. They house dozens of enzymes involved in biosynthetic reactions (reviewed in (Singh, 1997; Wanders and Waterham, 2006)), including those that produce ether phospholipids, as well as bile and docosahexaenoic acids. Among the ether phospholipids produced are plasmalogens, essential constituents of myelin, the nerve process insulating material. Bile acids are well

described participants in dietary fat metabolism; docosahexaenoic acids are omega-3 fatty acids essential for nervous system development and function. The latter molecules also appear to be derivatized into important mediators capable of inflammatory-suppression/modulation.

Peroxisomes also affect inflammation through their ability to degrade eicosanoids, signaling molecules with a wide array of biological targets and elicited effects. Peroxisomal enzymes degrade a number of other substrates including particular long-chain, very-long-chain, and branched-chain fatty acids. Defects in such processing results in accumulation of these molecules and, in many cases, disease and even death ensues. Metabolism of peroxisomal fatty acids occurs through biochemical oxidations; molecular oxygen is the electron acceptor and H_2O_2 is formed (see (Antonenkov et al., 2010) for an overview of peroxisomes as oxidative organelles). This H_2O_2 and related downstream ROS appear to play important roles in cell signaling and communication networks, in hormetic processes, as well as in initiating and progressing age-related declines in cell function (reviewed in (Titorenko and Terlecky, 2011)).

1.3.3 Contribution to cellular ROS levels

Peroxisomal H_2O_2 is subject to metabolism by organellar catalase, members of the peroxiredoxin family, and glutathione peroxidase (presumably in some combination with reduced glutathione and a reductase). As catalase is the most abundant and efficient H_2O_2 metabolizer, most discussions about peroxisomal antioxidant capacities focus on the heme-containing tetrameric enzyme.

1.4 Catalase

1.4.1 Overview of the antioxidant enzyme

Catalase is a tetrameric enzyme found in almost all living tissue. The iron-containing enzyme was the first to be isolated in 1937 by Summer and Dounce from bovine liver catalase. It contains four identical 60 kDa subunits each containing a heme (prosthetic) group and NADPH in the active center (Scibior and Czeczot, 2006) – and is primarily found in peroxisomes. This critical antioxidant enzyme protects the cell from the harmful metabolic by-product hydrogen peroxide, decomposing it to the less reactive molecules, water and oxygen. Catalase is known to be the most abundant and efficient hydrogen peroxide metabolizer (Vainshtein BK, 1981). It is most often studied in the context of free radical/reactive oxygen species metabolism and its role as a cellular antioxidant (Lardinois, 1995), among others.

Catalase is an extremely efficient enzyme and is known to have one of the highest turnover rates ever described. One molecule of catalase is capable of converting 6 million molecules of hydrogen peroxide into water and oxygen per minute (Rahman, 2007 and Mates et al., 1999).

The enzyme is sensitive to many molecules including cyanide, azide, hydroxyl amine, aminotriazole, and mercaptoethanol (Switala and Loewen, 2002). Their mechanism of inhibition includes interacting with catalase's active-site heme. Many experimental studies use 3-amino-1,2,4-triazole (3-AT) as a tool to inhibit catalase (Koepke JI, 2008 and Milton NG, 2001). 3-AT is an irreversible antagonist that covalently binds to the active center of the tetrameric form of catalase containing heme groups (Putnam CD, 2000).

In addition to catalases 'catalatic' activity in which it decomposes hydrogen peroxide to water and oxygen, catalase can act 'peroxidically' under conditions of low hydrogen peroxide concentrations. This reaction occurs where in the presence of hydrogen peroxide and a suitable hydrogen donor (ethanol, methanol, etc.) catalase removes the hydrogen peroxide but oxidizes its substrate (Scibior and Czeczot, 2006). Thus, catalases' peroxidatic activity may actually contribute to cellular damage (Koepke et al., 2007).

Because of catalases' important role in overall cellular detoxification and as the major protective enzyme against oxidative damage, our lab has investigated the use of a reengineered form of catalase as a potential targeted protein therapeutic described in greater detail below.

There exist individuals whose catalase levels are reduced due to instability of the protein or its mRNA; cells from these subjects display an accelerated aging phenotype (Wood et al., 2006). They amass H_2O_2, possess elevated levels of oxidized proteins and damaged DNA, contain functionally compromised peroxisomes and exhibit a growth stasis. Coupled with their altered, largely swollen and amorphous phenotypes, these cells could very well be described as senescent except that they do not express the histochemical biomarker, senescent-associated β-galactosidase (Wood et al., 2006). Similar progeric effects are seen in cells where catalase is deactivated with the irreversible inhibitor, 3-amino-1,2,4-triazole (Koepke et al., 2008). Coupled with powerful epidemiological evidence suggesting that the absence of cellular catalase is directly correlated with premature onset of age-related disease (Goth and Eaton, 2000;

Goth and Vitai, 2003) – a strong case emerges for a critical role of the enzyme in preventing oxidative stress in cells.

1.4.2 Catalase, lifespan, and rate of aging

Catalase received very high profile attention when studies published by Dr. Samuel Schriner and coauthors (Schriner et al., 2005; Schriner and Linford, 2006) showed that transgenic mice expressing catalase in mitochondria manifest a 20% increase in median lifespan and a 10% extension of maximum lifespan. (Peroxisomally targeted catalase showed a more muted effect, which may stem from how the molecule was directed to the organelle – a point considered further below.) Mitochondrial catalase delayed aging phenomena in the heart and eyes, reduced H_2O_2 levels in cells, and decreased mitochondrial DNA damage while maintaining mitochondrial function. Fitting these results into a simple model is somewhat problematic (Miller, 2005), however, it is probably safe to conclude, as the authors do (Schriner et al., 2005; Schriner and Linford, 2006), that reduced cellular oxidative stress positively impacts longevity. Another important conclusion drawn from their studies was that mitochondria were now seen as both sources of ROS, and targets of their destructive power.

More recent studies with these mice confirmed that age-associated declines in mitochondrial integrity and function were slowed, but also that (muscle) insulin sensitivity and lipid content were maintained at more youthful levels (Lee et al., 2010). Based on their important findings, the authors speculated that mitochondrial ROS damage the organelle and potentiate insulin resistance in the animals – leading ultimately to downstream pathologies including a type II diabetes phenotype.

As important as all of this is, we should not lose sight of the fact that normally, catalase is not found in the mitochondria – it is a peroxisomal enzyme. Perhaps, in future work, mechanisms could be developed to direct newly introduced/suitably expressed catalase, or an appropriate mimetic, to mitochondria. However, we are a long way off from this at present. What we are closer to, is understanding that a redox-sensitive interplay exists between mitochondria and peroxisomes – one that catalase may play a very important part. Moreover, unlike mitochondria, peroxisomes may very well be druggable targets in a way mitochondria cannot. The reader is directed to (Terlecky and Koepke, 2007) for further analysis of this latter point. Additional discussion of the peroxisome-mitochondria connection is included below – after a brief description of an important study linking catalase, caloric restriction, and longevity.

- - - -

As a critical antioxidant and one of the most efficient enzymes ever described, catalase has had its share of attention from the aging field. Studies have documented that catalase levels decline with age but are maintained or elevated in more long-lived species. One particularly interesting recent study, headed by Dr. Shugo Watabe, looked at the effects of caloric restriction in the freshwater animal, the rotifer (*Brachionus plicatilis*) (Kaneko et al., 2011). Rotifers live, on average, some 8.8 days. Calorically restricted animals live 13.5 – an approximately 50% increase in lifespan. Rotifers are parthenogenic zooplankton; they reproduce by an asexual process in which daughters are genetically identical to their mothers. The research team asked what happened to offspring of *ad libitum*-fed animals, versus those subjected to a restricted diet. Not unexpectedly, animals from fed mothers displayed a typical (~9.5 day)

lifespan, which could be extended to 14.4 days by a calorie limited diet. Interestingly, offspring from calorically restricted mothers lived 12.7 days when not nutritionally limited, and 16.8 days when the diet was modified. A lifespan enhancing trait was transmitted, presumably by an epigenetic process, to otherwise genetically identical offspring.

Dr. Watabe and colleagues identified that activity – it was catalase (Kaneko et al., 2011). The antioxidant enzyme was expressed at higher levels in offspring of calorically restricted mothers. Manganese superoxide dismutase, a powerful mitochondrial antioxidant enzyme, showed no such behavior. Does the increased catalase activity protect the organism from oxidative stress and contribute to its longevity? The overwhelming conclusion of this study was that it absolutely does. Two final points regarding this work; first, the research is of interest not only from a rate of aging perspective, but it also provides evidence of "transgenerational plasticity" with its accompanying "adaptive" potential (Kaneko et al., 2011). Second, regarding catalase and caloric restriction; this work confirms and extends what has already been shown in a number of model organisms. Specifically, levels of the enzyme are increased in cells of animals whose caloric intake is limited.

1.4.3 Catalase supplementation and a peroxisome-mitochondria redox interplay

Catalase is progressively mislocalized (to the cytosol) as cells age and approach replicative senescence (Legakis et al., 2002; Koepke et al., 2007). Concomitantly, these cells produce ROS, manifest an ever more compromised peroxisomal import apparatus, and proliferate the organelle in an apparent attempt to compensate for

functional shortfalls.[2] As pointed out above, these same phenomena are seen when catalase is missing due to protein or message instabilities, or when the enzyme is chemically inactivated (Wood et al., 2006; Koepke et al., 2008). Importantly, restoration of peroxisomal catalase through use of a genetically engineered variant of the enzyme, called catalase-SKL, delays appearance of senescence markers in aging cells (Koepke et al., 2007). Cellular ROS are reduced and, interestingly, mitochondrial integrity is restored. Specifically, catalase-SKL expression reestablishes mitochondrial membrane potential (normally dissipated as cells age (Hagen et al., 1997)) and reduces mitochondrial ROS production (normally elevated in senescing cells (Hagen et al., 1997; Koepke et al., 2007)).

The latter results suggest a redox-sensitive peroxisome-mitochondria interplay is at work in cells. Importantly, this extends evidence of organelle cross-talk and functional cooperation previously summarized by Dr. Michael Schrader and colleagues (Schrader and Yoon, 2007; Camoes et al., 2009). With the suggestion of such a relationship in mind, it is probably not surprising then, that inactivating catalase with 3-amino-1,2,4-triazole drives mitochondria to a depolarized (Koepke et al., 2008), ROS-producing, state (Koepke et al., 2008; Ivashchenko et al., 2011). Peroxisomal catalase is cytoprotective; its absence, mislocalization, or inactivation is progeric on cells. Which begs the question; can the antioxidant enzyme be introduced to cells – and if so, would we not expect a significant effect on age-, or oxidative stress-induced cellular pathologies?

[2] Peroxisome proliferation may also reflect impaired turnover of the organelle. Chaperone-mediated autophagy is compromised with age (Cuervo et al., 2000) ; whether or not autophagic processes directly responsible for peroxisome turnover are similarly affected is not clear. However, see relevant references included in Kuilman et al., 2010 and Hubbard et al., 2012 regarding links between cell senescence/aging and impaired autophagic pathways.

1.4.4 Cell penetrating catalase-SKL

Catalase-SKL contains a reengineered peroxisome targeting signal at its carboxy terminus. This enzyme interacts more avidly with the peroxisome import receptor, Pex5p (Koepke et al., 2007), and is more efficiently imported into peroxisomes (Koepke et al., 2007). It is important to note that the peroxisome contains a unique mechanistic import apparatus as it accommodates fully folded proteins – permitting the organelle to be druggable. The molecule was developed into a protein therapeutic by adding a cell penetrating peptide near the amino terminus, along with a polyhistidine tag – used for purifying the recombinant enzyme (see Fig. 1.1 schematic). The following is a brief summary of the demonstrated efficacy of the cell penetrating antioxidant enzyme (hereafter referred to as CAT-SKL) in a number of cell biological, physiological, and pathophysiological contexts.

Figure 1.1

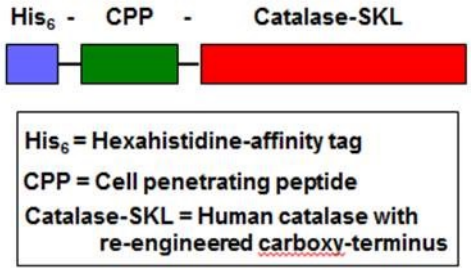

Figure 1.1. CAT-SKL construct. See text for additional description. Image appears in *Biochim Biophys Acta*. 2012 by Giordano, C.R. and Terlecky, S.R.

In a human cell model for psoriasis, CAT-SKL reduces tumor necrosis factor-α- (TNF-α) induced ROS and downstream inflammatory cytokine production (Young et al., 2008). In primary explants of human skin, a topically applied hydrogel preparation of CAT-SKL reduced ultraviolet light-induced lipid peroxidation by more than 60% as compared to a formulation base alone (Terlecky, unpublished). The molecule, when formulated with appropriate excipients including skin penetrating agents, enters (mouse) skin and reduces H_2O_2 levels (Terlecky, unpublished). Importantly, repeat insult patch test results indicate the CAT-SKL hydrogel elicited no "contact sensitization" reactions of any kind when applied over ten weeks to human subjects (Terlecky, unpublished).

The results in skin may be relevant to radiation dermatitis – a side effect of certain cancer treatments. Collaborative studies conducted at our own institution (Price et al., 2009) showed that CAT-SKL inhibited photodynamic therapy-induced apoptosis in murine leukemia cells. In contrast, the catalase inhibitor, 3-amino-1,2,4-triazole, potentiated the response. These studies are important in that they demonstrate a role for H_2O_2 in photodynamic therapy's pro-apoptotic effects, and suggest that CAT-SKL might be beneficial, that is, protective, if applied to tissue adjacent to that undergoing a photodynamic therapy-based treatment regimen. Also, the idea that inhibition of antioxidant activity enhances photo- or radiation-killing may have important implications for tumor elimination strategies.

ROS and resultant oxidative stress are thought to be the main drivers of ischemia-reperfusion and hypoxia-reoxygenation injury in the heart. Our work with a neonatal ventricular myocyte model showed CAT-SKL protected cells against these injurious events (Undyala et al., 2011). Coupled with our unpublished evidence that the

targeted antioxidant reduces the area of necrosis, as a function of the area at risk, in rats exposed to a 30 minute ischemic event – the suggestion is that CAT-SKL may represent a potentially powerful new therapeutic modality for the protection of heart tissue from oxidative damage.

In two other disease models included in chapters below, CAT-SKL reduced the toxic effects of soluble β-amyloid peptides on cultured embryonic rat hippocampal/cortical neurons, and sensitized otherwise resistant breast cancer cells to the tyrosine kinase inhibitor, gefitinib (Giordano et al., 2012). With respect to the former, these studies corroborate work from Dr. Nibaldo Inestrosa and colleagues (Inestrosa et al., 2013) showing a protective role for peroxisomes and peroxisomal catalase in β-amyloid induced neurodegeneration.

Non-SKL derivatized cell penetrating catalase molecules have also been employed in a number of systems including those designed to have the enzyme enter skin (Jin et al., 2001), to modulate ischemia-reperfusion injury in the heart (Huang et al., 2011), and to identify H_2O_2-dependent signaling pathways (Watanabe et al., 2003). Regarding this last point; our unpublished work looking at gene arrays and the effects of CAT-SKL suggest elimination of CAT-SKL-sensitive ROS may reintroduce cell cycle checkpoint control in senescing cells. The fact that catalase-SKL delays appearance of senescence markers (Koepke et al., 2007), whereas mislocalized catalase is associated with the senescent state (Legakis et al., 2002), is certainly consistent with these preliminary results.

One large omission from these completed or ongoing studies is a longitudinal analysis, in animals, of the effects of supplementing peroxisomal catalase. This could

be accomplished, for example, in a transgenic background with catalase-SKL as the introduced exogenous gene. Catalase-SKL would be the preferred transgene to assure more robust peroxisome trafficking with age (Legakis et al., 2002; Koepke et al., 2007). An alternative approach could involve regular (intraperitoneal or subcutaneous) administration of the recombinant protein, CAT-SKL. There are advantages and disadvantages of both approaches including the considerable time and expense of the requisite protocols. However, generation of these animals would permit not only a longevity study, but also an evaluation of their disease resistance after appropriate crosses or physiological perturbations. One could reasonably expect such animals to delay onset of age-related degenerative disease and perhaps even live longer than control animals. Of course, this is simply conjecture at this point.

- - - -

Some final thoughts on catalase. One recurring question is why does catalase possess a weak perosixome targeting signal – a property of the enzyme seen across evolutionary diverse organisms. Is it that a kinetically delayed import process permits proper folding and assembly of constituent protein and heme subunits? Is it, as speculated previously (Terlecky et al., 2006), that import of the enzyme is sufficiently robust in young cells/organisms and that the compromised compartmentalization seen in aging occurs after reproductive age and cannot be selected against evolutionarily? Is it that advantages exist for catalase to be partially localized to the cytosol? With respect to the latter, consider that during red blood cell development, precursor cells eliminate intracellular organelles (Gronowicz et al., 1984). Perhaps a partial cytosolic localization preserves antioxidant capacities in the mature red blood cell.

Lastly, overexpression of catalase in and of itself is not a panacea. Several studies over the years have shown that enhanced levels of antioxidant enzymes or mimetics may actually sensitize cells to toxic insult – not insulate them. As pointed out recently by Dr. Epstein and colleagues (Li et al., 2006), catalase overexpression in β-cells of the mouse pancreas actually sensitizes the animal to diabetes. Their explanation, and one supported by an emerging consensus, is that non discriminate metabolism of ROS in cells may very well be detrimental. ROS in small amounts (~bursts) and in particular locations, represent critical components of signaling cascades and related communication networks. They cannot be indiscriminately metabolized by broad-acting, non-targeted antioxidant strategies.

1.5 Conclusions and perspectives

Fig. 1.2 depicts a schematized version of two cells; a young cell at early passage, and an old cell at, or near, replicative senescence. The albeit simplified rendering reveals several important points. First, ROS can emanate from peroxisomes and mitochondria – even in young cells. The idea has emerged that these organelles might release a small but continuous stream of the reactive molecules to maintain readiness of the antioxidant response as well as to appropriately regulate cell signaling, cell communication, and network integrating activities. The sum total of these "hormetic" or "preconditioning" pathways may very well be the anti-aging programs reviewed in (Titorenko and Terlecky, 2011). However, the perspective of this article has been on what happens when these ROS are produced beyond a specific threshold – when they begin to amass and damage cell constituents and to initiate more pro-aging programs. As we depict in the figure, peroxisomes and

mitochondria release ROS – with each organelle affected by the process. Peroxisomes proliferate with age (Legakis et al., 2002; Ivashchenko et al., 2011), as do mitochondria (Lee et al., 2002). Peroxisomes are impaired in their ability to import their constituent enzymes, (Legakis et al., 2002; Ivashchenko et al., 2011), and begin to manifest functional deficits. Mitochondrial functionality is also reduced – for example, their ability to maintain a membrane potential is impaired (Hagen et al., 1997; Koepke et al., 2007). It should be noted that mitochondrial DNA is exquisitely sensitive to oxidative stress and an accumulation of mutations is seen as a major driver of mammalian aging (Kujoth et al., 2005).

Figure 1.2

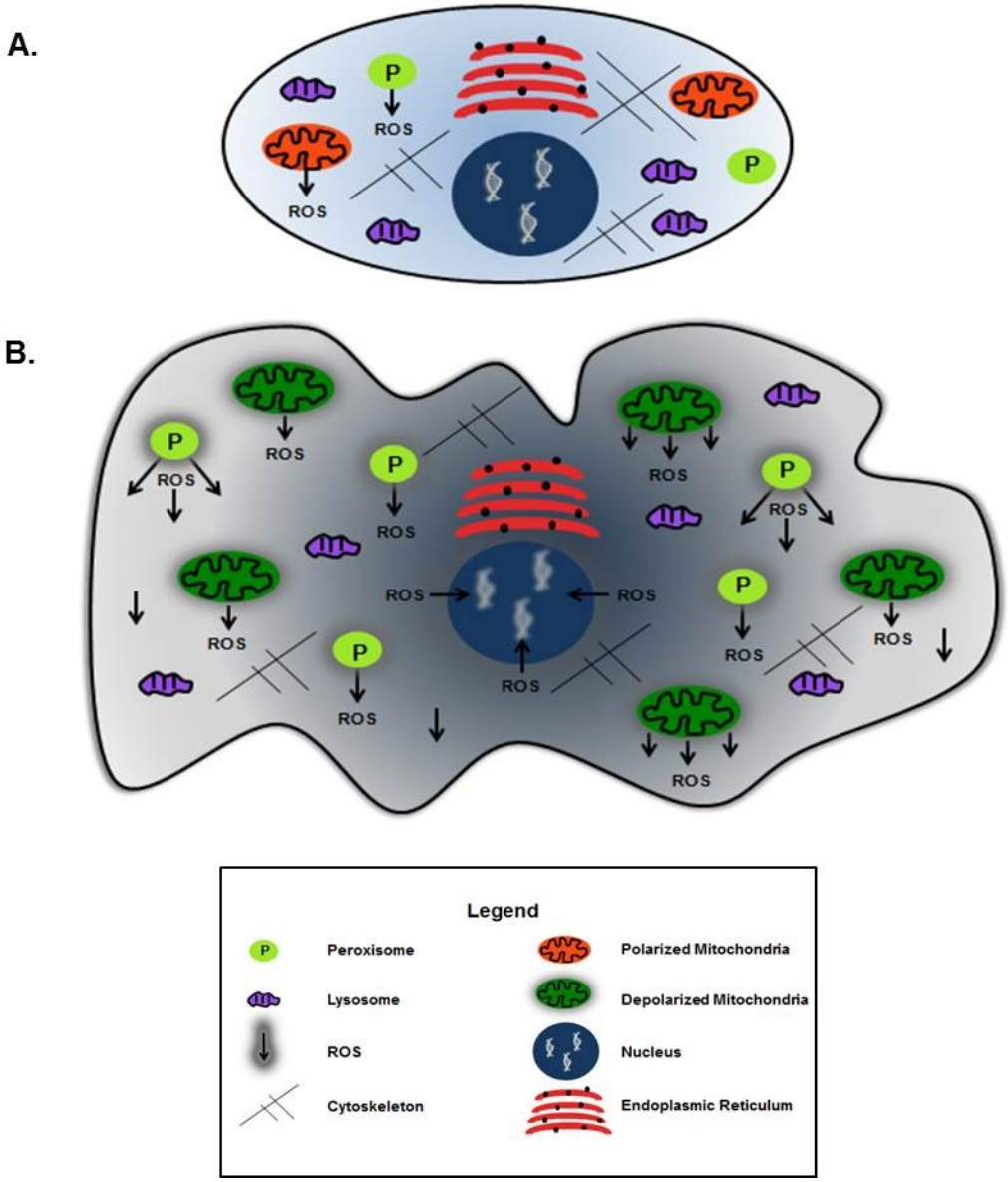

Figure 1.2. Schematic representation of cellular senescence and its impact on organelles, ROS production, and cell architecture. A. As described in the text, early passage/young cells contain peroxisomes and mitochondria that are fully capable of processing ROS produced *in situ*. B. Late passage/old cells are less able to carry out these processes and amass the reactive metabolites. As a consequence they manifest changes to organelles and the cell itself as illustrated. Image appears in *Biochim Biophys Acta*. 2012 by Giordano, C.R. and Terlecky, S.R.

It is nearly impossible to tease out where ROS begin and end in the cell. Is H_2O_2 produced first in the peroxisome and then "efficiently" diffused to mitochondria where it attacks perhaps more delicate components of the electron transport chain? Or does trafficking of the reactive metabolite and its downstream derivatives originate in mitochondria – the cell's "fiery furnace"? Continuing with unanswered questions, only little has been included here about the precise targets of organellar, or otherwise produced, ROS. What signaling pathways, communication networks, and pro- or anti-aging programs are actually modulated by these reactive molecules? It has been questioned whether aging represents a sort of end point with respect to oxidative damage to cellular constituents – or is it the culmination of an as yet undefined, development program? What is clear is that cellular ROS – and H_2O_2 in particular, is as suggested by Drs. Teng Lu and Toren Finkel, a "primary mediator" of *in vitro* senescence and *in vivo* aging (Lu and Finkel, 2008). Echoing the importance of H_2O_2, Drs. Michael Lisanti, Federica Sotgia and coauthors suggest the molecule, via its ability to "drive accelerated aging", constitutes a major player in the etiology of inflammation and cancer (Lisanti et al., 2011).

What has long been ignored when considering the nexus of oxidative stress, aging, and the development of degenerative disease is a role for peroxisomes. Although the extent of this role is yet to be completely defined – it is quite clear that peroxisomes will continue to emerge as critical contributors to these processes.

1.6 Overview of chapters

In the research described below, we investigate for the first time, a broader approach to disease treatment – focusing on the peroxisome and the restoration of

organellar catalase. We employ a novel antioxidant enzyme, CAT-SKL, which we show effectively targets appropriate oxidative stress and accompanying inflammatory mediators – the precise driving forces established for many degenerative diseases. The idea that metabolizing ROS may play a role in reducing toxic insult associated with disease models is not new; however, implicating peroxisomes as critical contributors to such defenses is.

As an overarching hypothesis then, we suggest that restoring cellular oxidative equilibrium with a peroxisomally targeted antioxidant will have protective effects against the cellular pathologies associated with cancer, diabetic retinopathy and amyloid-beta exposure. The work presented in the following chapter shows that in an *in vitro* breast cancer model, CAT-SKL sensitizes otherwise resistant human breast cancer cells to the tyrosine kinase inhibitor, gefitinib (Giordano et al., 2012). In chapter 3, the enzyme's ability to thwart early retinal dysfunction associated with the diabetic state *in vivo* is chronicled. These results are particularly important because they suggest an ability of CAT-SKL to cross the blood-retinal barrier – a boundary considered an extension of the blood brain barrier. With our evidence of the protein biologic efficacy in a neural setting, we asked whether or not it would thwart amyloid-beta-induced toxicity (chapter 4) in neuronal cell cultures. Our results show that it does, and we have embarked on experiments in an *in vivo*/preclinical setting to confirm and extend these observations. The data support an overall conclusion that the peroxisome is a major site of cellular ROS metabolism and critical metabolic pathway control.

1.7 References

Antonenkov VD, Grunau S, Ohlmeier S and Hiltunen JK (2010) Peroxisomes are oxidative organelles. *Antioxidants & redox signaling* **13**:525-537.

Baker DJ, Wijshake T, Tchkonia T, LeBrasseur NK, Childs BG, van de Sluis B, Kirkland JL and van Deursen JM (2011) Clearance of p16Ink4a-positive senescent cells delays ageing-associated disorders. *Nature* **479**:232-236.

Camoes F, Bonekamp NA, Delille HK and Schrader M (2009) Organelle dynamics and dysfunction: A closer link between peroxisomes and mitochondria. *Journal of inherited metabolic disease* **32**:163-180.

Campisi J (2005) Senescent cells, tumor suppression, and organismal aging: good citizens, bad neighbors. *Cell* **120**:513-522.

Collado M, Blasco MA and Serrano M (2007) Cellular senescence in cancer and aging. *Cell* **130**:223-233.

Coppe JP, Desprez PY, Krtolica A and Campisi J (2010) The senescence-associated secretory phenotype: the dark side of tumor suppression. *Annual review of pathology* **5**:99-118.

Cuervo AM and Dice JF (2000) Age-related decline in chaperone-mediated autophagy. *The Journal of biological chemistry* **275**:31505-31513.

Geuze HJ, Murk JL, Stroobants AK, Griffith JM, Kleijmeer MJ, Koster AJ, Verkleij AJ, Distel B and Tabak HF (2003) Involvement of the endoplasmic reticulum in peroxisome formation. *Molecular biology of the cell* **14**:2900-2907.

Giordano CR, Mueller KL, Terlecky LJ, Krentz KA, Bollig-Fischer A, Terlecky SR and Boerner JL (2012) A targeted enzyme approach to sensitization of tyrosine

kinase inhibitor-resistant breast cancer cells. *Experimental Cell Research* **318**:2014-2021.

Goth L and Eaton JW (2000) Hereditary catalase deficiencies and increased risk of diabetes. *Lancet* **356**:1820-1821.

Goth L and Vitai M (2003) The effects of hydrogen peroxide promoted by homocysteine and inherited catalase deficiency on human hypocatalasemic patients. *Free radical biology & medicine* **35**:882-888.

Gronowicz G, Swift H and Steck TL (1984) Maturation of the reticulocyte in vitro. *Journal of cell science* **71**:177-197.

Hagen TM, Yowe DL, Bartholomew JC, Wehr CM, Do KL, Park JY and Ames BN (1997) Mitochondrial decay in hepatocytes from old rats: membrane potential declines, heterogeneity and oxidants increase. *Proceedings of the National Academy of Sciences of the United States of America* **94**:3064-3069.

Herbig U, Ferreira M, Condel L, Carey D and Sedivy JM (2006) Cellular senescence in aging primates. *Science* **311**:1257.

Huang GQ, Wang JN, Tang JM, Zhang L, Zheng F, Yang JY, Guo LY, Kong X, Huang YZ, Liu Y and Chen SY (2011) The combined transduction of copper, zinc-superoxide dismutase and catalase mediated by cell-penetrating peptide, PEP-1, to protect myocardium from ischemia-reperfusion injury. *Journal of translational medicine* **9**:73.

Hubbard VM, Valdor R, Macian F and Cuervo AM (2012) Selective autophagy in the maintenance of cellular homeostasis in aging organisms. *Biogerontology* **13**:21-35.

Inestrosa NC, Carvajal FJ, Zolezzi JM, Tapia-Rojas C, Serrano F, Karmelic D, Toledo EM, Toro A, Toro J and Santos MJ (2013) Peroxisome proliferators reduce spatial memory impairment, synaptic failure, and neurodegeneration in brains of a double transgenic mice model of Alzheimer's disease. *Journal of Alzheimer's disease : JAD* **33**:941-959.

Ivashchenko O, Van Veldhoven PP, Brees C, Ho YS, Terlecky SR and Fransen M (2011) Intraperoxisomal redox balance in mammalian cells: oxidative stress and interorganellar cross-talk. *Molecular biology of the cell* **22**:1440-1451.

Jin LH, Bahn JH, Eum WS, Kwon HY, Jang SH, Han KH, Kang TC, Won MH, Kang JH, Cho SW, Park J and Choi SY (2001) Transduction of human catalase mediated by an HIV-1 TAT protein basic domain and arginine-rich peptides into mammalian cells. *Free radical biology & medicine* **31**:1509-1519.

Kaneko G, Yoshinaga T, Yanagawa Y, Ozaki Y, Tsukamoto K and Watabe S (2011) Calorie restriction-induced maternal longevity is transmitted to their daughters in a rotifer. *Functional Ecology* **25**:209-216.

Koepke JI, Nakrieko KA, Wood CS, Boucher KK, Terlecky LJ, Walton PA and Terlecky SR (2007) Restoration of peroxisomal catalase import in a model of human cellular aging. *Traffic (Copenhagen, Denmark)* **8**:1590-1600.

Koepke JI, Wood CS, Terlecky LJ, Walton PA and Terlecky SR (2008) Progeric effects of catalase inactivation in human cells. *Toxicology and applied pharmacology* **232**:99-108.

Kuilman T, Michaloglou C, Mooi WJ and Peeper DS (2010) The essence of senescence. *Genes & development* **24**:2463-2479.

Kujoth GC, Hiona A, Pugh TD, Someya S, Panzer K, Wohlgemuth SE, Hofer T, Seo AY, Sullivan R, Jobling WA, Morrow JD, Van Remmen H, Sedivy JM, Yamasoba T, Tanokura M, Weindruch R, Leeuwenburgh C and Prolla TA (2005) Mitochondrial DNA mutations, oxidative stress, and apoptosis in mammalian aging. *Science* **309**:481-484.

Lazarow PB and Fujiki Y (1985) Biogenesis of peroxisomes. *Annual review of cell biology* **1**:489-530.

Lardinois OM (1995) Reactions of bovine liver catalase with superoxide radicals and hydrogen peroxide. *Free Radic Res* **22**:251-274.

Lee HC, Yin PH, Chi CW and Wei YH (2002) Increase in mitochondrial mass in human fibroblasts under oxidative stress and during replicative cell senescence. *Journal of biomedical science* **9**:517-526.

Lee HY, Choi CS, Birkenfeld AL, Alves TC, Jornayvaz FR, Jurczak MJ, Zhang D, Woo DK, Shadel GS, Ladiges W, Rabinovitch PS, Santos JH, Petersen KF, Samuel VT and Shulman GI (2010) Targeted expression of catalase to mitochondria prevents age-associated reductions in mitochondrial function and insulin resistance. *Cell metabolism* **12**:668-674.

Legakis JE, Koepke JI, Jedeszko C, Barlaskar F, Terlecky LJ, Edwards HJ, Walton PA and Terlecky SR (2002) Peroxisome senescence in human fibroblasts. *Molecular biology of the cell* **13**:4243-4255.

Li X, Chen H and Epstein PN (2006) Metallothionein and catalase sensitize to diabetes in nonobese diabetic mice: reactive oxygen species may have a protective role in pancreatic beta-cells. *Diabetes* **55**:1592-1604.

Lisanti MP, Martinez-Outschoorn UE, Lin Z, Pavlides S, Whitaker-Menezes D, Pestell RG, Howell A and Sotgia F (2011) Hydrogen peroxide fuels aging, inflammation, cancer metabolism and metastasis: the seed and soil also needs "fertilizer". *Cell cycle* **10**:2440-2449.

Lu T and Finkel T (2008) Free radicals and senescence. *Exp Cell Res* **314**:1918-1922.

Ma C, Agrawal G and Subramani S (2011) Peroxisome assembly: matrix and membrane protein biogenesis. *The Journal of cell biology* **193**:7-16.

Mates JM, Perez-Gomez C, and De Castro IN (1999) Antioxidant enzymes and human disease. *Clinical Biochemistry* **32**:595-601.

Miller RA (2005) Biomedicine. The anti-aging sweepstakes: catalase runs for the ROSes. *Science* **308**:1875-1876.

Milton NG (2001) Inhibition of catalase activity with 3-amino-triazole enhances cytotoxicity of the Alzheimer's amyloid-beta peptide. *Neurotoxicity* **22**:767-774.

Price M, Terlecky SR and Kessel D (2009) A role for hydrogen peroxide in the pro-apoptotic effects of photodynamic therapy. *Photochemistry and photobiology* **85**:1491-1496.

Putnam CD, Arvai AS, Bourne Y, and Tainer JA (2000) Active and inhibited human catalase structures: ligand and NADPH binding and catalytic mechanism. *J Mol Biol* **296**:295-309.

Rahman K (2007) Studies on free radicals, antioxidants, and co-factors. *Clinical Interactions in Aging* **2**:219-236.

Rucktaschel R, Girzalsky W and Erdmann R (2011) Protein import machineries of peroxisomes. *Biochimica et biophysica acta* **1808**:892-900.

Schrader M and Yoon Y (2007) Mitochondria and peroxisomes: are the 'big brother' and the 'little sister' closer than assumed? *BioEssays : news and reviews in molecular, cellular and developmental biology* **29**:1105-1114.

Schriner SE and Linford NJ (2006) Extension of mouse lifespan by overexpression of catalase. *Age (Dordrecht, Netherlands)* **28**:209-218.

Schriner SE, Linford NJ, Martin GM, Treuting P, Ogburn CE, Emond M, Coskun PE, Ladiges W, Wolf N, Van Remmen H, Wallace DC and Rabinovitch PS (2005) Extension of murine life span by overexpression of catalase targeted to mitochondria. *Science* **308**:1909-1911.

Scibior D, and Czeczot H (2006) Catalase: structure, properties, functions. *Postepy Hig Med Dosw* **60**:170-180.

Singh I (1997) Biochemistry of peroxisomes in health and disease. *Molecular and cellular biochemistry* **167**:1-29.

Switala J, and Loewen PC (2002) Diversity of properties among catalases. *Arch Biochem Biophys* **401**:145-154.

Terlecky SR and Koepke JI (2007) Drug delivery to peroxisomes: employing unique trafficking mechanisms to target protein therapeutics. *Advanced drug delivery reviews* **59**:739-747.

Terlecky SR, Koepke JI and Walton PA (2006) Peroxisomes and aging. *Biochimica et biophysica acta* **1763**:1749-1754.

Titorenko VI and Terlecky SR (2011) Peroxisome metabolism and cellular aging. *Traffic (Copenhagen, Denmark)* **12**:252-259.

Undyala V, Terlecky SR and Vander Heide RS (2011) Targeted intracellular catalase delivery protects neonatal rat myocytes from hypoxia-reoxygenation and ischemia-reperfusion injury. *Cardiovascular pathology : the official journal of the Society for Cardiovascular Pathology* **20**:272-280.

Vainshtein BK, Melik-Adamyan WR, Barynin VV, Vagin AA, and Grebenko AI (1981) Three-dimensional structure of the enzyme catalase. **Nature 293**:411-412.

Wanders RJ and Waterham HR (2006) Biochemistry of mammalian peroxisomes revisited. *Annual review of biochemistry* **75**:295-332.

Watanabe N, Iwamoto T, Bowen KD, Dickinson DA, Torres M and Forman HJ (2003) Bio-effectiveness of Tat-catalase conjugate: a potential tool for the identification of H2O2-dependent cellular signal transduction pathways. *Biochemical and biophysical research communications* **303**:287-293.

Wood CS, Koepke JI, Teng H, Boucher KK, Katz S, Chang P, Terlecky LJ, Papanayotou I, Walton PA and Terlecky SR (2006) Hypocatalasemic fibroblasts accumulate hydrogen peroxide and display age-associated pathologies. *Traffic (Copenhagen, Denmark)* **7**:97-107.

Young CN, Koepke JI, Terlecky LJ, Borkin MS, Boyd Savoy L and Terlecky SR (2008) Reactive oxygen species in tumor necrosis factor-alpha-activated primary human keratinocytes: implications for psoriasis and inflammatory skin disease. *The Journal of investigative dermatology* **128**:2606-2614.

CHAPTER 2: A targeted enzyme approach to sensitization of tyrosine kinase inhibitor-resistant breast cancer cells

Published: **Giordano CR**, Mueller KL, Terlecky LJ, Krentz KA, Bollig-Fischer A, Terlecky SR, and Boerner JL (2012) A targeted enzyme approach to sensitization of tyrosine kinase inhibitor-resistant breast cancer cells *Experimental Cell Research* **318**:2014-2021.

2.1 Abstract

Gefitinib is an epidermal growth factor receptor (EGFR) tyrosine kinase inhibitor (TKI) of potential use in patients with breast cancer. Unfortunately, in clinical studies, gefitinib is often ineffective indicating that resistance to EGFR inhibitors may be a common occurrence in cancer of the breast. EGFR has been shown to be overexpressed in breast cancer, and in particular remains hyperphosphorylated in cell lines such as MDA-MB-468 that are resistant to EGFR inhibitors. Here, we investigate the cause of this sustained phosphorylation and the molecular basis for the ineffectiveness of gefitinib. We show that ROS, known to damage cellular macromolecules and to modulate signaling cascades in a variety of human diseases including cancers, appear to play a critical role in mediating EGFR TKI-resistance. Furthermore, elimination of these ROS through use of a cell-penetrating catalase derivative sensitizes the cells to gefitinib. These results suggest a new approach for the treatment of TKI-resistant breast cancer patients specifically, the targeting of ROS and attendant downstream oxidative stress and their effects on signaling cascades.

2.2 Introduction

Epidermal growth factor receptors (EGFR) are part of the ErbB family (or epidermal growth factor family) composed of receptor tyrosine kinases (Jorissen et al., 2003; DeYulia and Carcamo, 2005). EGFR is activated by binding of its ligand, epidermal growth factor (EGF), leading to dimerization of the receptor and stimulation of intracellular kinase activity. Upon dimerization, autophosphorylation occurs, eliciting downstream signaling cascades involved in cell survival and increased cellular proliferation (Jorissen et al., 2003; DeYulia and Carcamo, 2005). In some breast cancers, EGFR is overexpressed, although tyrosine kinase inhibitors targeting EGFR (EGFR TKIs) have yet to demonstrate uniform efficacy in the clinic (Tan et al., 2004; Baselga et al., 2005). Interestingly, in breast cancer cell lines resistant to EGFR TKIs, EGFR-phosphorylation is often maintained at high levels in the presence of the TKI (Mueller et al., 2008), indicating that EGFR may continue to signal to promote cell growth and survival. This is supported by evidence that targeted knockdown of EGFR expression can decrease growth and survival of EGFR TKI-resistant breast cancer cells (Irwin et al., 2011).

Mechanisms of EGFR inhibitor resistance in all cancers are the focus of many researchers and specific insights have been realized (Wheeler et al., 2010). The most common mutation known to occur in EGFR is a truncation resulting in a deletion of exons 2-7; the resultant molecule is known as EGFRvIII. Importantly, this mutation occurs in 86% of gliomas and is thought to mediate resistance to EGFR inhibitors (Lo, 2010). Resistance mechanisms involve upregulation of parallel signaling tyrosine kinase receptors including insulin like growth factor receptor (IGF-1R), vascular endothelial

growth factor (VEGFR), and Met as well as the constitutive activation of downstream molecules including Akt and MAPK (reviewed in (Wheeler et al., 2010)). These EGFR TKI resistance pathways circumvent EGFR TKIs by the activation of additional signaling pathways.

An additional mechanism to explain the somewhat disappointing overall response of breast tumors to EGFR TKIs is the possibility that the EGFR still has the ability to signal in the absence of innate EGFR kinase activity. Indeed, it has been clearly demonstrated that additional tyrosine kinases can phosphorylate the EGFR independent of ligand. For example, c- Src phosphorylates a kinase-impaired EGFR on its autophosphorylation sites as well as several additional tyrosines (Stover et al., 1995; Amos et al., 2005). In addition, another EGFR family member, HER2, also has the ability to phosphorylate the EGFR on its autophosphorylation sites (Spivak-Kroizman et al., 1992). Furthermore, it has been shown that a point mutation in the HER2 kinase domain results in constitutive phosphorylation of EGFR in the presence of EGFR TKIs (Wang et al., 2006). These data indicate that, even without the EGFR kinase activity, phosphorylation of the EGFR may occur to promote cell growth and survival pathways.

The EGFR TKI-resistance seen in certain cancer cells may result from an ROS-induced inactivation of an EGFR-associated tyrosine phosphatase (Chen et al., 2006). In this context, a role for ROS and accompanying oxidative stress in the initiation and progression of breast cancer has been suggested and variously supported in a number of studies (Benhar et al., 2002; Bollig-Fischer et al., 2010; Liou and Storz, 2010). Oncogenes with tyrosine kinase activity, including HER2 in breast cancer cells, can induce the upregulation of cellular/oncogenic ROS and influence the metabolic

transformation of cancer cells (Lee et al., 1998). Furthermore, the cancer cell redox state can affect the function of oncogenic kinases (Benhar et al., 2002).

In order to examine the potential link between cellular ROS and EGFR TKI-resistance, we employed a targeted antioxidant enzyme, CAT-SKL, to reduce oxidant levels in breast cancer cell line models expressing high levels of ROS and EGFR. Our results indicate that CAT-SKL sensitizes previously resistant MDA-MB-468 cells to the anti-cancer effects of the EGFR-targeted TKI, gefitinib. EGFR inhibitors are of great potential value as therapies in breast cancer models; resistance presents a major challenge to this treatment modality. CAT-SKL, a H_2O_2 metabolizing protein therapeutic shown to be effective in a number of *in vitro* and pre-clinical indications (Koepke et al., 2007; Young et al., 2008; Undyala et al., 2011), thus represents a potentially powerful new means of combating this devastating disease.

2.3 Results

2.3.1 EGFR remains tyrosine phosphorylated in breast cancer cells resistant to TKIs

Despite EGFR overexpression in more than 30% of breast cancers, clinical trials using EGFR targeted therapies have failed to show a significant benefit in disease-free and overall survival (Tan et al., 2004; Baselga et al., 2005). Breast cancers overexpressing EGFR have a poor clinical outcome, therefore emphasizing a need to more effectively target EGFR in these cancers. To examine the effects of gefitinib on EGFR phosphorylation, we cultured two human breast cancer cell lines in the presence of the TKI. In SUM149 cells, phosphorylation of EGFR at tyrosine 1068 was reduced in response to gefitinib, whereas EGFR phosphorylation at tyrosine 1068 in MDA-MB-468

cells was unaffected (Fig. 2.1A). Inhibitory growth curves further document the sensitivity of SUM149 cells to gefitinib (IC50 values of 6.8 μM for SUM149 cells and 14.1 μM for the MDA-MB-468 cells (Fig. 2.1B; dotted lines = 95% confidence intervals)). We previously documented this trend of EGFR tyrosine phosphorylation in the presence of gefitinib correlating with resistance to effects on viability by EGFR TKIs and established the inhibition of EGFR kinase activity with gefitinib ((Mueller et al., 2008); Supplementary figure a2.1). Here we further demonstrate that in MDA-MB-468 cells, autophosphorylation specifically at tyrosine 1068 is regulated independently of EGFR kinase activity.

Figure 2.1A

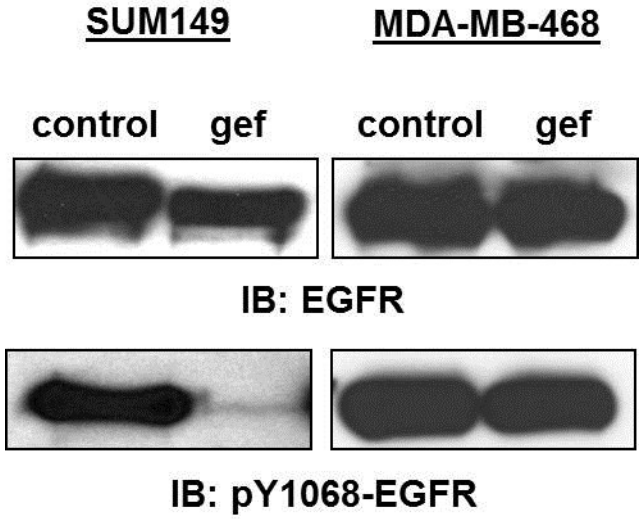

Figure 2.1B

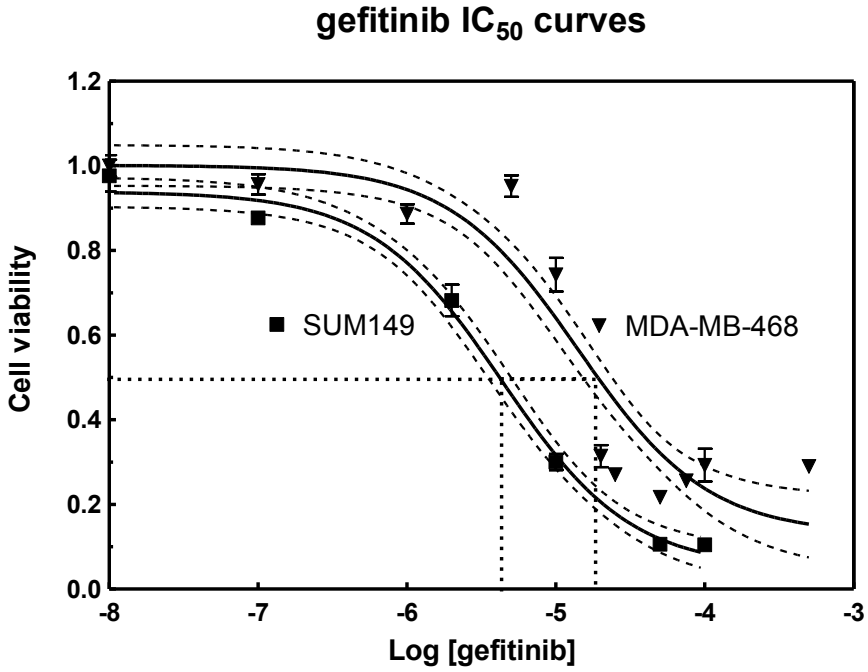

Figure 2.1. EGFR phosphorylation and TKI sensitivity of breast cancer cell lines. (A) SUM149 and MDA-MB-468 cells were treated with 0.5 μM gefitinib for 30 minutes. Lysates were then prepared, separated by SDS-PAGE, and immunoblotted using anti-EGFR or anti-pY1068-EGFR antibodies. Control = vehicle control treated; gef = gefitinib treated; IB = immunoblot. (B) SUM149 or MDA-MB-468 cells were cultured with increasing concentrations of gefitinib for 72 hours. MTT colorimetric assays were performed to assess cell viability. Fraction of surviving cells was determined and IC50 values were calculated from sigmoidal dose response curves. 95% confidence intervals for each curve appear as dashed lines. Log [geftinib] = log of each dose of gefitinib used in M. Image appears in *Experimental Cell Research*. 2012 by Giordano, CR et al. Figure contributed by Boerner JL.

2.3.2 Elevated ROS levels in TKI-resistant breast cancer cells

Deregulation of EGFR tyrosine phosphorylation could be elevated by ROS through any number of distinct mechanisms. Therefore, we sought to determine the baseline level of ROS in MDA-MB-468 cells compared to a gefitinib-sensitive breast cancer cell line, in this case, SUM149. Using a DCF-fluorescence assay that measures total intracellular ROS, we found that oxidant levels in MDA-MB-468 cells were nearly 10 fold higher when directly compared to the SUM149 cells (Fig. 2.2; black bars). To determine if ROS production was altered by gefitinib treatment, we incubated both cell lines with 0.5 μM gefitinib for 30 minutes. Interestingly, ROS production was not altered by gefitinib in either cell line (Fig. 2.2; white bars). These results led us to consider that ROS production in MDA-MB-468 cells may regulate EGFR tyrosine phosphorylation and subsequent biological resistance to gefitinib.

2.3.3 EGFR tyrosine phosphorylation is regulated by reactive oxygen

To examine the role of ROS in modulating EGFR tyrosine phosphorylation, we examined the process in cells treated with the antioxidant, N-acetyl cysteine (NAC), or the oxidizer, H_2O_2, as seen in Fig. 2.3A and 2.3B (immunoblots quantified in Supplementary figures a2.2A and a2.2B). Quenching ROS decreased EGFR tyrosine phosphorylation in gefitinib-treated MDA-MB-468 cells. In contrast, enhancing oxidative stress in SUM149 cells with H_2O_2 rendered them unable to decrease EGFR tyrosine phosphorylation.

Figure 2.2

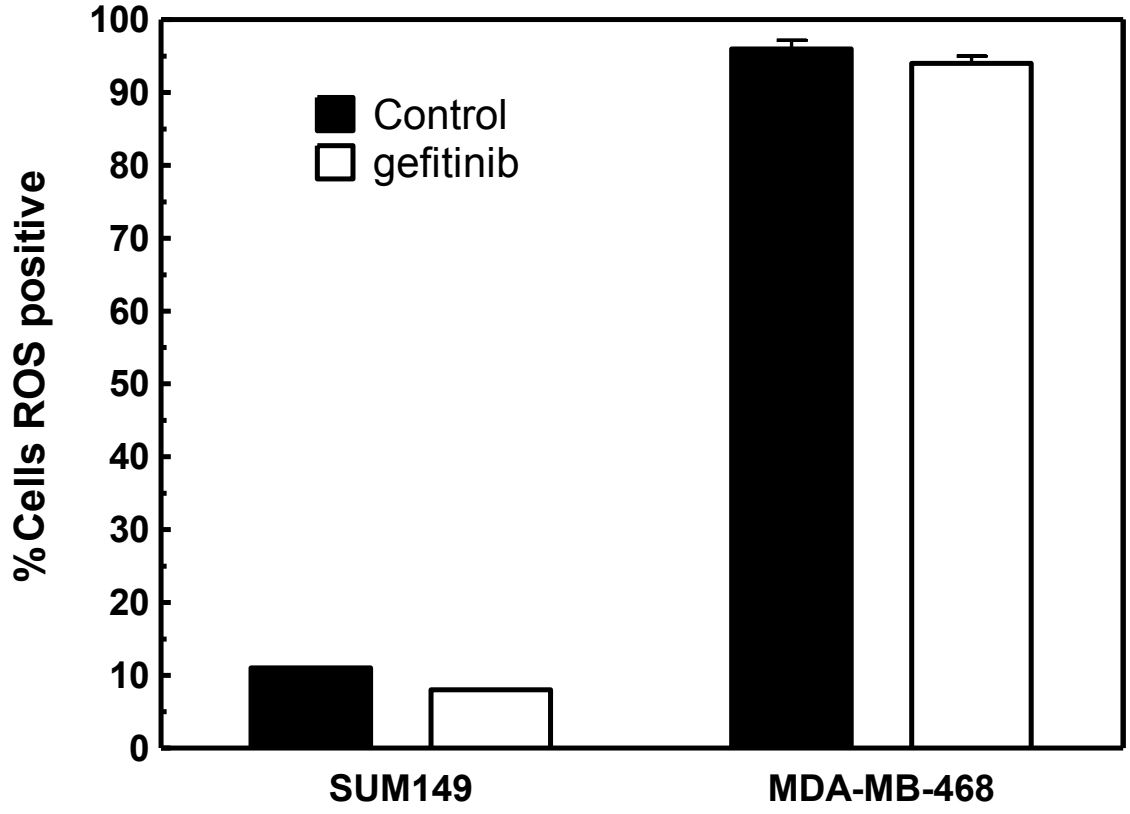

Figure 2.2. ROS levels are elevated in TKI-resistant breast cancer cells. SUM149 and MDA-MB-468 cells were treated with 0.5 μM gefitinib for 30 minutes. ROS production was measured using the fluorescent dye, 2',7'-dichlorofluorescin diacetate (DCF-DA), which measures reactive oxygen on a per cell basis. The percentage of cells positive for ROS was determined from an average of three independent experiments. Control = vehicle control treated; gef = gefitinib treated. Image appears in *Experimental Cell Research*. 2012 by Giordano, CR et al. Figure contributed by Boerner, JL.

Figure 2.3A

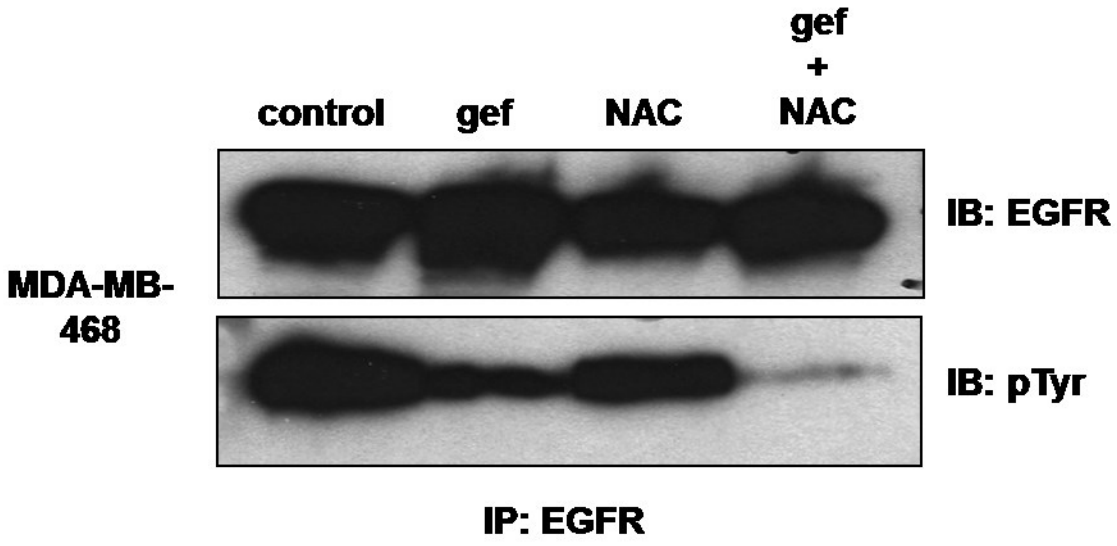

Figure 2.3B

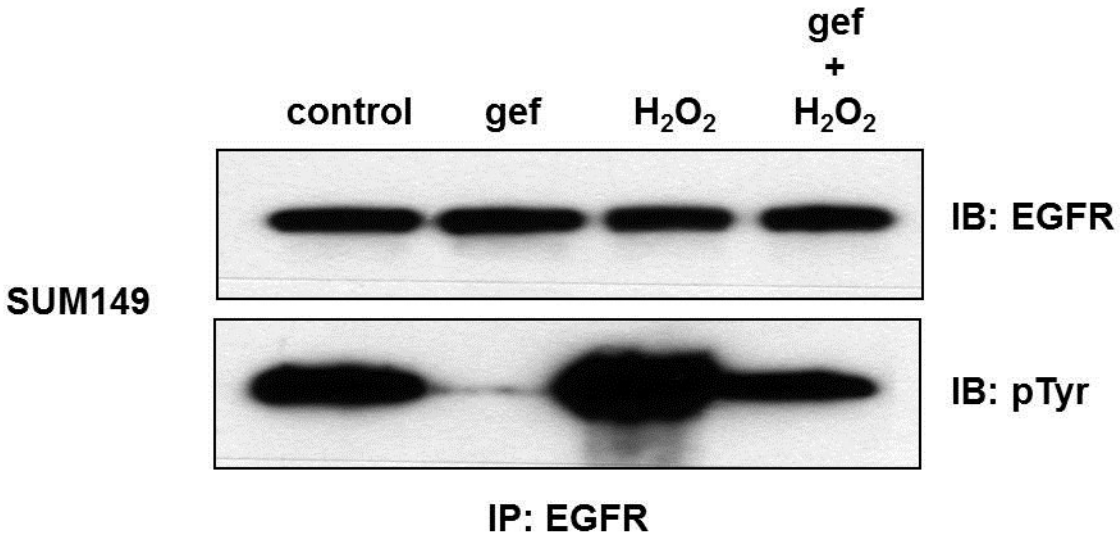

Figure 2.3. EGFR tyrosine phosphorylation is regulated by reactive oxygen. (A) MDA-MB-468 cells were treated with 0.5 μM gefitinib for 30 minutes and/or 50 mM N-acetyl cysteine for the last 10 minutes as indicated. Cell lysates were immunoprecipitated using anti-EGFR antibodies and immunoblotted with anti-EGFR or anti-phosphotyrosine antibodies. (B) SUM149 cells were treated with 0.5 μM gefitinib and/or 5 mM H_2O_2. Cell lysates were immunoprecipitated using anti-EGFR antibodies and immunoblotted with anti-EGFR or anti-phosphotyrosine antibodies. Control = vehicle control treated; gef = gefitinib treated; NAC = N-acetyl cysteine treated; IB = immunoblot; IP = immunoprecipitation. Image appears in *Experimental Cell Research*. 2012 by Giordano, CR et al. Figures contributed by Boerner,JL.

These results support the model that in breast cancer cells, ROS modulates EGFR phosphorylation in the presence of an EGFR TKI.

2.3.4 CAT-SKL transduction of MDA-MB-468 cells

NAC was abandoned as a potential therapeutic due to its toxicity in our long-term growth assays (data not shown). Instead, we employed a novel cell-penetrating catalase derivative, called CAT-SKL (Wood et al., 2006; Terlecky and Koepke, 2007; Price et al., 2009; Undyala et al., 2011). This molecule is designed to enter cells and, by virtue of a modified targeting signal, efficiently traffic to peroxisomes. Once there, it metabolizes H_2O_2 produced both within the organelle, as well as elsewhere in the cell, and restores, to varying extents, oxidative balance in cells (Wood et al., 2006; Terlecky and Koepke, 2007; Price et al., 2009; Undyala et al., 2011). This targeted enzyme approach has shown efficacy in a number of cellular and preclinical indications and works, at least in part, by controlling inflammatory processes (Young et al., 2008; Undyala et al., 2011). In order to demonstrate transduction of MDA-MB-468 breast cancer cells, we biotinylated CAT-SKL and tracked its entry into the cells (Fig. 2.4A). MDA-MB- 468 cells were incubated with 100 nM CAT-SKL for 1 to 4 hours. Protein lysates were isolated and blotted with streptavidin-alkaline phosphatase labeled antibodies. Importantly, biotinylated- CAT-SKL was detected inside the MDA-MB-468 cells after 1 hour of incubation (Fig. 2.4B).

2.3.5 CAT-SKL reduces ROS in MDA-MB-468 cells

Although we have shown that CAT-SKL was able to enter MDA-MB-468 cells, we needed to confirm that the enzyme was able to quench ROS in this breast cancer model. To accomplish this, MDA-MB-468 cells were incubated with 1 μM CAT-SKL for 4

hours and ROS production was determined by measuring DCF-fluorescence (Figs. 2.5A and 2.5B). Importantly, CAT-SKL was able to decrease ROS production by about 48% in MDA-MB-468 cells (Fig. 2.5B). In addition, when H_2O_2 specifically was measured using an Amplex® Red based assay, a 21% decline was seen (Fig. 2.5C). Taken together, these experiments demonstrate that CAT-SKL is able to enter MDA-MB-468 cells and significantly reduce ROS production.

Figure 2.4A

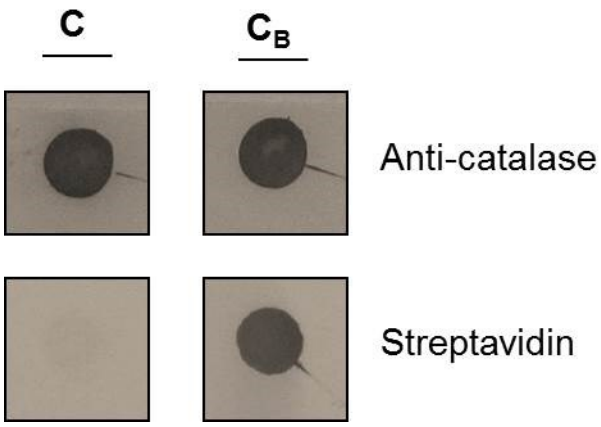

Figure 2.4B

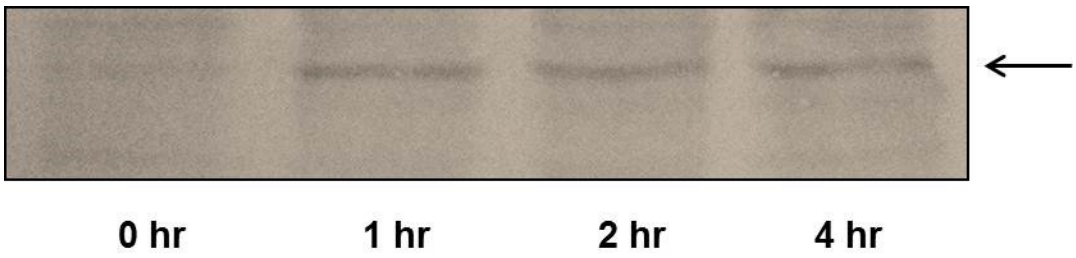

Figure 2.4. CAT-SKL transduction of MDA-MB-468 cells. (A) CAT-SKL was biotinylated as described (16-18). CAT-SKL ("C") and CAT-SKL after biotinylation ("C_B") were dot-blotted onto nitrocellulose and probed with anti-catalase antibodies (and alkaline phosphatase secondary antibodies) or streptavidin alkaline phosphatase as indicated. (B) MDA-MB-468 cells were incubated with biotinylated CAT-SKL (100 nM) for 0, 1, 2, and 4 hours as indicated. Cells were then washed, harvested, and blotted with streptavidin-alkaline phosphatase. Arrow indicates migration of biotinylated-CAT-SKL. Image appears in *Experiment Cell Research*. 2012 by Giordano, CR et al. Figures contributed by Giordano, CR.

To determine if H_2O_2 decreased viability of the MDA-MB-468 cells, 1 mM H_2O_2 was added to the cells for 2 hours and the effects on cell viability were assessed by the MTT assay, a measure of mitochondrial reductase activity. As expected, H_2O_2 decreased viability in the MDA-MB-468 cells by almost 50% (Fig. 2.5D; black bars). In contrast, in cells pretreated with CAT-SKL, exogenously added H_2O_2 was largely without effect (Fig. 2.5D). CAT-SKL treatment alone had no effect on cell viability, demonstrating that the enzyme is not toxic to human breast cancer cells. Essentially similar results were obtained when trypan blue (dye) exclusion assays were employed to directly determine cell viability (Fig. 2.5E).

2.3.6 CAT-SKL sensitizes MDA-MB-468 cells to gefitinib

To determine if CAT-SKL reduction of ROS production is sufficient to reduce EGFR tyrosine phosphorylation in the presence of 1 μM gefitinib, we measured EGFR phosphorylation at tyrosine 1068 in MDA-MB-468 cells after a 4 hour treatment with 1 μM CAT-SKL. Once again, EGFR tyrosine phosphorylation was not reduced with gefitinib treatment; however, co-treatment with gefitinib and CAT-SKL resulted in an almost complete loss of EGFR tyrosine phosphorylation at 1068 (Fig. 2.6A; left panel). This is in contrast to the treatment of SUM149 cells with gefitinib and CAT-SKL. Specifically, EGFR tyrosine phosphorylation is abrogated with gefitinib treatment and actually modestly inhibited by CAT-SKL itself (Fig. 2.6A; right panel). These data suggest that the general phenomenon of inhibiting ROS production in cancer cells may decrease tyrosine phosphorylation of key pro-growth and survival proteins.

To determine if CAT-SKL could sensitize MDA-MB-468 cells to the anti-proliferation effects of gefitinib, we treated cells with vehicle or 1 μM gefitinib in the

presence or absence of 1 μM CAT-SKL in a 7 day proliferation assay. MDA-MB-468 cells continued to proliferate with 1 μM gefitinib or 1 μM CAT-SKL treatment alone (Fig. 2.6B; triangles). However, co-treatment of MDA-MB-468 cells with gefitinib and CAT-SKL decreased cell proliferation by nearly 50% (Fig. 2.6B; left panel; diamonds). This decrease in proliferation was statistically significant and provides evidence, for the first time, of a targeted antioxidant enzyme sensitizing cancer cells to a TKI. Taken together, these data suggest that CAT-SKL may represent a new therapeutic approach for the treatment of EGFR TKI-resistant breast cancers.

Previously we have shown that SUM149 cells are sensitive to EGFR inhibitors including gefitinib (Figure 2.1B; 2.3). Here we demonstrate that gefitinib treatment decreases cell proliferation by 50% in the SUM149 cells (Fig. 2.6B; right panel). As with the MDA-MB-468 cells, CAT-SKL alone failed to inhibit cell proliferation in the SUM149 cells. However, combining gefitinib and CAT-SKL produced an additional 25% decrease in cell proliferation compared to gefitinib treatment alone (Fig. 2.6B; right panel). Taken together, these data suggest that for breast cancers that express high levels of EGFR and ROS, a combination antioxidant and TKI treatment strategy may elicit a greater effect than, or overcome resistance to, EGFR-targeted TKI therapy

Figure 2.5A

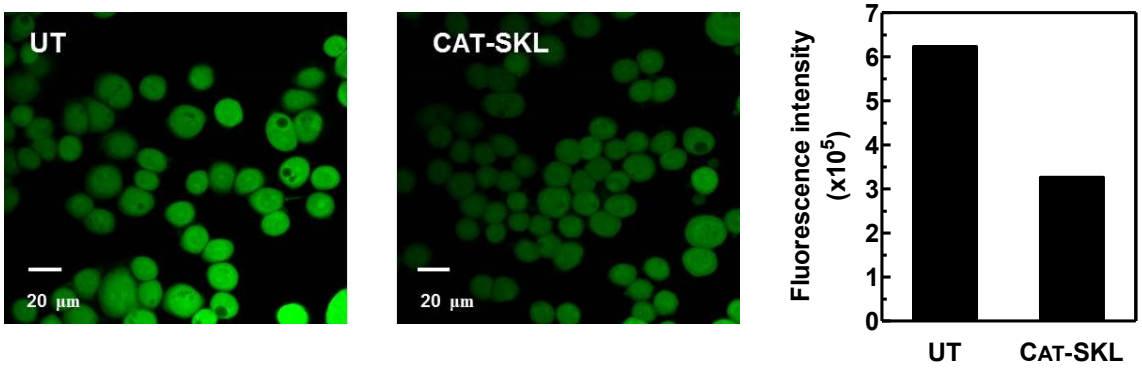

Figure 2.5B and C

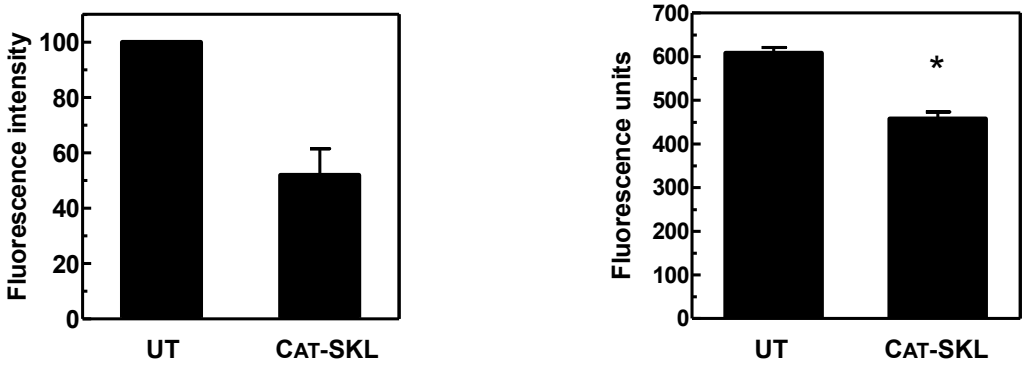

Figure 2.5D and E

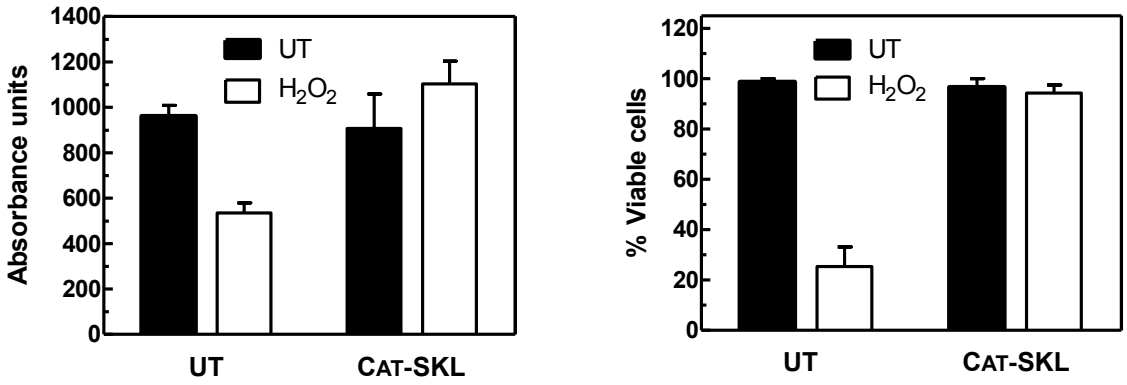

Figure 2.5. Effect of CAT-SKL on ROS levels in MDA-MB-468 cells. (A) Cells were pretreated or not ("UT") with CAT-SKL (1 μM) for 4 hours and then examined for the presence of ROS using DCF-DA (25 μM). The accompanying histogram represents MetaMorph®-based quantification of the cellular fluorescence intensities seen in the ROS images. (B) Cellular fluorescence intensities from three experiments (including the one shown in (A)) were pooled and normalized to the untreated control value (arbitrarily set at 100) to permit comparison. Results presented are the mean ± 1 SD. (C) H_2O_2 was specifically measured employing the Amplex® Red Reagent (10-acetyl-3,7-dihydroxy-phenoxazine). The decline is statistically significant; *p-value < 0.01. (D,E) MDA-MB-468 cells were pretreated with CAT-SKL (1 μM) for 4 hours and then challenged with H_2O_2 for 2 hours (1 mM). Cell viability was determined either using the water soluble tetrazolium cell proliferation assay (WST-1) (D), or by quantitative trypan blue exclusion assays (E). Image appears in *Experimental Cell Research*. 2012 by Giordano, CR et al. Figures contributed by Giordano, CR.

Figure 2.6A

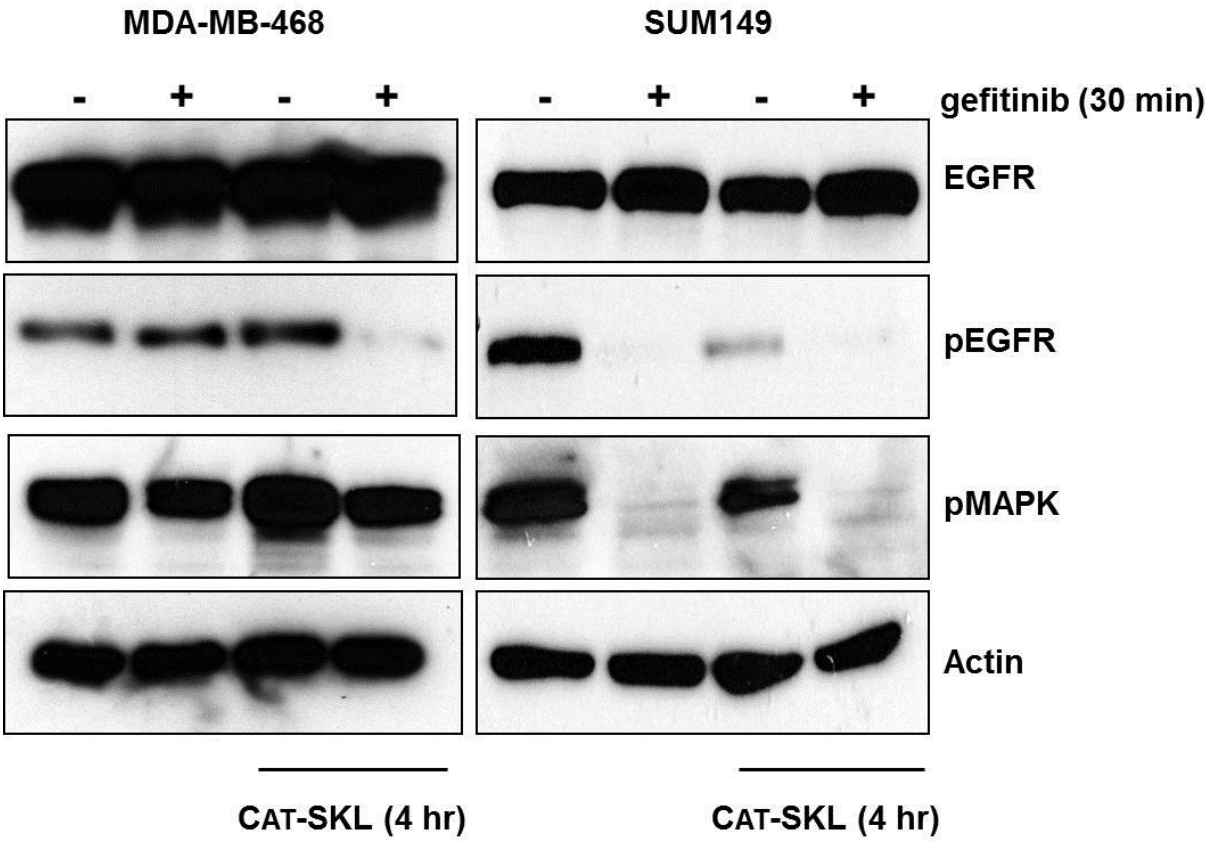

Figure 2.6B

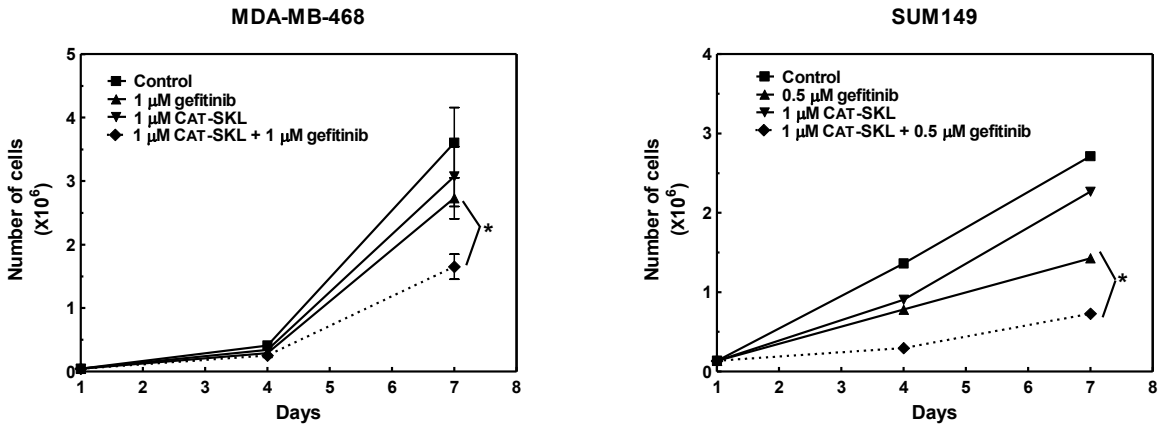

Figure 2.6. CAT-SKL decreases EGFR tyrosine phosphorylation in the presence of gefitinib and sensitizes MDA-MB-468 cells to the TKI. (A) MDA-MB-468 and SUM149 cells were incubated with 1 μM CAT-SKL for 4 hours followed by 30 minutes with 1 μM or 0.5 μM gefitinib, respectively. Cell lysates were prepared, separated by SDS-PAGE, and immunoblotted using anti-EGFR, anti-pY1068-EGFR, anti-pMAPK, or anti-β-actin antibodies. (B) MDA-MB-468 and SUM149 cells were treated with 1 μM or 0.5 μM gefitinib, respectively, 1 μM CAT-SKL, or the combination for 7 days. Cells were counted on days 1, 4 and 7 as described in materials and methods. Growth curves were plotted over time. * p-value = 0.05. Image appears in *Experimental Cell Research*. 2012 by Giordano, CR et al. Figures contributed by Boerner, JL.

2.4 Discussion

In this report we have provided evidence of a role for ROS production in mediating resistance to EGFR inhibitors through maintenance of EGFR tyrosine phosphorylation. Specifically, we found that inhibiting ROS production using a novel inhibitor of H_2O_2 production, CAT-SKL, sensitized resistant MDA-MB-468 breast cancer cells to EGFR kinase inhibition by gefitinib. In doing so, EGFR tyrosine phosphorylation, and cell proliferation were reduced. As EGFR inhibitors have yet to show consistent value in the clinical treatment of breast cancer, these data provide striking evidence for the efficacy of a combination of CAT-SKL and gefitinib in the treatment of EGFR expressing tumors.

How CAT-SKL elicits its effect remains to be further investigated, but in light of our observations that CAT-SKL treatment has a role in attenuating EGFR phosphorylation, a plausible mechanistic explanation may involve CAT-SKL-dependent reactivation of a phosphatase (PTP) that targets the EGFR. It is known that PTPs contain an active cysteine that is required for phosphorylation and that ROS modify this site (reviewed in (Tonks, 2006)). Inhibition of ROS production by antioxidants has been shown to “reactivate” tyrosine PTPs; including PTP1B, TCPTP, SHP2, SHP1, CD45, PTPκ, and PTP-PEST (Tonks, 2006). Importantly, PTP1B, SHP1, and PTPκ have been shown to dephosphorylate EGFR. In addition, SHP1 and PTPκ have been implicated as tumor suppressors, implying that loss of the function of these PTPs promotes cancer progression. Future work will address the hypothesis that downregulation of ROS by CAT-SKL treatment can reverse PTP inactivation and thus allow for dephosphorylation of EGFR, and re-establishment of sensitivity to gefitinib.

The work of others has established that dysregulated ROS production/metabolism plays a crucial role in many human diseases, including cancer (Benhar et al., 2002; Liou and Storz, 2010). Furthermore, ROS have been linked to aberrant EGFR phosphorylation resulting in modifications of downstream signaling cascades. Our work here has shown that treatments with antioxidants such as NAC were able to reduce ROS and potentiate the effects of gefitinib on EGFR phosphorylation. However, when growth curves were performed with NAC, cell viability was compromised, suggesting it is a poor clinical option for breast cancer patients. Our results indicate that transduced CAT-SKL was able to significantly reduce cellular ROS and gefitinib-sensitize otherwise resistant breast cancer cells that express high levels of ROS without compromising cell viability. Breast cancer treatment is limited for certain patients due to insensitivity to EGFR TKIs. Furthermore, constitutively active EGFR phosphorylation is a common characteristic of many breast cancers. Reducing ROS production with a safe, targeted enzyme approach employing CAT-SKL may represent a new treatment modality for a deadly disease.

2.5 Materials and Methods

Cell culture. SUM149 cells were maintained in Ham's F-12 supplemented with 5% FBS, 1 µg/mL hydrocortisone, and 5 µg/mL insulin. MDA-MB-468 cells were grown in DMEM supplemented with 10% FBS. Both cell lines were cultured with 2.5 µg/mL amphotericin B and 25 µg/mL gentamicin. For vehicle control treated cells, dimethyl sulfoxide was added at 0.1% final concentration.

SDS-PAGE/Immunoblotting. Lysates were prepared from the indicated cells in CHAPS lysis buffer (10 mM CHAPS, 50 mM Tris-pH 8.0, 150 mM NaCl, and 2 mM

EDTA with 10 μM NaOVa and 1X protease inhibitor cocktail (EMD Biosciences, Philadelphia, PA)). For immunoblotting, 10 μg of protein lysates were separated by SDS-PAGE and transferred to Immobilon P. Membranes were blocked in either 5% nonfat dry milk or 5% BSA for 1 hour at 25°C or 5% BSA. Primary antibodies utilized in this study include: anti-EGFR and anti-pY1068 EGFR from Cell Signaling (Danvers, MA); anti-pMAPK and anti-actin from Sigma (St. Louis, MO); and anti-pTyrosine from Invitrogen (Carlsbad, CA). Anti-mouse and anti-rabbit IgG-HRP was used from Cell Signaling and enhanced chemiluminescence (ECL) reagents were from GE Healthcare Life Sciences (Piscataway, NJ). Experiments were repeated at least three times.

Dot blot analyses were performed with streptavidin alkaline-phosphatase (1:1000) or anti-catalase antibodies (1:4000) and goat anti-rabbit-alkaline-phosphatase (1:5000) and developed with the NBT/BCIP color development substrate (Thermo Scientific). Protein transduction was performed as follows; 100 nM of biotinylated CAT-SKL was added for 0, 1, 2, and 4 hours, cells were washed with PBS, and harvested directly into standard 2X sample buffer. Proteins were separated by 10% SDS-PAGE, and then transferred to a nitrocellulose membrane and blocked for 1 hour in 5% nonfat dry milk in Tween-containing, tris buffered saline. Membranes were probed with anti-streptavidin alkaline phosphatase (1:1000) and developed with NBT/BCIP.

Biotinylation of CAT-SKL. CAT-SKL containing an 11 arginine peptide transduction domain and a modified peroxisomal targeting signal was expressed, purified, and biotinylated as described in (Terlecky et al., 2001; Terlecky, 2002; Koepke et al., 2007; Young et al., 2008).

Cell viability and cell growth assays. For testing cell viability, two approaches were employed; enzymatic assays that measure metabolic activity and a dye-exclusion assay that distinguishes live from dead cells. For the generation of IC50 curves, 1,000 MDA-MB-468 or SUM149 cells per well were incubated for 72 hours with various concentrations of gefitinib (dissolved in dimethyl sulfoxide). At this point, cell viability was determined with 3-(4,5-dimethylthiazol-2-yl)-2,5-diphenyltetrazolium bromide (MTT), as per manufacturer's protocol. For the sensitivity to H_2O_2 experiments, cells were plated at 400,000 cells per well, pretreated with CAT-SKL (1 μM) for 4 hours, and challenged with H_2O_2 (1 mM) for 2 hours. MDA-MB-468 cell viability was determined using the water soluble tetrazolium cell proliferation assay (WST-1) from Millipore following the manufacturer's protocol. For the latter, 200,000 cells, pretreated with CAT-SKL and challenged with H_2O_2 as described above, were incubated with 0.2% trypan blue (final concentration) for 3-5 minutes and the percentage of non-viable (blue) cells were determined microscopically with a hemocytometer.

Growth assays were performed by plating MDA-MB-468 or SUM149 cells in triplicate in 6-well plates at 35,000 cells per well (day 0). The next day, and every other day thereafter for seven days, the cells were treated with 0.1% dimethyl sulfoxide (vehicle control), or gefitinib, and/or CAT-SKL at the indicated dosages. The number of cells was determined using a Coulter counter on days 1, 4, and 7. Each experiment was repeated at least three times.

Measurement of ROS. H_2O_2 measurements were performed using the Amplex® Red Hydrogen Peroxide/Peroxidase Assay Kit from Molecular Probes® following the manufacturer's protocol. After treatment with 1 μM CAT-SKL for 4 hours at 37°C, cells

were washed twice with Hank's balanced salt solution, harvested in the Amplex® Red reagent/horse radish peroxidase working solution, incubated at room temperature for 30 minutes, and fluorescence was measured on a microplate reader (excitation 530 nm and emission 590 nm). 2',7'-dichlorofluorescin diacetate (DCF-DA) was used as previously described (Legakis et al., 2002); live cells were imaged for ROS production. Briefly, cells were treated with or without 1 μM CAT-SKL for 4 hours, washed twice with Hank's balanced salt solution and incubated for 10 minutes with 25 μM DCF-DA. After washing again, microscopic analysis was performed using the Zeiss LSM 510 META NLO confocal microscope at the Wayne State University School of Medicine Microscopy, Imaging, & Cytometry Resources Core. Cellular ROS was quantified either by counting the cells that stain positive for ROS or by using MetaMorph® (Molecular Devices) image analysis software to quantitate cellular fluorescence intensities.

Appendix Chapter 2

Supplementary figure a2.1

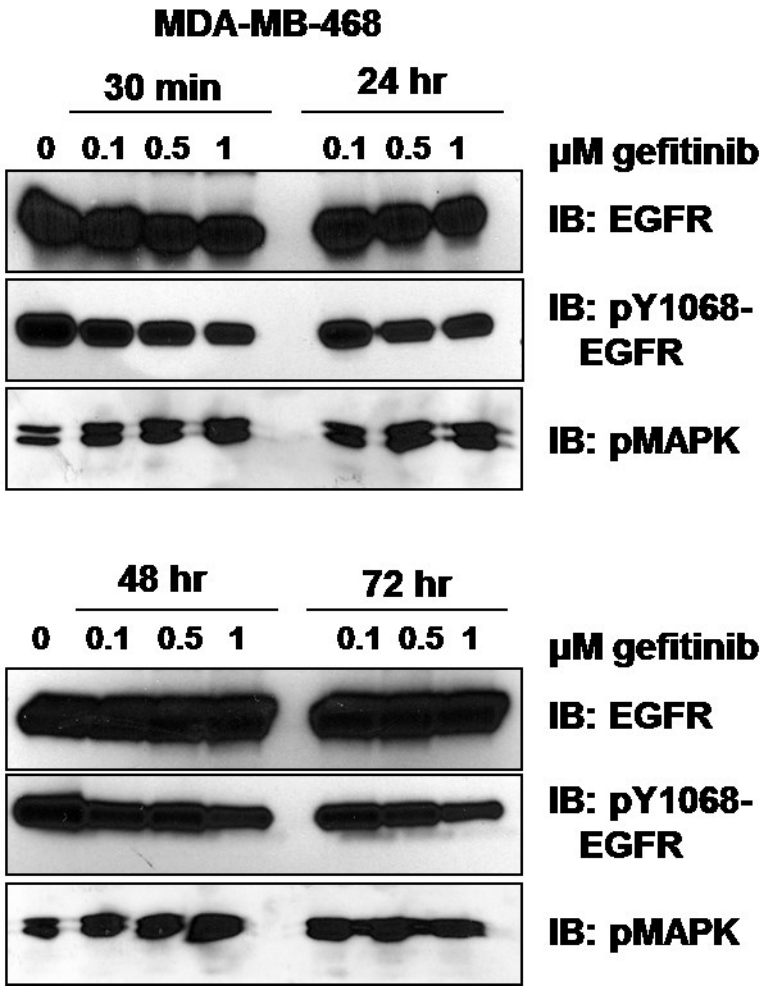

Supplementary figure a2.1. EGFR remains tyrosine phosphorylated in MDA-MB-468 in the presence of gefitinib. MDA-MB-468 cells were treated with 0.1, 0.5, and 1 μM gefitinib for 30 minutes, 24 hours, 48 hours, or 72 hours as indicated. Lysates were prepared and immunoblotted using antibodies to EGFR, pEGFR Y1068, and pMAPK. Image appears in *Experimental Cell Research*. 2012 by Giordano, CR et al. Figures contributed by Boerner, JL.

Supplementary figure a2.2A and a2.2B

A

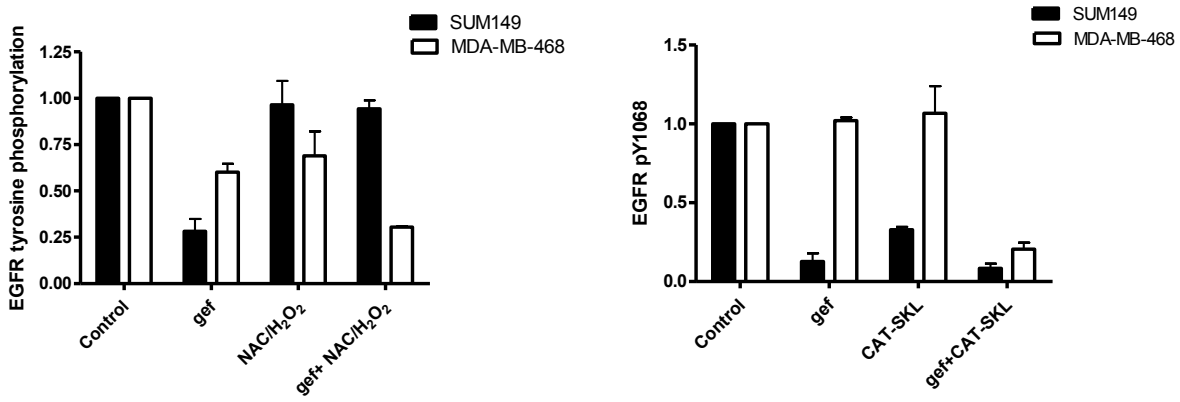

Supplementary figure a2.2. Quantification of immunoblots. (A and B) EGFR tyrosine phosphorylation immunoblots were digitized and quantified using AlphaEaseFC. Immunoblots from three experiments represented by Fig. 2.3A (A) or Fig. 2.6A (B) were included in the quantification. Image appears in *Experimental Cell Research*. 2012 by Giordano, CR et al. Figures contributed by Boerner, JL.

2.6 References

Amos S, Martin PM, Polar GA, Parsons SJ and Hussaini IM (2005) Phorbol 12-myristate 13-acetate induces epidermal growth factor receptor transactivation via protein kinase Cdelta/c-Src pathways in glioblastoma cells. *The Journal of biological chemistry* **280**:7729-7738.

Baselga J, Albanell J, Ruiz A, Lluch A, Gascon P, Guillem V, Gonzalez S, Sauleda S, Marimon I, Tabernero JM, Koehler MT and Rojo F (2005) Phase II and tumor pharmacodynamic study of gefitinib in patients with advanced breast cancer. *Journal of clinical oncology : official journal of the American Society of Clinical Oncology* **23**:5323-5333.

Benhar M, Engelberg D and Levitzki A (2002) ROS, stress-activated kinases and stress signaling in cancer. *EMBO Rep* **3**:420-425.

Bollig-Fischer A, Dziubinski M, Boyer A, Haddad R, Giroux CN and Ethier SP (2010) HER-2 signaling, acquisition of growth factor independence, and regulation of biological networks associated with cell transformation. *Cancer research* **70**:7862-7873.

Chen CH, Cheng TH, Lin H, Shih NL, Chen YL, Chen YS, Cheng CF, Lian WS, Meng TC, Chiu WT and Chen JJ (2006) Reactive oxygen species generation is involved in epidermal growth factor receptor transactivation through the transient oxidization of Src homology 2-containing tyrosine phosphatase in endothelin-1 signaling pathway in rat cardiac fibroblasts. *Molecular pharmacology* **69**:1347-1355.

DeYulia GJ, Jr. and Carcamo JM (2005) EGF receptor-ligand interaction generates extracellular hydrogen peroxide that inhibits EGFR-associated protein tyrosine phosphatases. *Biochemical and biophysical research communications* **334**:38-42.

Irwin ME, Mueller KL, Bohin N, Ge Y and Boerner JL (2011) Lipid raft localization of EGFR alters the response of cancer cells to the EGFR tyrosine kinase inhibitor gefitinib. *Journal of cellular physiology* **226**:2316-2328.

Jorissen RN, Walker F, Pouliot N, Garrett TP, Ward CW and Burgess AW (2003) Epidermal growth factor receptor: mechanisms of activation and signalling. *Exp Cell Res* **284**:31-53.

Koepke JI, Nakrieko KA, Wood CS, Boucher KK, Terlecky LJ, Walton PA and Terlecky SR (2007) Restoration of peroxisomal catalase import in a model of human cellular aging. *Traffic (Copenhagen, Denmark)* **8**:1590-1600.

Lee SR, Kwon KS, Kim SR and Rhee SG (1998) Reversible inactivation of protein-tyrosine phosphatase 1B in A431 cells stimulated with epidermal growth factor. *The Journal of biological chemistry* **273**:15366-15372.

Legakis JE, Koepke JI, Jedeszko C, Barlaskar F, Terlecky LJ, Edwards HJ, Walton PA and Terlecky SR (2002) Peroxisome senescence in human fibroblasts. *Molecular biology of the cell* **13**:4243-4255.

Liou GY and Storz P (2010) Reactive oxygen species in cancer. *Free radical research* **44**:479-496.

Lo HW (2010) EGFR-targeted therapy in malignant glioma: novel aspects and mechanisms of drug resistance. *Current molecular pharmacology* **3**:37-52.

Mueller KL, Hunter LA, Ethier SP and Boerner JL (2008) Met and c-Src cooperate to compensate for loss of epidermal growth factor receptor kinase activity in breast cancer cells. *Cancer research* **68**:3314-3322.

Price M, Terlecky SR and Kessel D (2009) A role for hydrogen peroxide in the pro-apoptotic effects of photodynamic therapy. *Photochemistry and photobiology* **85**:1491-1496.

Spivak-Kroizman T, Rotin D, Pinchasi D, Ullrich A, Schlessinger J and Lax I (1992) Heterodimerization of c-erbB2 with different epidermal growth factor receptor mutants elicits stimulatory or inhibitory responses. *The Journal of biological chemistry* **267**:8056-8063.

Stover DR, Becker M, Liebetanz J and Lydon NB (1995) Src phosphorylation of the epidermal growth factor receptor at novel sites mediates receptor interaction with Src and P85 alpha. *The Journal of biological chemistry* **270**:15591-15597.

Tan AR, Yang X, Hewitt SM, Berman A, Lepper ER, Sparreboom A, Parr AL, Figg WD, Chow C, Steinberg SM, Bacharach SL, Whatley M, Carrasquillo JA, Brahim JS, Ettenberg SA, Lipkowitz S and Swain SM (2004) Evaluation of biologic end points and pharmacokinetics in patients with metastatic breast cancer after treatment with erlotinib, an epidermal growth factor receptor tyrosine kinase inhibitor. *Journal of clinical oncology : official journal of the American Society of Clinical Oncology* **22**:3080-3090.

Terlecky SR (2002) In vitro analysis of peroxisomal protein import. *Current protocols in cell biology / editorial board, Juan S Bonifacino [et al]* **Chapter 11**:Unit 11 15.

Terlecky SR and Koepke JI (2007) Drug delivery to peroxisomes: employing unique trafficking mechanisms to target protein therapeutics. *Advanced drug delivery reviews* **59**:739-747.

Terlecky SR, Legakis JE, Hueni SE and Subramani S (2001) Quantitative analysis of peroxisomal protein import in vitro. *Exp Cell Res* **263**:98-106.

Tonks NK (2006) Protein tyrosine phosphatases: from genes, to function, to disease. *Nature reviews Molecular cell biology* **7**:833-846.

Undyala V, Terlecky SR and Vander Heide RS (2011) Targeted intracellular catalase delivery protects neonatal rat myocytes from hypoxia-reoxygenation and ischemia-reperfusion injury. *Cardiovascular pathology : the official journal of the Society for Cardiovascular Pathology* **20**:272-280.

Wang SE, Narasanna A, Perez-Torres M, Xiang B, Wu FY, Yang S, Carpenter G, Gazdar AF, Muthuswamy SK and Arteaga CL (2006) HER2 kinase domain mutation results in constitutive phosphorylation and activation of HER2 and EGFR and resistance to EGFR tyrosine kinase inhibitors. *Cancer cell* **10**:25-38.

Wheeler DL, Dunn EF and Harari PM (2010) Understanding resistance to EGFR inhibitors-impact on future treatment strategies. *Nature reviews Clinical oncology* **7**:493-507.

Wood CS, Koepke JI, Teng H, Boucher KK, Katz S, Chang P, Terlecky LJ, Papanayotou I, Walton PA and Terlecky SR (2006) Hypocatalasemic fibroblasts accumulate hydrogen peroxide and display age-associated pathologies. *Traffic (Copenhagen, Denmark)* **7**:97-107.

Young CN, Koepke JI, Terlecky LJ, Borkin MS, Boyd Savoy L and Terlecky SR (2008) Reactive oxygen species in tumor necrosis factor-alpha-activated primary human keratinocytes: implications for psoriasis and inflammatory skin disease. *The Journal of investigative dermatology* **128**:2606-2614.

CHAPTER 3: **Towards peroxisome-targeted therapy for diabetic retinopathy**

3.1 Abstract

Preclinical studies have highlighted retinal oxidative stress in the pathogenesis of diabetic retinopathy. Here we evaluated whether or not a treatment designed to enhance peroxisomal catalase reduces oxidative stress in retinal cells cultured in high glucose and corrects early retinal pathophysiology as determined by a surrogate biomarker in diabetic mice. Human retinal Müller, pigment epithelial, and photoreceptor cells were chronically exposed to normal or high glucose levels and treated with a cell-penetrating derivative of the peroxisomal enzyme catalase (called CAT-SKL). H_2O_2 levels were measured using a quantitative fluorescence-based assay. For *in vivo* studies, streptozotocin (STZ)-induced diabetic C57Bl/6 mice were treated subcutaneously once a week for 4 months with CAT-SKL; untreated age-matched non-diabetic controls and untreated diabetic mice were also studied. Manganese-enhanced magnetic resonance imaging (MEMRI) was used to analytically assess the efficacy of CAT-SKL treatment on diabetes-evoked oxidative stress-related pathophysiology *in vivo*. Both Müller and retinal pigment epithelial cells (RPE) demonstrated an increase in high glucose-induced H_2O_2 production. After catalase transduction, peroxide production was significantly lowered in both lines. In contrast, the photoreceptors, a transformed line, showed no such induction of H_2O_2 in response to high glucose culture conditions, but did respond to the targeted antioxidant. In studies *in vivo*, CAT-SKL-treated diabetic mice had similar body weights and glycated hemoglobin levels as untreated diabetic mice; these metrics were different from those in controls. Subnormal intraretinal uptake

of manganese in the diabetic mice was improved by catalase supplementation. This proof-of-concept study sets the stage for future more thorough investigations involving augmentation of peroxisomal catalase as a potential therapy for diabetic retinopathy.

3.2 Introduction

Accumulating evidence supports diabetes-evoked retinal oxidative stress as a pathogenic factor in experimental diabetic retinopathy (Du et al., 2003; Kowluru et al., 2006a; Kowluru et al., 2006b; Kanwar et al., 2007). However, targeting such stress using conventional antioxidant treatment is complicated by the fact that ROS play a central role in a number of normal cellular activities including endomembrane signaling cascades, communication networks, and metabolic regulatory complexes (Lee et al., 2012). Here, we examine a new targeted approach to addressing these concerns that is focused on peroxisomes.

The peroxisome is a critical but understudied subcellular constituent that is involved in a number of important redox-based metabolic processes in the cell (Ivashchenko et al., 2011; Terlecky et al., 2012). These peroxisomal reactions are significant contributors to the oxidative load in aged cells and in several degenerative diseases - including diabetes (Giordano et al., 2012; Terlecky et al., 2012). Peroxisomal ROS accumulates for a number of reasons including, perhaps most importantly, mislocalization or impaired activity of catalase, its major resident antioxidant enzyme (Terlecky et al., 2006; Terlecky et al., 2012). Diabetes reduces whole retinal catalase levels, although a specific contribution from peroxisomes has not been extensively investigated (Zhang et al., 1996; Kowluru et al., 1997; Kocak et al., 2000; Obrosova et al., 2006; Sadi et al., 2008). The goal of this study was to begin to

determine if targeting peroxisomes with catalase supplementation could reduce oxidative stress in retinal cells exposed to high glucose conditions, and, if an *in vivo* biomarker sensitive to antioxidant treatment in diabetic models was also positively responsive to targeted catalase treatment. These initial studies were designed to set the stage for more extensive long term drug testing.

In this feasibility study, H_2O_2 levels were first evaluated in retinal (Müller, RPE, and photoreceptor) cell lines chronically exposed to high glucose levels and treated with CAT-SKL - a cell penetrating catalase derivative designed to traffic to peroxisomes ((as described above) and references therein). Next, we examined whether or not CAT-SKL might be useful *in vivo* using MEMRI, a non-invasive measurement of intraretinal uptake of manganese ion (Mn^{2+}, a strong MRI contrast agent) as an analytical biomarker for the extent of calcium ion inflow that occurs in the retina in awake and freely moving animals (Berkowitz et al., 2006; Berkowitz et al., 2008; Berkowitz et al., 2009b). In diabetic rats and mice, intraretinal uptake of manganese is subnormal well before the appearance of diabetes-evoked retinal histopathology (Berkowitz et al., 2007b; Berkowitz et al., 2009a; Berkowitz et al., 2012). Importantly, antioxidant therapies that correct these early MEMRI impairments also correct later diabetic retinopathy (Berkowitz et al., 2007b; Berkowitz et al., 2009a). For these reasons, we employed MEMRI to begin an analysis of CAT-SKL's *in vivo* efficacy.

3.3 Results

3.3.1 Cell culture

First we confirmed that CAT-SKL can enter retinal cells. Müller and RPE cell lines in normal and high glucose media conditions were treated with biotinylated CAT-

SKL for 0, 1, 2, and 4 hours. Transduction was observed within 1 hour of incubation (Figure 3.1A). To confirm transduced CAT-SKL increases peroxisomal catalase, the protein was measured in both Müller and RPE cells by SDS-PAGE and then immunoblotted for anti-catalase antibodies in the presence or absence of 1 μM CAT-SKL for 24 hours (Figure 3.1B and D). In addition, the activity of catalase was measured enzymatically showing a significant increase ($p<0.05$) in catalase activity when treated with 1 μM CAT-SKL for 24 hours (Figure 3.1C and E.) Both Müller and RPE cell lines cultured with chronically higher glucose concentrations (HG) demonstrated an increase in H_2O_2 levels compared to those cultured in normal glucose (NG) conditions (Figure 3.2A and 2B). Importantly, supplementing peroxisomal catalase with CAT-SKL was found to prevent supernormal peroxide buildup in both cell lines (Figure 3.2). Furthermore, enzymatically inactive CAT-SKL elicited no significant effect on cellular H_2O_2 levels (Figure 3.2A). Since RPE cells are normally polarized in the retina, culturing cells on a filtered transwell plate was employed to obtain a physical and metabolic state that is theoretically more closely aligned with the cells' normal physiological circumstance. Again, an increase in H_2O_2 was observed between NG and HG concentrations and CAT-SKL treatment in HG conditions reduced H_2O_2 levels back to approximately those seen in the NG condition (Figure 3.3A).

In contrast to RPE and Müller cells, when transformed photoreceptors were examined (Figure 3.3B), no induction in H_2O_2 between NG and HG cultured conditions was noted. Nonetheless, treatment with CAT-SKL significantly reduced H_2O_2 levels in a manner requiring the active recombinant enzyme (Figure 3.3B).

These results demonstrate that supplementing peroxisomal catalase can be an effective treatment for reducing levels of hyperglycemia-evoked H_2O_2 in retinal cells.

Figure 3.1A

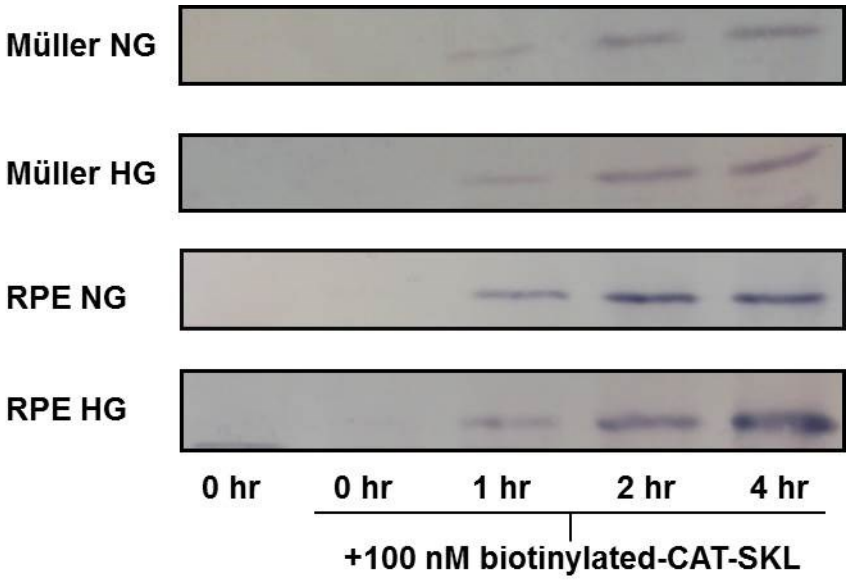

Figure 3.1 B

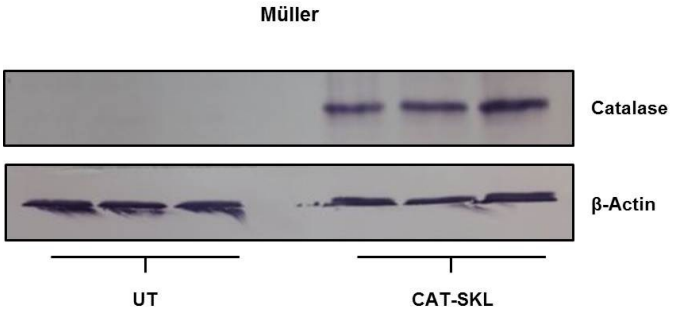

Figure 3.1C

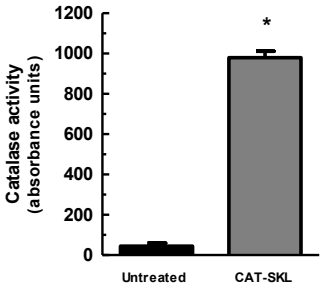

Figure 3.1 D

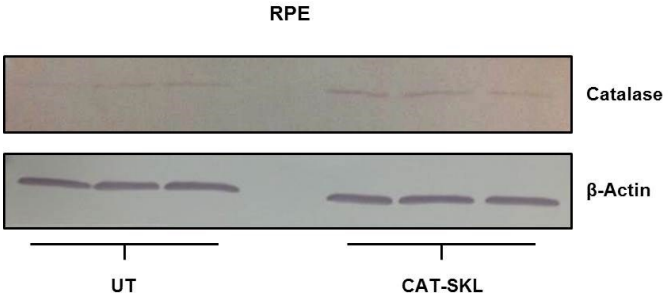

Figure 3.1E

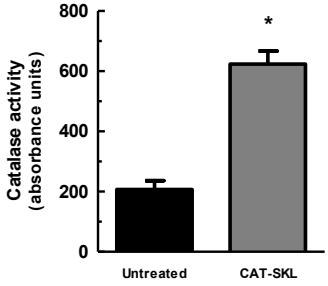

Figure 3.1. CAT-SKL transduction of retinal cells. (A) Müller and RPE cells were cultured in normal (5 mM) glucose (NG) or high (17.5 mM) glucose (HG) media as indicated. The cells were treated for 0, 1, 2, and 4 hours with biotinylated CAT-SKL (100 nM), washed, and harvested. Transduction was documented by blotting with streptavidin-alkaline phosphatase. Bands shown migrate at position expected for CAT-SKL. Müller (B,C.) and RPE (D,E.) cells were transduced with 1 μM CAT-SKL (indicated as "CAT-SKL") or without (indicated as "UT") for 24 hours, washed and harvested in PBS. Equal amounts of protein were separated by SDS-PAGE and probed with anti-catalase and anti-β-actin antibodies or catalase activity was measured enzymatically (* indicates $p<0.05$).

Figure 3.2A

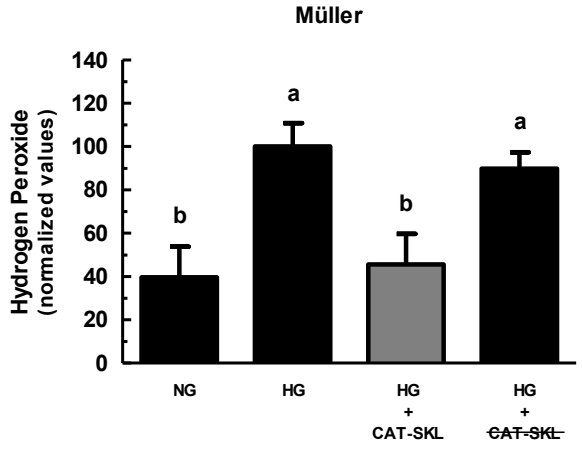

Figure 3.2B

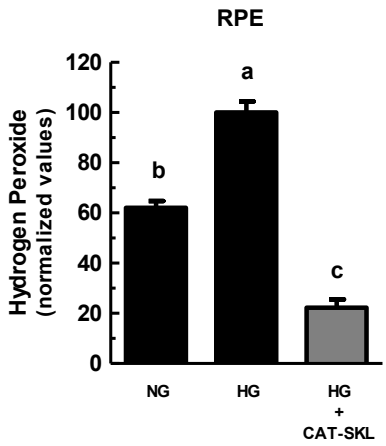

Figure 3.2. Enzymatically-active CAT-SKL reduces H2O2 levels in Müller and RPE cells. Müller (A) and RPE (B) cells were cultured over several passages in normal (5 mM) glucose (NG) or high (17.5 mM) glucose (HG) media. Replicate cultures of HG cells were then treated with 1 μM CAT-SKL for 24 hours as indicated. H_2O_2 levels was measured using the Amplex® Red reagent (10-acetyl-3,7-dihydroxyphenoxazine) assay kit. Results presented, means +/- one standard deviation of four or more samples, are normalized to the HG value (arbitrarily set at 100). In (A), cells were also transduced with 1 μM enzymatically-inactive (heat denatured) CAT-SKL (indicated as ~~CAT-SKL)~~. Bars represent mean ± SEM for triplicate samples. Means followed by the same letter are not significantly different according to Tukey's Multiple Comparison Test ($p>0.05$).

Figure 3.3A

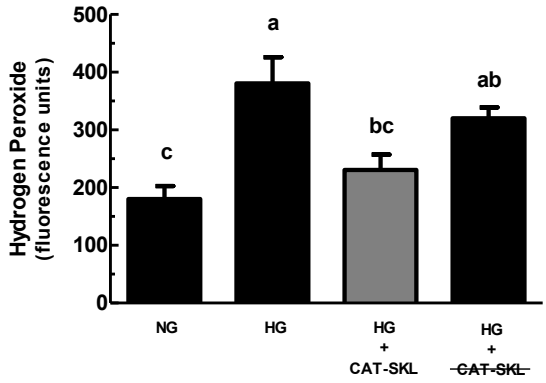

Figure 3.3B

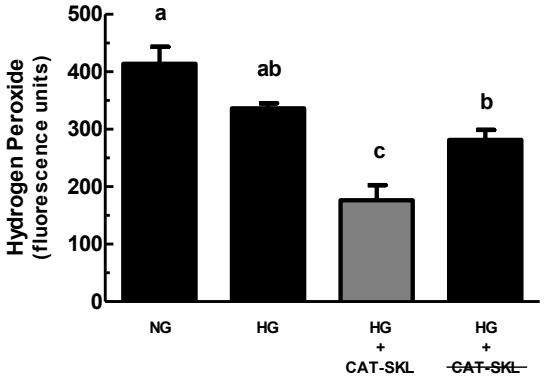

Figure 3.3. CAT-SKL's effects on polarized RPE and photoreceptor cells. Polarized RPE (A) and photoreceptor (B) cells were treated as in Figure 3.2 except that for the polarized RPE cells, H_2O_2 levels were measured in the basolateral receiving well. Bars represent mean ± SEM for quadruplicate samples. Means followed by the same letter are not significantly different according to Tukey's Multiple Comparison Test ($p>0.05$).

3.3.2 Model characteristics

Having established the usefulness of CAT-SKL as an effective antioxidant in retinal cells, we next began an investigation into its effectiveness *in vivo*. First we examined staining of the 70 kDa peroxisomal membrane protein (PMP70) in both control and diabetic mice. We have previously noted increased peroxisome numbers in aged, diseased or xenobiotic treated cells (Legakis et al., 2002; Wood et al., 2006; Koepke et al., 2008; Ivashchenko et al., 2011). Perhaps not unexpectedly, we found that in the diabetic animal's retina, PMP70 staining (red intensity) is substantially increased compared to their counterpart controls (Figure 3.4A and B). The reason for this induction is not clear – one explanation is that the disease state causes an alteration in regulating peroxisome growth and division, leading to increased growth of the organelle in the absence of normal cellular cues. Alternatively the organelle proliferates to compensate for mitochondrial deficits – recall the mitochondrial-peroxisomal interplay discussed above. Compromised degradation (pexophagy) in the diabetic retina may also be considered.

Glycated hemoglobin (A1c) was examined in all groups and as expected for the diabetic mouse model, the A1c range was lower ($p<0.05$) in age-matched non-diabetic controls (5.3 – 7.0%) as compared to either the non-treated diabetic animals (12.0 – 14.4%) or the treated diabetic mice (10.9 – 15.7%); no differences in A1c between diabetic groups were found ($p>0.05$). The range of body weights were also different between age-matched non-diabetic controls (30 – 36 g) and untreated (17 – 23 g) and treated (18 – 23 g) diabetic groups; again the two diabetic groups did not differ ($p>0.05$) in their final body weight.

Figure 3.4A and B

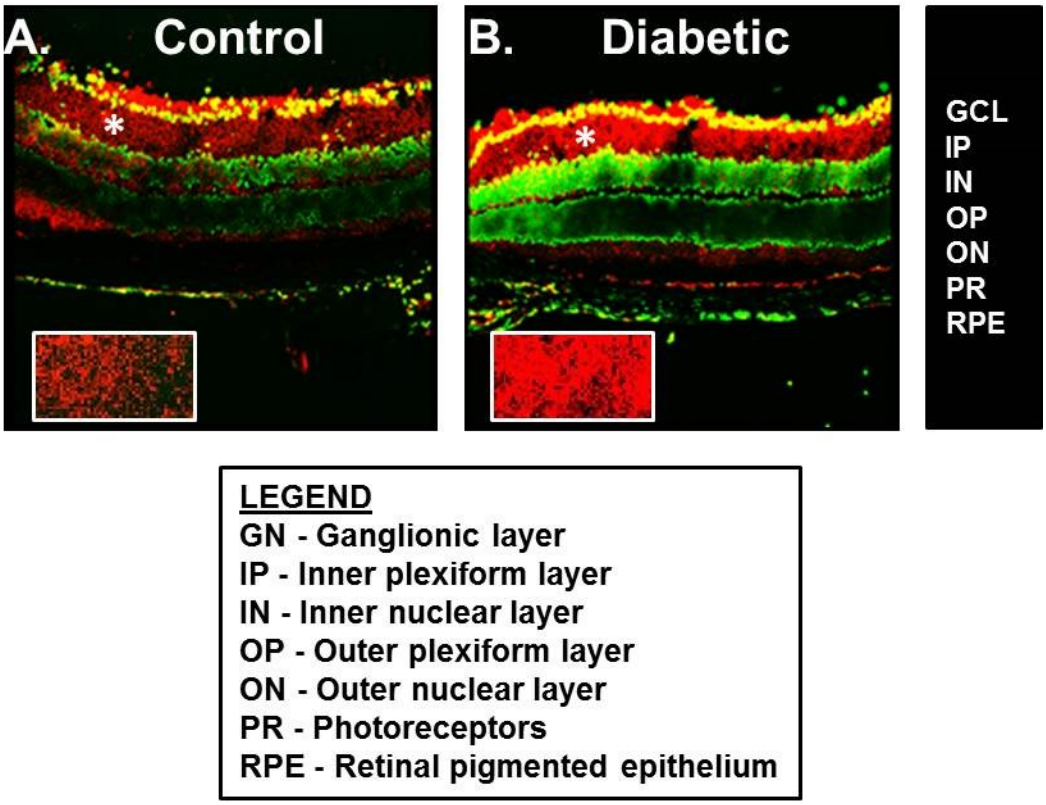

Figure 3.4. Peroxisomal staining in diabetic and control mouse retinas. Control (A) and diabetic (B) mouse retinas were stained with the peroxisomal membrane protein marker PMP70 (red) and SYTOX® Green Nucleic Acid Stain (green). Asterisks indicate area of inserts; higher magnifications of the inner plexiform layer of the retina showing increased peroxisomal staining in diabetic mice compared to control counterparts.

3.3.3 MEMRI

We next began to determine the effectiveness of CAT-SKL treatment *in vivo* using the previously established antioxidant-sensitive early diabetes-evoked metric: decreased intraretinal manganese uptake as measured by MEMRI (Berkowitz et al., 2007b; Berkowitz et al., 2009a). As summarized in Figure 3.5, CAT-SKL treatment significantly ($p<0.05$) improved uptake in both the inner and outer retina.

Figure 3.5

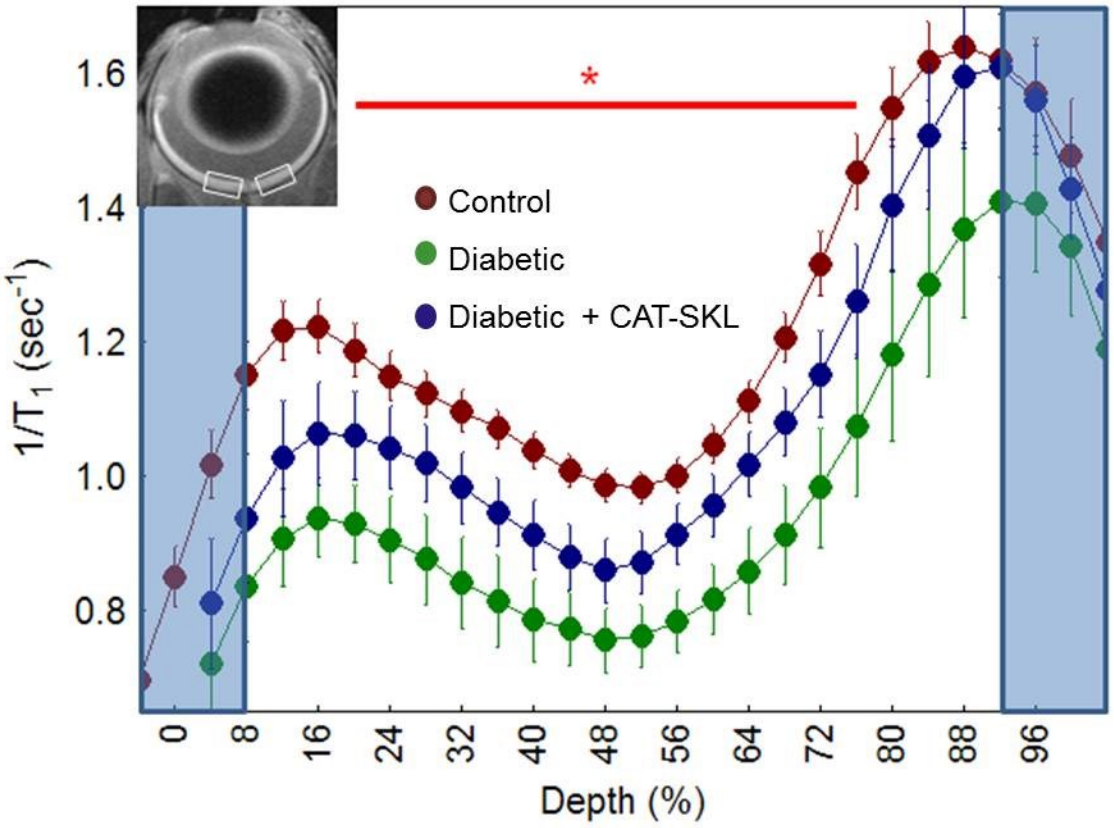

Figure 3.5. Manganese uptake in the retina of diabetic mice is partially corrected with the targeted antioxidant CAT-SKL. Data are shown as a function of distance from the retina/non-retina borders, where 0% is the vitreous/retina border and 100% is the retina/choroid border. Shaded regions near borders likely include some signal from outside of the retina and were not included in the analysis. White boxes outline central retinal regions analyzed. For those areas tested, * indicates common depths in untreated and treated diabetic groups that are significantly different Mn^{2+} in uptake from controls ($p<0.05$, two-tailed t-tests). Red line = control, blue line = diabetic + CAT-SKL, green line = diabetic. Experiments contributed by Giordano, CR along with Berkowitz BA.

3.4 Discussion

In this study, we found, for the first time, that treatment with a peroxisome-specific catalase molecule (CAT-SKL) significantly corrected hyperglycemia-induced oxidative stress in retinal cells as well as improved early ion channel dysregulation in diabetic retinopathy *in vivo*. The present studies take advantage of the recent availability of CAT-SKL to begin to test for a contribution of peroxisomal oxidative stress to diabetic retinopathy. It is now clear that retinal oxidative stress is a pathogenic factor in diabetic retinopathy, based, in part, on previous studies using a variety of non-specific/non-targeted antioxidants, all of which prevented the development of diabetic retinopathy (Kowluru et al., 1996; Kowluru et al., 1997; Kowluru et al., 2001; Kowluru et al., 2006b; Kanwar et al., 2007). Questions remain as to how antioxidants are best introduced into the retina with minimal perturbation of normal cellular functions involving brief and often continuous oxidative bursts on endomembrane signaling, inter- and intracellular communication networks, and coordinated metabolic regulation (Lee et al., 2012). The results in this study raise the possibility that targeting peroxisomal oxidative stress is a novel and effective treatment strategy for diabetic retinopathy.

This proof-of-concept study had some limitations. For example, we were unable to determine how effectively CAT-SKL reduced retinal oxidative stress in the diabetic mice. Furthermore, based on the incomplete correction of the diabetes-induced subnormal MEMRI retinal profiles - possibly because the dose employed was suboptimal, it is clear that additional, more thorough dose-response studies are warranted. We anticipate that once CAT-SKL's pharmacodynamics and pharmacokinetics are better defined, we will be able to further examine the impact of the

protein therapeutic on retinal ROS levels and catalase levels, as well as the actual development of diabetic retinopathy. Also, we did not examine the impact of CAT-SKL in non-diabetic controls *in vivo*. Collecting data from this control group would have informed about the drug's toxicity which is relevant in future studies but not necessary in this proof-of-concept phase.

These present results are in-line with our previous studies showing that MEMRI is a powerful and sensitive assay to document beneficial effects of antioxidant strategies designed to treat early diabetes-evoked retinal pathophysiology (Marmorstein et al., 2006; Berkowitz et al., 2007b; Lu et al., 2007; Berkowitz et al., 2009a). For example, we found that α-lipoic acid effectively reversed the subnormal intraretinal manganese uptake (measured by MEMRI) in diabetic mice (Berkowitz et al., 2007b). Furthermore, we showed that overexpression of the copper/zinc binding antioxidant, superoxide dismutase, dramatically impacted diabetes-induced early MEMRI lesions and later diabetic retinopathy (Berkowitz et al., 2009a). MEMRI is a non-invasive technique that measures retinal open / closed status of L-type voltage gated calcium ion channels, crucial components of intracellular communication (Drapeau and Nachshen, 1984; Carlson et al., 1994; Marmorstein et al., 2006; Berkowitz et al., 2007a; Cross et al., 2007; Lu et al., 2007; Berkowitz et al., 2011). While it is not yet clear how retinal oxidative stress (due to diabetes) leads to impaired intraretinal uptake on MEMRI, the current data, and those from our other studies, continue to underscore the usefulness of MEMRI as providing a sensitive surrogate for antioxidant efficacy.

The pathogenesis of diabetic retinopathy is not completely understood, although there is strong consensus that increased oxidative stress is a major contributor (Kowluru

et al., 1996; Kowluru et al., 1997; Kowluru et al., 2001; Kowluru et al., 2006b; Kanwar et al., 2007). There are several potential ways in which oxidative stress in diabetic mice could be generated including impaired activity of the major antioxidant defense enzymes, including catalase and/or superoxide dismutase (Kowluru et al., 1997; Obrosova et al., 2006). Also, because in this study we found improvements in both inner and outer retina, it is intriguing that the photoreceptor inner segments contain at least 60-65% of retinal mitochondria and are the primary retinal region that immunostains for catalase (and presumably peroxisomes) (Atalla et al., 1987). Perhaps improvements in outer retinal oxidative stress lead to downstream improvements in inner retina oxidative stress. To the best of our knowledge, treatment targeted to increasing peroxisomal catalase levels alone has not been investigated in diabetic retinopathy. The present findings raise the possibility that such highly specific supplementation of the powerful antioxidant enzyme will be useful in diabetic retinopathy.

3.5 Materials and Methods

All animals were treated in accordance with the National Institutes of Health Guide for the Care and Use of Laboratory Animals, the Association for Research in Vision and Ophthalmology Statement for the Use of Animals in Ophthalmic and Vision Research, and Institutional Animal and Care Use Committee authorization. Animals were housed and maintained in normal 12 h:12 h light-dark cycle laboratory lighting, unless otherwise noted.

Cell culture. Human retinal pigment epithelium (ARPE-19) cells were obtained from American Type Culture Collection (ATCC, Manassas, VA). Spontaneously immortalized human Müller cells (MIO-M1) were a gift from Dr. G. Astrid Limb and were maintained

as previously described (Shamsuddin and Kumar, 2011). Transformed 661W photoreceptor cells were grown and maintained as described previously (al-Ubaidi et al., 1992; Tan et al., 2004). The retinal cell lines were grown in Dulbecco's Modified Eagle Medium (DMEM) or Dulbecco's Modified Eagle Medium: Nutrient Mixture F-12 (DMEM:F12) with normal glucose (NG) (5 mM) or DMEM with high glucose (HG) (17.5 mM). Chronic normal or high glucose cells were acquired after 10 passages in media supplemented with either normal or high glucose concentrations.

CAT-SKL transduction. CAT-SKL was purified and characterized as previously described (Koepke et al., 2007; Young et al., 2008; Giordano et al., 2012). To track entry into cells, the molecule was biotinylated on primary amines (Koepke et al., 2007; Giordano et al., 2012). Cells were treated with biotinylated-CAT-SKL (100 nM) for 0, 1, 2, and 4 hours at which time they were harvested into sample buffer. Proteins were separated by SDS-PAGE and then transferred to a nitrocellulose membrane. The membrane was blocked using 5% non-fat milk and probed with streptavidin-alkaline phosphatase (diluted 1:1000). Reactive proteins were visualized with the NBT/BCIP 1-Step Solution (Thermo Scientific).

Catalase activity. Catalase enzymatic activity was determined by its ability to decompose H_2O_2 as described in (Storrie and Madden, 1990). Here, equal numbers of cells where added to 1 mg/ml BSA, 0.02 M imidazole (pH 7.0), 0.2% Triton-X 100, 0.06% H_2O_2 (prepared fresh) in PBS, and the reaction incubated at room temperature for 15 min. Titanium oxysulfate stop solution was then added and resultant absorbance at 405 nm was measured on a microplate reader. Catalase transduction of Müller and RPE cells was accomplished by treating cells (or not) with 1 μm CAT-SKL for 24 hours.

Confirmation of transduction was made by western blot analysis. Cells were harvested in PBS, equal amounts of protein were separated by SDS and transferred to a nitrocellulose membrane. Antibodies utilized included anti-catalase and anti-β-actin, diluted 1:4000 and 1:10000, respectively.

Measurement of H_2O_2. Müller, RPE, and photoreceptor cells were plated at 20,000 cells per well in 96-well plates and treated with or without 1 μM CAT-SKL for 24 hours at 37°C. Where indicated, heat inactivated CAT-SKL was prepared by boiling at 100°C for 3 min, cooling to room temperature, and resuspending as appropriate in cell culture media. For polarized RPE experiments, HTS Transwell-96 System, 0.4 μm polycarbonate membranes were utilized (Corning Incorporated, New York). Cells were plated at 6,000 cells per well and treated as described above except that oxidant measurements were performed on the conditioned media in the receiving well. H_2O_2 levels were determined using the Amplex® Red Hydrogen Peroxide/Peroxidase Assay Kit (Molecular Probes®) following the manufacturer's protocol. Briefly, cells were washed with Hank's balanced salt solution, treated with the Amplex® Red reagent (10-acetyl-3,7-dihydroxyphenoxazine)/horseradish peroxidase working solution and incubated for 2 hours at room temperature protected from light. Fluorescence units were obtained using a microplate reader (excitation 544 nm and emission 590 nm). Background fluorescence in wells containing media alone was subtracted from all data points.

Mice. At 2 months of age, 20 g male C57Bl/6 mice (Jackson Laboratories, Bar Harbor, ME) were randomly divided into the following groups: non-diabetic age-matched controls, diabetics, diabetics with treatments (diabetic + CAT-SKL).

Diabetes. Diabetes was induced in mice with starting weights of 16 to 20 g by streptozotocin (STZ), (60 mg/kg; 10 mM citrate buffer (pH 4.5) intraperitoneal injection, within 10 minutes of preparation, once a day for 5 consecutive days. Body weight and blood glucose levels were monitored twice weekly. Insulin (neutral protamine Hagedorn), administered to mice as needed based on bodyweight and blood glucose levels but not more than twice weekly, allowed slow weight gain while maintaining hyperglycemia (blood glucose levels higher than 400 mg/dl). Mice that lost weight and/or had blood glucose levels greater than 600 mg/dl were given 0.1 - 0.2 units of Lilly Humulin N insulin. Normal rodent chow (Purina TestDiet 5001; Richmond, IN, which contains 11.2% fat, 26% protein, and 62.7% carbohydrate) and water were provided *ad libitum*. Dehydrated animals were administered saline as needed. A1c was measured (Glyco-Tek affinity columns, kit 5351; Helena Laboratories, Beaumont, TX) from blood collected after each MEMRI experiment. Blood was drawn from the left ventricle, after puncture, into a capillary tube and stored in an Eppendorf tube with a small amount of heparin to prevent coagulation. The blood was kept at 4°C until analysis within one week following the MEMRI experiment.

CAT-SKL. A random subset of diabetic mice treated subcutaneously with CAT-SKL (1 mg/kg) weekly for 3 months, starting 1 week after initiation and confirmation of the diabetic state. Two treated diabetic mice had relatively low A1c values (8.6 and 8.9%) and were excluded from the final analysis. Note that the control and diabetic mice data had been reported in a previous study (Berkowitz et al., 2012). At the end of the 4-month study period, untreated controls (n = 7), diabetic animals (n = 7), and diabetic animals treated with CAT-SKL(n = 5) underwent MEMRI examination.

Immunohistochemical staining. Mouse retinas were fixed in 4% paraformaldehyde, 0.05 M L-lysine, and 0.01 M sodium periodate in 0.01 M phosphate buffer pH 7.4 for 5 minutes at room temperature. Permeabilization was performed using 0.05% Triton X-100 in phosphate buffered saline solution for 10 minutes in a moist chamber environment and then washed three times with 0.01 M phosphate buffer. Tissue was blocked with 1% BSA (Sigma-Aldrich) and 10% goat serum (Invitrogen) in 0.01 M phosphate buffer for 30 minutes to block unspecific binding of antibodies. Tissue was then incubated with rabbit anti-PMP70 (abcam) 1:500 for 1 hour at room temperature. Slides were washed three times with 0.01 M phosphate buffer and incubated with the secondary antibody Alexa Fluor 546 goat anti-rabbit (Molecular Probes) 1:1500 for 1 hour at room temperature covered from light. Slides were washed and incubated with SYTOX® GREEN nuclear label 1:150,000 for two minutes and rinsed with deionized water. Coverslips were mounted with VECTASHIELD (Vector Laboratories, Inc.). Microscopic analysis was performed using the Leica TCS SP2 confocal microscope located in the Department of Anatomy and Cell Biology's microscope facility at Wayne State University School of Medicine.

MEMRI. The methodologies for measuring MEMRI in mice has been described in detail previously (Berkowitz et al., 2012). Briefly, all animals were maintained in darkness for 16 to 20 hours before manganese injection. All procedures (i.e., weighing, injecting $MnCl_2$, anesthetic administration, and MRI examination) were performed under dim red light or darkness. $MnCl_2$ was administered as an intraperitoneal injection (66 mg $MnCl_2 \cdot 4H_2O$ / kg) on the right side of the awake animal. After this injection, animals were maintained in dark conditions for another 3.5 to 4 hours. Immediately before the

MRI experiment, animals were anesthetized with urethane (36% solution intraperitoneally; 0.083 ml/20 g animal weight, prepared fresh daily; Aldrich, Milwaukee, WI). MRI data were acquired on a 7T system (Clinscan). Retinal partial saturation T_1 data were acquired using a dual coil mode on a 7 T BrukerClinscan system: Several single spin-echo (time to echo [TE] 13 ms, 7 x 7 mm^2, matrix size 160×320, slice thickness 600 µm) images were acquired at different repetition times [TRs] in the following order (number per time between repetitions in parentheses): TR 0.15 s (6), 3.50 s (1), 1.00 s (2), 1.90 s (1), 0.35 s (4), 2.70 s (1), 0.25 s (5), and 0.50 s (3). To compensate for reduced signal-noise ratios at shorter TRs, progressively more images were collected as the TR decreased.

MRI analysis. MEMRI data of central retinal data (± 1 mm from the center of the optic nerve) were analyzed using the region-of-interest such as those highlighted in the top insert of Figure 3.5 for mice. The white region-of-interest indicates the part of central retina (including optic nerve (ON)) that was linearized for the control, untreated diabetic and treated diabetic (diabetic + CAT-SKL) groups. Quantitative analysis was as follows: single images acquired with the same TR were first registered (rigid body) and then averaged. These averaged images were then registered across TRs. The same regions-of-interest as above were analyzed by calculating $1/T_1$ maps by first fitting to a three-parameter T_1 equation (y=a + b*(exp(-c*TR)), where a, b, and c are fitted parameters) on a pixel-by-pixel basis using R (v.2.9.0, R Development Core Team [2009]). R: A language and environment for statistical computing. R Foundation for Statistical Computing. ISBN 3–900051–07–0) scripts developed in-house, and the minpack.lm package (v.1.1.1, Timur V. Elzhov and Katharine M. Mullen minpack.lm: R

interface to the Levenberg-Marquardt nonlinear least-squares algorithm found in MINPACK. R package version 1.1–1). The reciprocal ($1/T_1$) values directly reflect manganese levels. Central intraretinal $1/T_1$ profiles were obtained as detailed elsewhere (Bissig and Berkowitz, 2011). Values from the superior and inferior retina were averaged. Note that only those animals that took up manganese above baseline (i.e., ~0.6 s^{-1}) were included in the final analysis.

Statistical analysis. Drug-treated versus untreated cell culture H_2O_2 values were compared using student t-tests. Comparison of MEMRI data between groups were performed using individual t-tests at different locations of the intraretinal profiles. In all cases, $p<0.05$ was considered statistically significant.

3.6 References

al-Ubaidi MR, Font RL, Quiambao AB, Keener MJ, Liou GI, Overbeek PA and Baehr W (1992) Bilateral retinal and brain tumors in transgenic mice expressing simian virus 40 large T antigen under control of the human interphotoreceptor retinoid-binding protein promoter. *The Journal of cell biology* **119**:1681-1687.

Atalla L, Fernandez MA and Rao NA (1987) Immunohistochemical localization of catalase in ocular tissue. *Current eye research* **6**:1181-1187.

Berkowitz BA, Bissig D, Bergman D, Bercea E, Kasturi VK and Roberts R (2011) Intraretinal calcium channels and retinal morbidity in experimental retinopathy of prematurity. *Molecular vision* **17**:2516-2526.

Berkowitz BA, Bissig D, Patel P, Bhatia A and Roberts R (2012) Acute systemic 11-cis-retinal intervention improves abnormal outer retinal ion channel closure in diabetic mice. *Molecular vision* **18**:372-376.

Berkowitz BA, Gradianu M, Bissig D, Kern TS and Roberts R (2009a) Retinal ion regulation in a mouse model of diabetic retinopathy: natural history and the effect of Cu/Zn superoxide dismutase overexpression. *Investigative ophthalmology & visual science* **50**:2351-2358.

Berkowitz BA, Gradianu M, Schafer S, Jin Y, Porchia A, Iezzi R and Roberts R (2008) Ionic dysregulatory phenotyping of pathologic retinal thinning with manganese-enhanced MRI. *Investigative ophthalmology & visual science* **49**:3178-3184.

Berkowitz BA, Roberts R, Goebel DJ and Luan H (2006) Noninvasive and simultaneous imaging of layer-specific retinal functional adaptation by manganese-enhanced MRI. *Investigative ophthalmology & visual science* **47**:2668-2674.

Berkowitz BA, Roberts R, Oleske DA, Chang M, Schafer S, Bissig D and Gradianu M (2009b) Quantitative mapping of ion channel regulation by visual cycle activity in rodent photoreceptors in vivo. *Investigative ophthalmology & visual science* **50**:1880-1885.

Berkowitz BA, Roberts R, Penn JS and Gradianu M (2007a) High-resolution manganese-enhanced MRI of experimental retinopathy of prematurity. *Investigative ophthalmology & visual science* **48**:4733-4740.

Berkowitz BA, Roberts R, Stemmler A, Luan H and Gradianu M (2007b) Impaired apparent ion demand in experimental diabetic retinopathy: correction by lipoic Acid. *Investigative ophthalmology & visual science* **48**:4753-4758.

Bissig D and Berkowitz BA (2011) Same-session functional assessment of rat retina and brain with manganese-enhanced MRI. *NeuroImage* **58**:749-760.

Carlson RO, Masco D, Brooker G and Spiegel S (1994) Endogenous ganglioside GM1 modulates L-type calcium channel activity in N18 neuroblastoma cells. *The Journal of neuroscience : the official journal of the Society for Neuroscience* **14**:2272-2281.

Cross DJ, Flexman JA, Anzai Y, Sasaki T, Treuting PM, Maravilla KR and Minoshima S (2007) In vivo manganese MR imaging of calcium influx in spontaneous rat pituitary adenoma. *AJNR American journal of neuroradiology* **28**:1865-1871.

Drapeau P and Nachshen DA (1984) Manganese fluxes and manganese-dependent neurotransmitter release in presynaptic nerve endings isolated from rat brain. *The Journal of physiology* **348**:493-510.

Du Y, Miller CM and Kern TS (2003) Hyperglycemia increases mitochondrial superoxide in retina and retinal cells. *Free radical biology & medicine* **35**:1491-1499.

Giordano CR, Mueller KL, Terlecky LJ, Krentz KA, Bollig-Fischer A, Terlecky SR and Boerner JL (2012) A targeted enzyme approach to sensitization of tyrosine kinase inhibitor-resistant breast cancer cells. *Experimental Cell Research* **318**:2014-2021.

Ivashchenko O, Van Veldhoven PP, Brees C, Ho YS, Terlecky SR and Fransen M (2011) Intraperoxisomal redox balance in mammalian cells: oxidative stress and interorganellar cross-talk. *Molecular biology of the cell* **22**:1440-1451.

Kanwar M, Chan PS, Kern TS and Kowluru RA (2007) Oxidative damage in the retinal mitochondria of diabetic mice: possible protection by superoxide dismutase. *Investigative ophthalmology & visual science* **48**:3805-3811.

Kocak G, Aktan F, Canbolat O, Ozogul C, Elbeg S, Yildizoglu-Ari N and Karasu C (2000) Alpha-lipoic acid treatment ameliorates metabolic parameters, blood pressure, vascular reactivity and morphology of vessels already damaged by streptozotocin-diabetes. *Diabetes, nutrition & metabolism* **13**:308-318.

Koepke JI, Nakrieko KA, Wood CS, Boucher KK, Terlecky LJ, Walton PA and Terlecky SR (2007) Restoration of peroxisomal catalase import in a model of human cellular aging. *Traffic (Copenhagen, Denmark)* **8**:1590-1600.

Koepke JI, Wood CS, Terlecky LJ, Walton PA and Terlecky SR (2008) Progeric effects of catalase inactivation in human cells. *Toxicology and applied pharmacology* **232**:99-108.

Kowluru RA, Atasi L and Ho YS (2006a) Role of mitochondrial superoxide dismutase in the development of diabetic retinopathy. *Investigative ophthalmology & visual science* **47**:1594-1599.

Kowluru RA, Kern TS and Engerman RL (1997) Abnormalities of retinal metabolism in diabetes or experimental galactosemia. IV. Antioxidant defense system. *Free radical biology & medicine* **22**:587-592.

Kowluru RA, Kern TS, Engerman RL and Armstrong D (1996) Abnormalities of retinal metabolism in diabetes or experimental galactosemia. III. Effects of antioxidants. *Diabetes* **45**:1233-1237.

Kowluru RA, Kowluru V, Xiong Y and Ho YS (2006b) Overexpression of mitochondrial superoxide dismutase in mice protects the retina from diabetes-induced oxidative stress. *Free radical biology & medicine* **41**:1191-1196.

Kowluru RA, Tang J and Kern TS (2001) Abnormalities of retinal metabolism in diabetes and experimental galactosemia. VII. Effect of long-term administration of antioxidants on the development of retinopathy. *Diabetes* **50**:1938-1942.

Lee J, Giordano S and Zhang J (2012) Autophagy, mitochondria and oxidative stress: cross-talk and redox signalling. *The Biochemical journal* **441**:523-540.

Legakis JE, Koepke JI, Jedeszko C, Barlaskar F, Terlecky LJ, Edwards HJ, Walton PA and Terlecky SR (2002) Peroxisome senescence in human fibroblasts. *Molecular biology of the cell* **13**:4243-4255.

Lu H, Xi ZX, Gitajn L, Rea W, Yang Y and Stein EA (2007) Cocaine-induced brain activation detected by dynamic manganese-enhanced magnetic resonance

imaging (MEMRI). *Proceedings of the National Academy of Sciences of the United States of America* **104**:2489-2494.

Marmorstein LY, Wu J, McLaughlin P, Yocom J, Karl MO, Neussert R, Wimmers S, Stanton JB, Gregg RG, Strauss O, Peachey NS and Marmorstein AD (2006) The light peak of the electroretinogram is dependent on voltage-gated calcium channels and antagonized by bestrophin (best-1). *The Journal of general physiology* **127**:577-589.

Obrosova IG, Drel VR, Kumagai AK, Szabo C, Pacher P and Stevens MJ (2006) Early diabetes-induced biochemical changes in the retina: comparison of rat and mouse models. *Diabetologia* **49**:2525-2533.

Sadi G, Yilmaz O and Guray T (2008) Effect of vitamin C and lipoic acid on streptozotocin-induced diabetes gene expression: mRNA and protein expressions of Cu-Zn SOD and catalase. *Molecular and cellular biochemistry* **309**:109-116.

Shamsuddin N and Kumar A (2011) TLR2 mediates the innate response of retinal Muller glia to Staphylococcus aureus. *Journal of immunology* **186**:7089-7097.

Storrie B and Madden EA (1990) Isolation of subcellular organelles. *Methods in enzymology* **182**:203-225.

Tan E, Ding XQ, Saadi A, Agarwal N, Naash MI and Al-Ubaidi MR (2004) Expression of cone-photoreceptor-specific antigens in a cell line derived from retinal tumors in transgenic mice. *Investigative ophthalmology & visual science* **45**:764-768.

Terlecky SR, Koepke JI and Walton PA (2006) Peroxisomes and aging. *Biochimica et biophysica acta* **1763**:1749-1754.

Terlecky SR, Terlecky LJ and Giordano CR (2012) Peroxisomes, oxidative stress, and inflammation. *World journal of biological chemistry* **3**:93-97.

Wood CS, Koepke JI, Teng H, Boucher KK, Katz S, Chang P, Terlecky LJ, Papanayotou I, Walton PA and Terlecky SR (2006) Hypocatalasemic fibroblasts accumulate hydrogen peroxide and display age-associated pathologies. *Traffic (Copenhagen, Denmark)* **7**:97-107.

Young CN, Koepke JI, Terlecky LJ, Borkin MS, Boyd Savoy L and Terlecky SR (2008) Reactive oxygen species in tumor necrosis factor-alpha-activated primary human keratinocytes: implications for psoriasis and inflammatory skin disease. *The Journal of investigative dermatology* **128**:2606-2614.

Zhang H, Agardh CD and Agardh E (1996) Retinal nitro blue tetrazolium staining and catalase activity in rat models of diabetes. *Graefe's archive for clinical and experimental ophthalmology = Albrecht von Graefes Archiv fur klinische und experimentelle Ophthalmologie* **234**:324-330.

CHAPTER 4: Amyloid-beta neuroprotection mediated by a targeted antioxidant

Publilshed: **Giordano CR**, Terlecky LJ, Bollig-Fischer A, Walton PA, and Terlecky SR (2014) *Scientific Reports* **4**:4983.

4.1 Abstract

Amyloid-beta (Aβ)-induced neurotoxicity is a major contributor to the pathologies associated with Alzheimer's disease (AD). The formation of ROS, an early response induced by the peptide and oligomeric derivatives of Aβ, plays a significant role in effecting cellular pathogenesis. Here we employ particularly toxic forms of Aβ with cultured primary cortical/hippocampal neurons to elicit ROS and drive cellular dysfunction. To prevent and even reverse such effects, we utilized a cell-penetrating, peroxisome-targeted, protein biologic – called CAT-SKL. We show the recombinant enzyme enters neurons, reverses Aβ-induced oxidative stress, and increases cell viability. Dramatic restorative effects on damaged neuronal processes were also observed. In addition, we used DNA microarrays to determine Aβ's effects on gene expression in neurons, as well as the ability of CAT-SKL to modify such Aβ-induced expression profiles. Our results suggest that CAT-SKL, a targeted antioxidant, may represent a new therapeutic approach for treatment of disorders, like Alzheimer's disease, that are driven through oxidative stress. Preclinical testing is ongoing.

4.2 Introduction

AD is a progressive neurodegenerative disorder caused by multiple conspiring pathologies including misprocessing of the amyloid precursor protein (to Aβ peptide and related higher order structures); tau phosphorylation, relocalization, and deposition; activity of presenilins and the effects of specific ε4 alleles of apolipoprotein E; α

synuclein/Lewey body accumulation; and is potentiated by the effects of aging (Selkoe, 2011; Holtzman et al., 2012; Huang and Mucke, 2012). Thus, a barrage of anti-proteostatic effects are brought to bear on neurons, with devastating consequences.

In this report, we concentrate on the neurocompromising effects of Aβ peptides, molecules thought to trigger a cascade of early neuropathogenic activities. In particular, we focus on soluble forms of the toxic Aβ-peptide, called amyloid β-derived diffusible ligands - or ADDLs(Klein, 2002). These Aβ-derivatives are thought to interact with specific cell surface receptors to trigger ROS formation and associated downstream cytotoxic effects(Klein, 2002). Indeed, ADDLs may initiate a self-perpetuating spiral of toxic Aβ-formation/deposition, and cell pathology (Saraiva et al., 2012).

To confer neuroprotection in our culture model, we targeted the response arm of Aβ-toxicity; specifically the formation of ROS. This was accomplished in a manner distinct from previously employed (and failed (Petersen et al., 2005; Brewer, 2010; Polidori and Nelles, 2013; Persson et al., 2014)) approaches of flooding cells with non-targeted antioxidants. It is becoming well understood that cells employ ROS as effectors of signaling, communication and metabolic regulatory networks, and that these molecules cannot be indiscriminately quenched (Droge, 2002; Hsieh and Yang, 2013). Our approach is to target a powerful antioxidant, in this case catalase(Chance, 1948; Vainshtein et al., 1981), to the peroxisome where an accumulating literature suggests the enzyme maintains and/or reestablishes oxidative balance without side-effects. To accomplish this, we employed CAT-SKL, a genetically engineered recombinant derivative of catalase containing a cell penetrating peptide at its amino terminus and an altered, more efficient peroxisomal targeting signal at its carboxy terminus. The results

with CAT-SKL have been dramatic in a number of cellular and preclinical settings (Young et al., 2008; Price et al., 2009; Undyala et al., 2011; Giordano et al., 2012; Giordano and Terlecky, 2012). Here the targeted catalase molecule was able to protect rat primary cortical/hippocampal cultures from ADDL-induced cytotoxicity as manifest by effects on ROS production, gene expression, neurite formation, and overall cell viability.

4.3 Results

4.3.1 ADDL characterization and toxicity.

Freshly prepared ADDLs were characterized to document the nature of the oligomeric species created. The Aβ peptide used to generate ADDLs is 42 amino acids (~4.5 kDa). A gel filtration column was prepared with G-50 Sephadex beads, a sizing column that excludes proteins greater than 30 kDa. Sample fractions of ADDLs were collected and compared to the behavior of 67 kDa and 1.4 kDa control polypeptides. The prepared ADDLs were confirmed to be mainly larger oligomeric species, displaying an excluded migration pattern similar to the 67 kDa protein (Fig. 4.1A). Therefore, in our hands, ADDLs contain largely oligomeric assemblies of Aβ – consistent with the results reported by others (Lue et al., 1999; McLean et al., 1999; Wang et al., 1999; Klein, 2002). Soluble forms of Aβ accumulate in the human brain and are thought to cause the functional deficits that precede neuronal death. Indeed, these ADDLs are considered to be a major driver of the early stages and progression of AD. To determine if freshly prepared ADDLs were toxic to primary neuronal cultures, several concentrations of the oligomeric peptide were added to cells. The cells employed were embryonic day 18 Sprague Dawley rat cortical/hippocampal neurons. Cells were harvested from fresh brain tissue, plated, and differentiated as described in the

methods. After 7 days of differentiation, the neurons displayed axons and dendrites, and are known to form synapses and conduct action potentials(Brewer et al., 1993; Brewer and Price, 1996). Our neuronal cultures stained positive for the dendritic marker, MAP-2, (see Fig. 4.4 below) and the axonal marker, neurofilament-68 (data not shown).

Cellular mitochondrial dehydrogenase activity was measured by absorbance spectroscopy to determine cellular viability after treatment with ADDLs at 0.1, 1, and 10 μM for 24 hours (Fig. 4.1B). Compared to untreated neurons, 1 and 10 μM ADDLs significantly reduced metabolic activity as indicated by the decrease in formazan dye formed ($p<0.05$), thus confirming toxicity of the ADDL preparations to neurons as previously reported (Klein, 2002). Metastable intermediates of insoluble Aβ fibrils, called protofibrils were also prepared for this study but showed no toxicity compared to a vehicle control (Fig. 4.1B); further strengthening the notion that soluble oligomers of Aβ are the more harmful state of the peptide.

As introduced above, Aβ induces ROS production in cells of the brain. Here, we specifically measured H_2O_2 in primary neuronal cultures and found that addition of 1 μM ADDLs for 24 hours significantly increased levels of ROS ($p<0.05$) (Fig. 4.1C). An unrelated peptide had no such effects (Fig. 4.1C).

Figure 4.1A

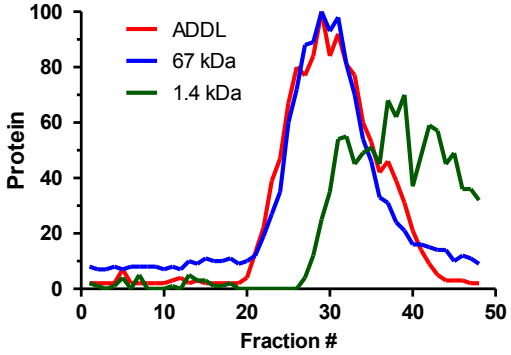

Figure 4.1B

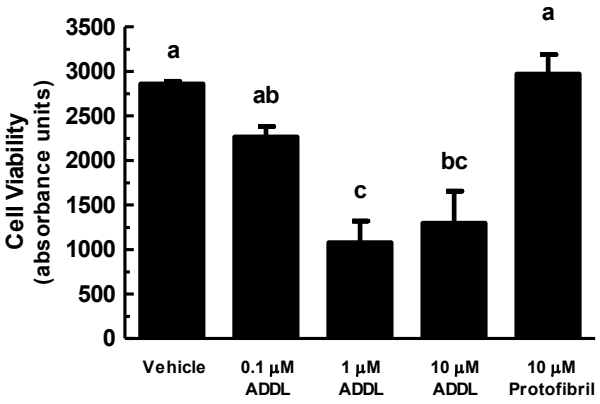

Figure 4.1C

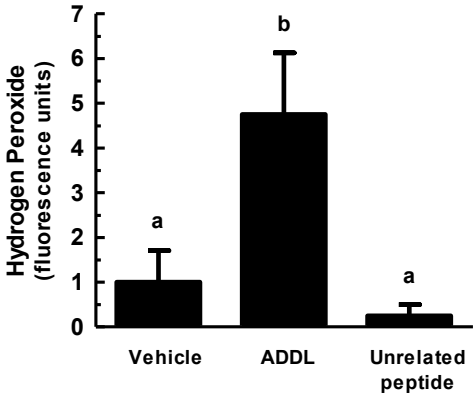

Figure 4.1. ADDL-induced toxicity in primary cortical/hippocampal neurons. (A) ADDLs were subjected to gel filtration (using Sephadex G-50 beads) to characterize their sizing behavior. Any molecule greater than 30 kDa is excluded from the column (~fraction 20). Red line = ADDLs, blue line = 67 kDa protein, and green line = 1.4 kDa peptide. Y-axis is normalized protein intensity as quantified by Image J software. (B) Primary rat cortical/hippocampal cultures were treated with ADDLs (0.1, 1, and 10 µM), and protofibrils (10 µM) as indicated, for 24 hours. Cell viability was determined using the water soluble tetrazolium cell proliferation assay (WST-1). Bars represent mean ± SEM for triplicate samples. Means followed by the same letter are not significantly different according to Tukey's Multiple Comparison Test ($p>0.05$). (C) Hydrogen peroxide production was measured using the Amplex® Red reagent (10-acetyl-3,7-dihydroxyphenoxazine). ADDLs (1 µM for 24 hours) induced hydrogen peroxide production in primary rat cortical/hippocampal neurons. Statistical analysis was performed using one-way analysis of variance (ANOVA). When ANOVA indicated significant treatment effects, means were separated using Tukey's Multiple Comparison Test. Bars represent mean ± SEM for quadruplicate samples. Means followed by the same letter are not significantly different ($p>0.05$). Similar results were seen in three additional experiments.

4.3.2 CAT-SKL transducibility.

We utilized CAT-SKL, which has been shown to robustly metabolize H_2O_2 within the peroxisome and other cellular compartments, and restore oxidative equilibrium within cells (Koepke et al., 2007; Young et al., 2008; Price et al., 2009; Undyala et al., 2011; Giordano et al., 2012), to determine the role of H_2O_2 and related ROS in ADDL-induced neurotoxicity. Transduction of the targeted antioxidant has been documented in a number of cell types, with entry confirmed within 1 hour of addition (Giordano et al., 2012). To demonstrate transduction of CAT-SKL in neurons, we tracked cell entry of a biotinylated form of the recombinant enzyme (Fig. 4.2A). Immunofluorescence analysis confirmed catalase staining was significantly increased in CAT-SKL treated neurons compared to vehicle or a non-transducible form of the recombinant enzyme (Fig. 4.2B). Similar transduction results were obtained in live cells with a CAT-SKL molecule covalently conjugated to red fluorescent spheres (Supplementary figure a4.1A), ruling out potential artefactual fixation anomalies. Importantly, CAT-SKL - FluoSpheres® was enzymatically active – confirming no loss of quaternary structure for the obligate tetramer (Supplementary figure a4.1B). As expected, catalase activity and immunoreactivity were increased in CAT-SKL-treated neuronal cultures after a 24 hour incubation (Fig. 2C,D).

Figure 4.2A

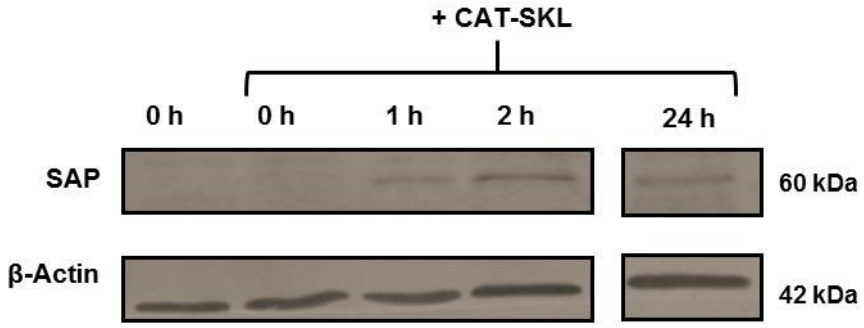

Figure 4.2B

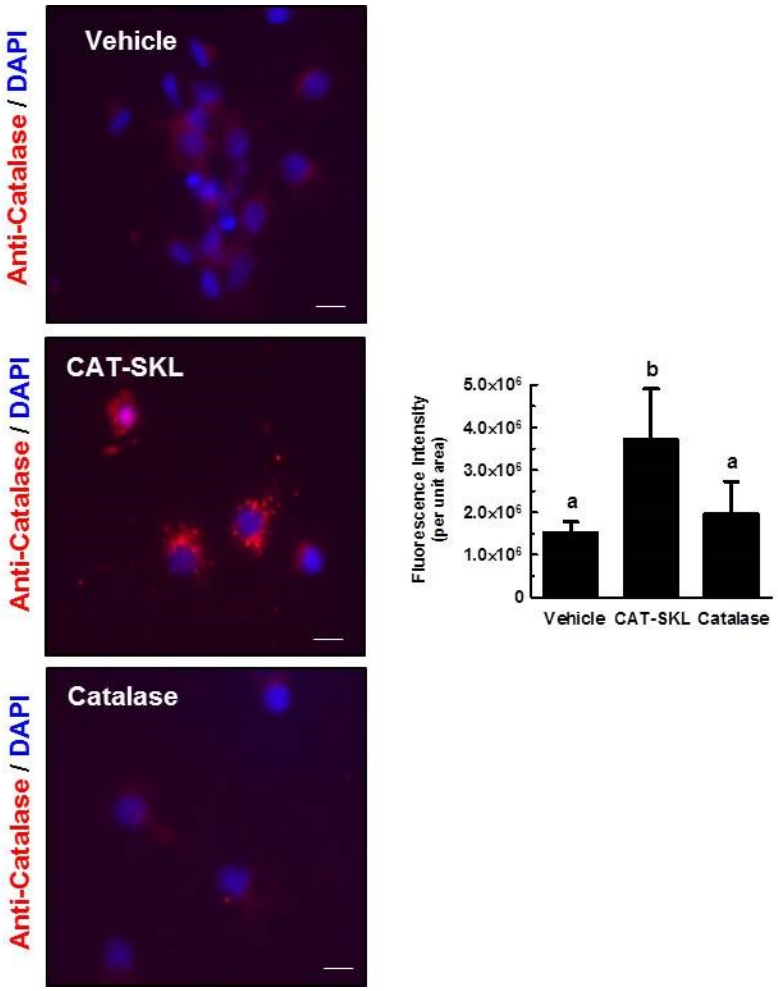

Figure 4.2C

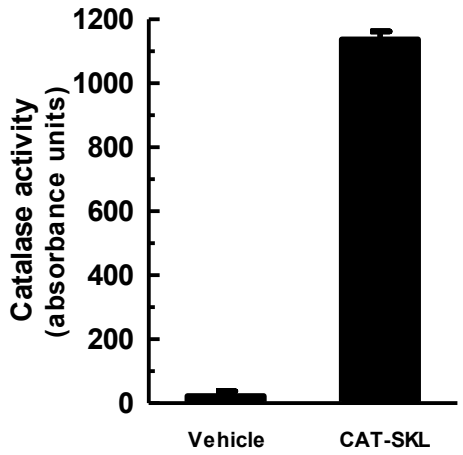

Figure 4.2D

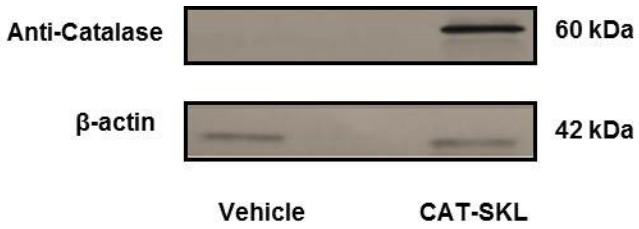

Figure 4.2. CAT-SKL transduction of primary cortical/hippocampal neurons. (A) Primary rat cortical/hippocampal neurons were treated with 100 nM biotinylated CAT-SKL for 0, 1, 2, and 24 hours, washed, and harvested in sample buffer. Transduction was demonstrated by probing cell extracts with streptavidin alkaline phosphatase (SAP). β-actin was used as a loading control. Results shown are from same probed blot. Full-length blots are presented in Supplementary Figure 2a. (B) Cells were treated with vehicle, 1 μM CAT-SKL, or 1 μM catalase for 24 hours. Cells were then washed, fixed, and immunostained for catalase (red fluorescence) and 4',6-diamidino-2-phenylindole (DAPI) (blue fluorescence). Statistical analysis was performed using one-way ANOVA. When ANOVA indicated significant treatment effects, means were separated using Tukey's Multiple Comparison Test. Bars represent mean ± SEM for replicate samples (n=8). Means followed by the same letter are not significantly different ($p>0.05$). Scale bar = 20 μm. Catalase enzymatic activity (C) and immunoreactivity (D) was measured after 24 hour treatment with 1 μM CAT-SKL or without (indicated as vehicle). Cells were washed, harvested in PBS, and equal amounts of protein were separated by SDS-PAGE. Antibodies utilized include anti-catalase and anti-β-actin (n=3).

4.3.3 Neuroprotective effects of CAT-SKL.

We next examined the protective effects of CAT-SKL against ADDL-induced neuronal toxicity. To accomplish this, cellular mitochondrial dehydrogenase activity was measured by absorbance spectroscopy to determine cell viability in neurons pretreated with 1 μM CAT-SKL and subsequently challenged with 1 μM ADDLs. Pretreatment with CAT-SKL exhibited a protective effect against ADDLs as evidenced by an increase in cell viability (Fig. 4.3A). Likewise the peroxisomal proliferator Wy-14,643, which previously has been shown to increase endogenous catalase levels (Santos et al., 2005; Inestrosa et al., 2013), also is protective when added prior to ADDL challenge (Fig. 4.3B). Furthermore, pretreatment with 1 μM CAT-SKL and/or 100 μM Wy-14,643 also reduced ADDL-induced H_2O_2 levels (Fig. 4.3C).

Fluorescence microscopy was employed to extend our quantitative biochemical results. Here, primary neuronal cultures were stained for microtubule associated protein-2 (MAP-2), a dendritic marker. Compared to a vehicle control (Fig. 4.4A), 1 μM ADDLs triggered a retraction in dendritic arborization (branching of dendrites), which resulted in decreased cell body clustering (Fig. 4.4B). Importantly, CAT-SKL added before or after ADDL treatment protected against these effects (Fig. 4.4C,D). Similar effects on dendrites were observed with the peroxisome proliferator Wy-14,643 (data not shown).

Figure 4.3A

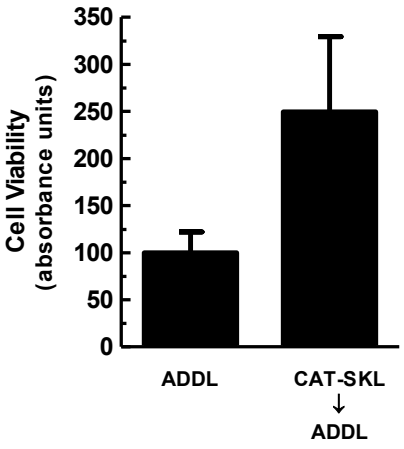

Figure 4.3B

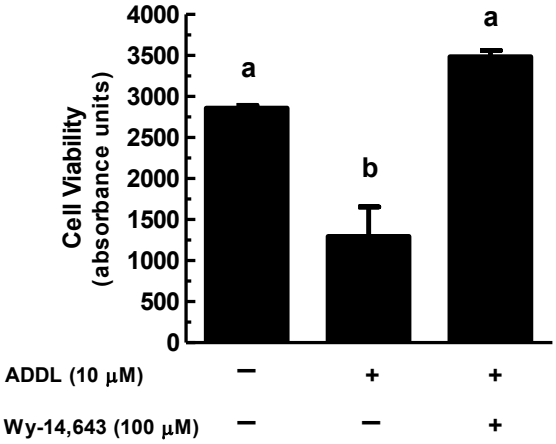

Figure 4.3C

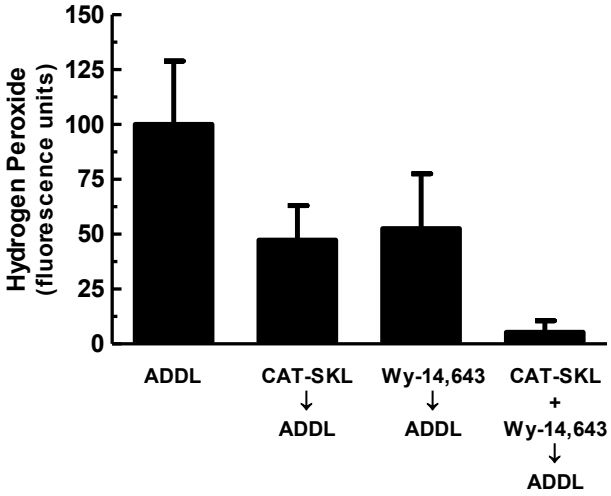

Figure 4.3. Neuroprotective effects of CAT-SKL against ADDL-induced neurotoxicity. (A) Primary rat cortical/hippocampal neurons were pretreated with CAT-SKL (1 μM) for 24 hours and subsequently challenged with ADDLs (1 μM) for 24 hours. (B) Cells were pretreated with the peroxisomal proliferator Wy-14,643 (100 μM) for 48 hours and then challenged with ADDLs (10 μM) for an additional 24 hours. Cell viability was determined using the water soluble tetrazolium cell proliferation assay (WST-1). Statistical analysis was performed using one-way ANOVA. When ANOVA indicated significant treatment effects, means were separated using Tukey's Multiple Comparison Test. Bars represent mean ± SEM for triplicate samples. Means followed by the same letter are not significantly different ($p>0.05$). (C) Neurons were pretreated with CAT-SKL (1 μM) for 24 hours and/or Wy-14,643 (100 μM) for 48 hours. Amount of H_2O_2 produced in cells was determined by the Amplex® Red reagent (10-acetyl-3,7-dihydroxy-phenoxazine) (n=4). Similar results were seen in three additional experiments.

Figure 4.4A-D

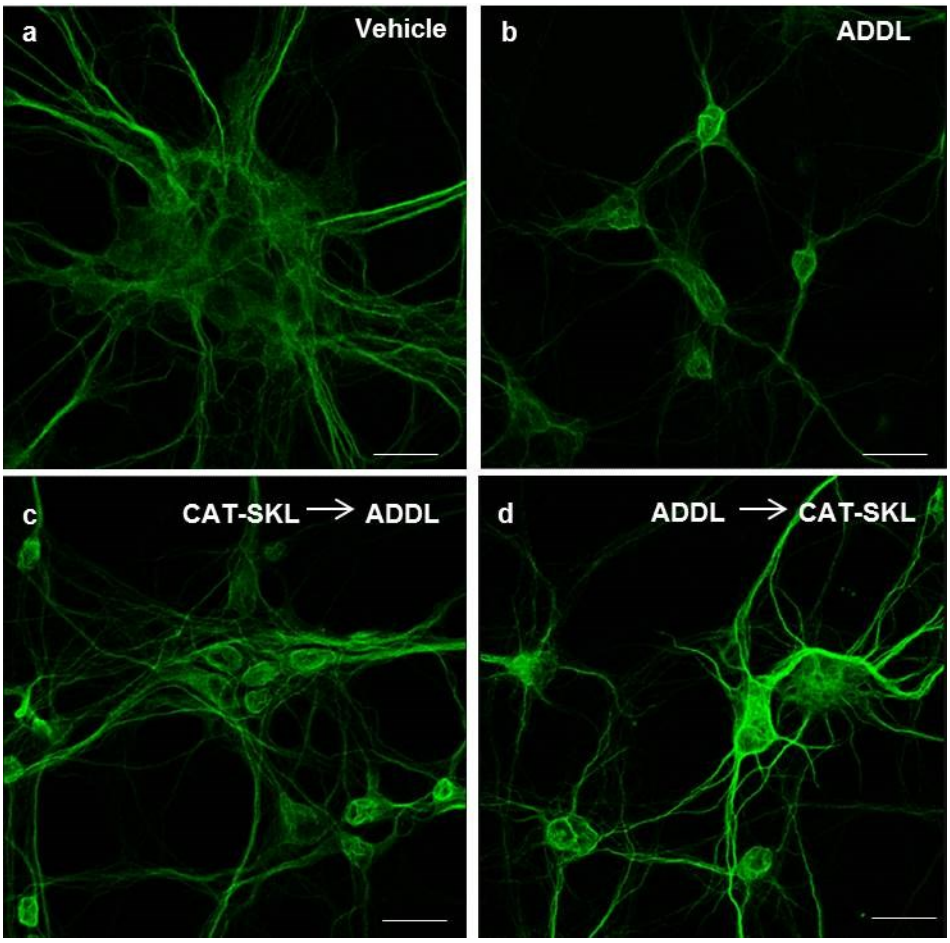

Figure 4.4. Effects of CAT-SKL on ADDL-induced neurite degeneration in primary rat cortical/hippocampal neurons. Primary rat cortical/hippocampal neurons were treated as follows: (A) Vehicle control for 24 hours. (B) ADDLs (1 μM) for 24 hours. (C) CAT-SKL (1 μM) for 24 hours, followed by ADDLs (1 μM) for 24 hours. (D) ADDLs (1 μM) for 24 hours, followed by CAT-SKL (1 μM) for 24 hours. Neurons were immunostained with anti-MAP-2 antibodies (a dendritic marker), and visualized with AlexaFluor 488-goat anti-mouse antibodies (green fluorescence). Scale bar = 20 μm.

Primary neuronal cultures were also stained for PMP70, a peroxisomal membrane protein. Since CAT-SKL resides in the peroxisome and alters its oxidative environment, we hypothesized that there would be an effect on peroxisome number or morphology between treatments. We have previously reported peroxisomal proliferation in aged, diseased, or xenobiotic-treated cells(Legakis et al., 2002; Wood et al., 2006; Koepke et al., 2008; Ivashchenko et al., 2011). The molecular basis for this induction is unclear; we have speculated that it happens to compensate for compromised peroxisome functioning or to assist mitochondria in metabolizing pathological levels of ROS (Giordano and Terlecky, 2012). Alternatively, rates of pexophagy may be compromised (Huybrechts et al., 2009). Here, in neurons, we find that ADDLs also triggered significant increases in peroxisomal numbers, evident both within cell processes and cell bodies (Fig. 5a,b) ($p<0.05$). Importantly, pre-and post-treatments with CAT-SKL significantly reversed these changes, resulting in peroxisomal staining more akin to that seen in untreated cells (Fig. 5c,d) ($p<0.05$).

4.3.4 CAT-SKL and ADDL-induced mitochondrial impairment.

Mitochondria and peroxisomes may share a redox-based dynamic relationship whereby changes in oxidant handling or overall function of one organelle, impacts the structural and functional integrity of the other(Koepke et al., 2007; Koepke et al., 2008; Ivashchenko et al., 2011; Walton and Pizzitelli, 2012; Wang et al., 2013). For example, if the ability of peroxisomes to metabolize H_2O_2 is abrogated, mitochondria depolarize and begin producing ROS themselves (Koepke et al., 2007; Koepke et al., 2008; Ivashchenko et al., 2011; Walton and Pizzitelli, 2012). In contrast, if peroxisomal

antioxidant capacity is enhanced, mitochondria repolarize and reduce oxidant production (Koepke et al., 2007).

In our culture studies, ADDLs cause neuronal mitochondria ROS production and depolarization (Fig. 6). The former is seen as an increase in red fluorescence emitted by a mitochondrial ROS-sensitive dye; the latter by an increase in the monomeric (green fluorescence) form of the JC-1 dye. Importantly, CAT-SKL significantly reversed these effects if supplied after ADDL treatment; or prevented them if provided prophylactically ($p<0.05$) (Fig. 6).

4.3.5 ADDLs, CAT-SKL, and glutathione S-transferase.

DNA microarray experiments were performed to determine the gene expression profiles of cells treated with ADDLs, CAT-SKL or CAT-SKL → ADDLs, as compared to untreated (control) cells. Importantly, 79 genes showing significant expression level changes were in common between treatments (see Venn diagram – Fig. 7a). Mining of functional association pathways with Ingenuity Systems' Pathway Analysis software highlighted glutathione S-transferase (GST), a critical cellular detoxifying enzyme, among genes specifically altered by the treatments. Furthermore, upstream regulatory analysis predicted that the specific isoform, GSTπ, was inactivated by ADDLs (Fig. 7b). This analysis, which was implemented using Ingenuity Systems software, can predict transcription factors involved in the gene expression changes observed in the data sets, and whether or not they are activated or inhibited. GST was investigated further because of the dramatically reduced levels in post-mortem brains of AD patients (Lovell et al., 1998).

Western blotting of ADDL-treated neurons revealed GSTπ levels to be reduced (Fig. 7c). However, the effects of ADDL treatment on GSTπ were reversed when CAT-SKL was present, either before or after ADDL treatment (Fig. 7d). A heat inactivated form of CAT-SKL had no such effects on restoring GSTπ levels (Fig. 7d).

Figure 4.5A-D

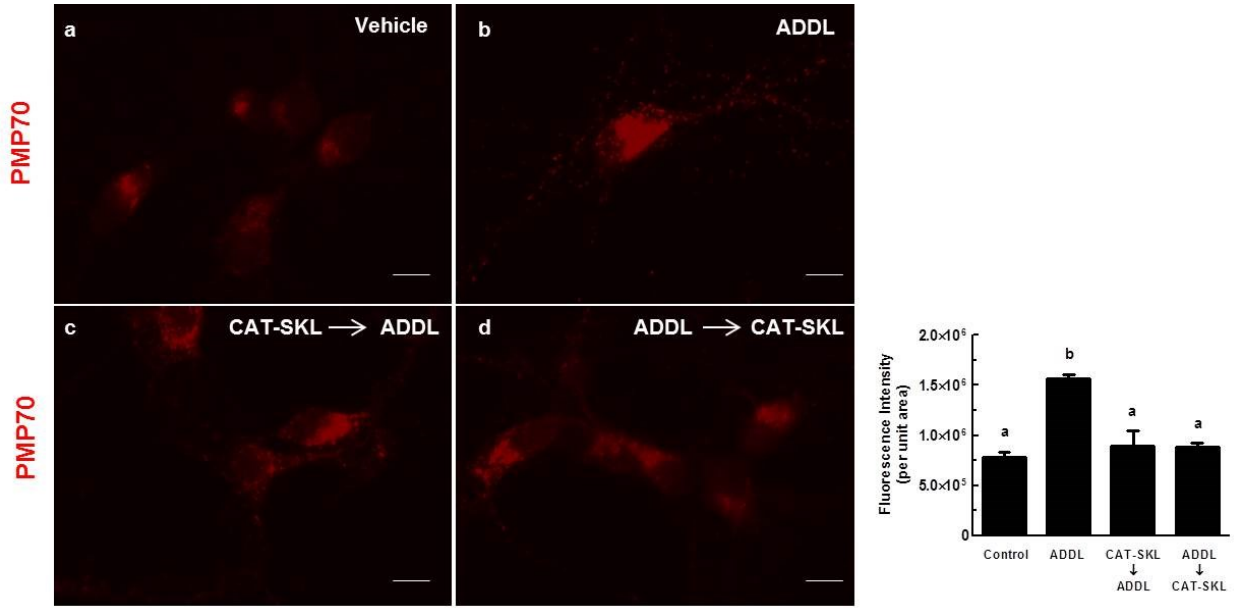

Figure 4.5. CAT-SKL thwarts ADDL-induced proliferation of peroxisomes. Primary rat cortical/hippocampal neurons were treated as follows: (A) Vehicle control for 24 hours. (B) ADDLs (1 μM) for 24 hours. (C) CAT-SKL (1 μM) for 24 hours followed by ADDLs (1 μM) for 24 hours. (D) ADDLs (1 μM) for 24 hours followed by CAT-SKL (1 μM) for 24 hours. Neurons were immunostained with anti-PMP70 (70 kDa peroxisomal membrane protein) antibodies followed by AlexaFluor 546 goat anti-rabbit antibodies (red fluorescence). Quantification (inset) was accomplished using Image J shareware. Statistical analysis was performed using one-way ANOVA. When ANOVA indicated significant treatment effects, means were separated using Tukey's Multiple Comparison Test. Bars represent mean ± SEM for replicate samples (n=5). Means followed by the same letter are not significantly different ($p>0.05$). Scale bar = 20 μm.

Figure 4.6 left and right panels

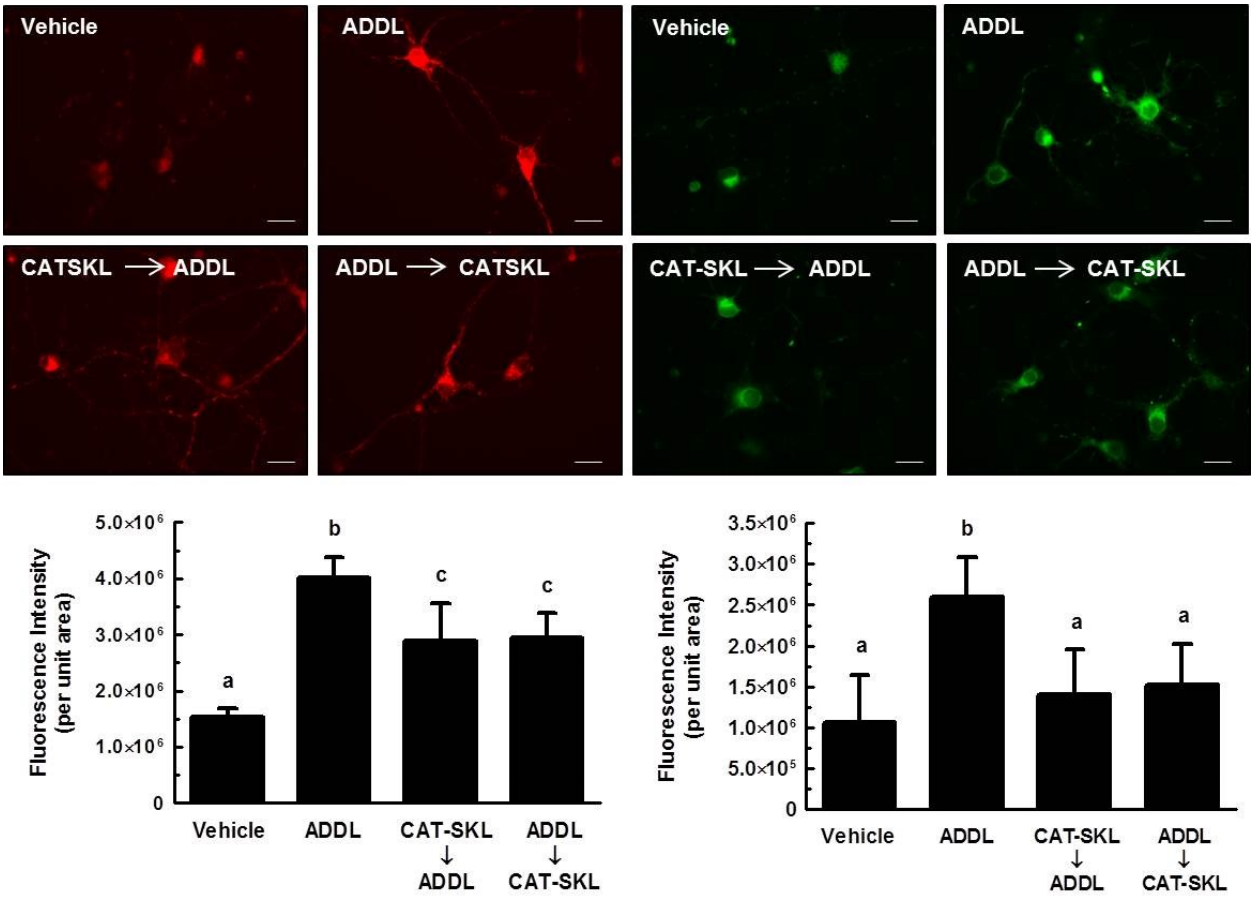

Figure 4.6. CAT-SKL's effects on mitochondria in ADDL-treated neurons. Left panel: Mitochondrial ROS was determined using the MitoTracker® Red CM-H_2XRos selective probe (red fluorescence). Right panel: Mitochondrial depolarization was visualized using the JC-1 mitochondrial potential sensor (green fluorescence). Quantification (insets) was accomplished using Image J shareware. Statistical analysis was performed using one-way ANOVA. When ANOVA indicated significant treatment effects, means were separated using Tukey's Multiple Comparison Test. For left and right inset graphs, bars represent mean ± SEM for replicate samples (n=6 and n=8, respectively). Means followed by the same letter are not significantly different ($p>0.05$). Scale bar = 20 μm.

Figure 4.7A

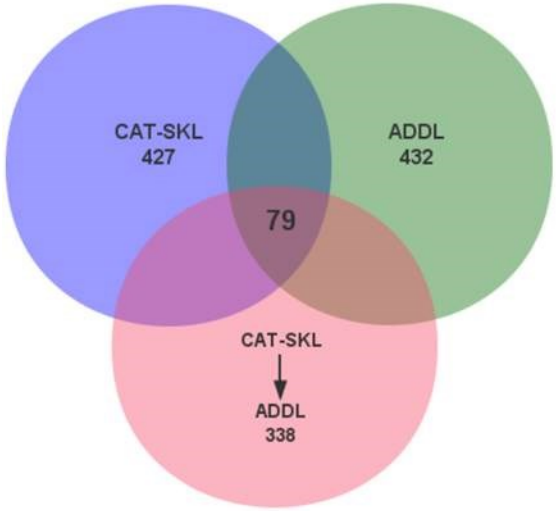

Figure 4.7B

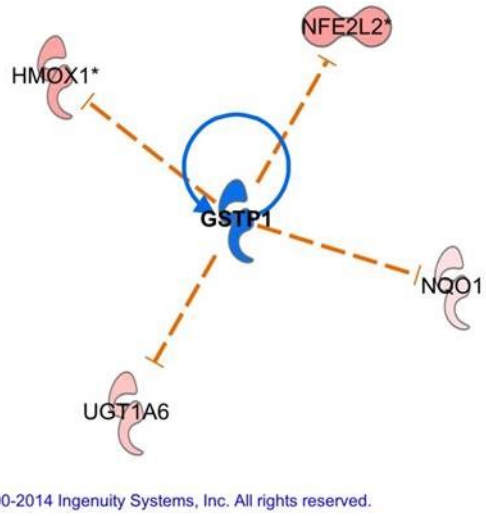

Figure 4.7C

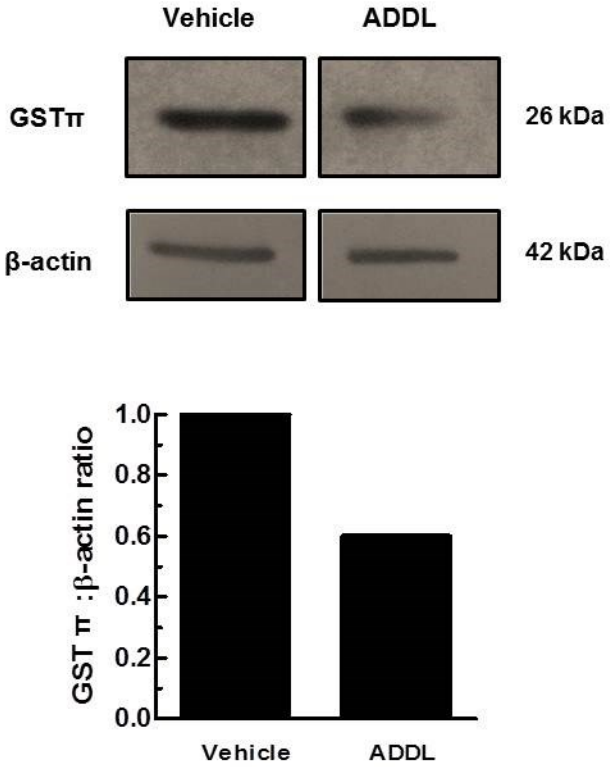

Figure 4.7D

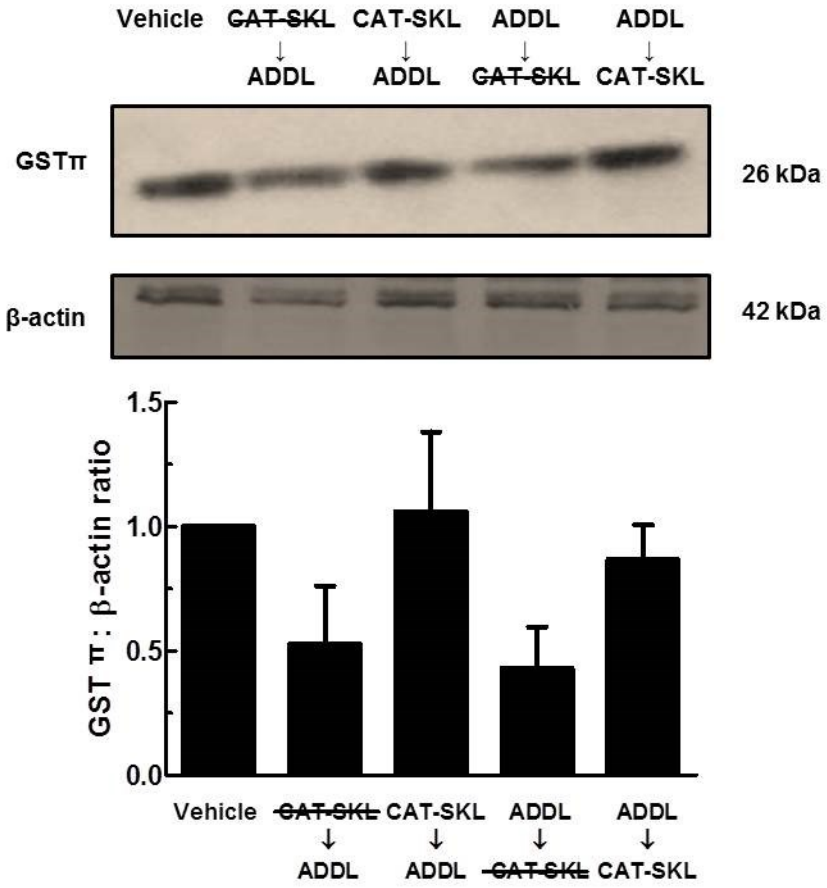

Figure 4.7. CAT-SKL protects neurons from GSTπ depletion in ADDL treated neurons. (A) Venn diagram illustrating 79 overlapping genes between treatments. A total of 432 genes were altered in ADDLs, 427 in CAT-SKL, and 338 in CAT-SKL followed by ADDL treatments. Complete lists of genes are available in Supplementary Table a4.1. (B) Upstream regulator analysis was used to identify potential molecules upstream responsible for the observed gene expression changes in the dataset. Blue indicates upstream regulator GSTπ is predicted to be inactivated. Nuclear factor (erythroid-derived 2)-like 2 (NFE2L2) is a transcription factor involved in increasing the expression of various antioxidant enzymes including: heme oxygenase-1 (HMOX1), UDP-glucuronosyltransferase (UGT1A6), and NAD(P)H quinone oxidoreductase 1 (Nqo1), among others. (C) Vehicle and ADDL (1 μM) treated neurons for 24 hours. Bands are taken from same western blot. Quantification of western blots normalized to β-actin. (D) Lane assignments left to right: Vehicle control: cells pretreated with enzymatically inactive CAT-SKL (1 μM) - indicated with line through for 24 hours, followed by ADDL (1 μM) for 24 hours; cells pretreated with CAT-SKL (1 μM) for 24 hours, followed by ADDL (1 μM) for 24 hours; cells treated with ADDL (1 μM) for 24 hours, followed by enzymatically inactive CAT-SKL (1 μM) for 24 hours; cells treated with ADDL (1 μM) for 24 hours, followed by CAT-SKL (1 μM) for 24 hours. Quantification of western blots normalized to β-actin (n=3).

4.4 Discussion

The importance of soluble oligomeric forms of Aβ as a major driving force in the initial stages of AD has been receiving ever wider acceptance (Lue et al., 1999; McLean et al., 1999; Wang et al., 1999; Klein, 2002; Selkoe, 2011). Here, we confirm the toxicity of ADDLs in rat primary neuronal cultures. In addition, we show these effects are prevented or reversed by the peroxisomally targeted antioxidant enzyme, CAT-SKL. How catalase supplementation of peroxisomes exerts such dramatic protective effects on neurons is not completely clear. Indeed, there is only limited understanding of peroxisome involvement in AD, despite the clear importance of the organelle in overall cell physiology. What is known is that peroxisome activity is upregulated in early states of the disease, an apparent initial response to Aβ's effects (Cimini et al., 2009; Fanelli et al., 2013). At later stages of the disease, changes in peroxisome number, activity, and oxidative balance are observed (Santos et al., 2005; Inestrosa et al., 2013). Plasmalogens, critical ether-linked phospholipids synthesized initially in peroxisomes, are present at diminished levels in the AD brain. Accompanying this lipid perturbation are elevated levels of very long chain fatty acids, potentially toxic molecules normally metabolized in the organelle. Finally, in the AD brain peroxisome density increases in neuronal cell bodies (Kou et al., 2011).

Despite the uncertainty regarding peroxisomes and their role in neuronal health and Aβ-induced cytotoxicity, the results presented in this work suggest that an oxidatively-balanced peroxisome is a desirable goal. Neuronal cells with peroxisomes made resistant to enhanced oxidative stress by addition of catalase, are robustly protected against the toxic effects of Aβ. ROS are present at reduced levels, the

exquisitely complex neuronal architecture is maintained or regenerated, and viability is enhanced.

Effects of CAT-SKL are not restricted to peroxisomes. The targeted antioxidant once again reverses mitochondrial dysfunction, at least at the level of oxidant production and organelle polarity (Fig. 6). Changes in mitochondrial form and function are known to accompany AD pathogenesis (Hirai et al., 2001; Garcia-Escudero, 2013; Xie et al., 2013). The nature of the redox-based interplay between peroxisomes and mitochondria is a fascinating topic for future investigation, both within and without the context of AD.

An important validation of the culture system employed in these studies was the demonstration, by DNA microarray analysis, that expression of the detoxifying enzyme GSTπ was compromised by ADDLs (and reversed by CAT-SKL). GSTπ is a critically important cellular enzyme and there is no clear understanding of why the enzyme is present in greatly diminished concentrations in the AD brain. It is not known to what extent decreased transcription and translation contributes – versus a destabilization or degradation of the fully synthesized molecule. In our culture model, whatever mechanism is responsible for reduced levels of the enzyme, they are sensitive to CAT-SKL's redox-balance-creating effects. The fact that GST is inactivated by the lipid peroxidation product 4-hydroxynonenal, supports the damage by oxidation theory (Lovell et al., 1998).

Targeted antioxidant prophylaxis is a relatively new concept, and is gaining momentum in this time of considerable question about the safety and efficacy of more

traditional antioxidants (Petersen et al., 2005; Brewer, 2010; Polidori and Nelles, 2013; Watson, 2013; Persson et al., 2014). Is it the non-selective quenching of oxidants that is detrimental? Or perhaps the high concentrations required of molecules needed in stoichiometric amounts. Regardless, our work suggests CAT-SKL possess powerful neuroprotective effects against Aβ-induced neurotoxicity; preclinical testing is the next step and has commenced.

4.5 Materials and Methods

Primary neuronal cultures. E18 Sprague Dawley rat cortex/hippocampus tissue was obtained from BrainBits®. Preparation and cell plating was performed following the manufacturer's protocol. Briefly, cell culture plates were coated overnight using standard cell culture conditions with poly-D-lysine (50 µg/mL) (Sigma-Aldrich). Rat cortex/hippocampus tissue was incubated in 2 mg/mL papain for 10 minutes at 37°C. Cell dispersal was performed using a sterile glass Pasteur pipette. Sample containing the dispersed cells was transferred to a new tube and centrifuged at 200 x g for 1 minute. The supernatant was discarded and the pellet was resuspended in NbActiv1™ media (BrainBits®). Cells were plated and incubated under normal cell culture conditions for 7 days to allow differentiation. Media was changed every 3 days.

ADDL preparation. Aβ 1-42 peptide was purchased from California Peptide Research, Inc. ADDL preparation was carried out as previously documented (Klein, 2002). Briefly, monomerization of amyloid-beta 1-42 was performed by incubating with 1,1,1,3,3,3-hexafluoror-2-propanol (HFIP) (Sigma-Aldrich) to a final concentration of 1 mM and incubated at room temperature for 1 hour. The amyloid-beta-HFIP solution was then placed on ice for an additional 10 minutes and aliquoted under a fume hood in

Eppendorf tubes which allowed for HFIP evaporation overnight. ADDL preps were performed by resuspending the dried peptide in dimethyl sulfoxide to generate a 5 mM stock. The 5 mM solution was additionally diluted into NbtActiv1^{TM} medium for 24 hours at 5°C and then centrifuged for 10 minutes at 14,000 x g. The resultant supernatant was transferred to a new tube to make a 100 µM ADDL preparation to work from. Protofibrils were formed by modifying the above protocol and leaving the peptide in dimethyl sulfoxide for 24 hours at 37°C and then diluting into NbtActiv1^{TM}.

Gel filtration. Sephadex G-50 beads were suspended and gently swirled in dH_2O and allowed to swell at room temperature. A Poly-Prep column (BIO-RAD) was filled with the swollen bead suspension and allowed to settle to a ~10 mL bed volume. The column was then re-equilibrated with PBS. Equal volumes/concentrations of polypeptide samples were added to the top of the bed volume and additional PBS was added through the column. A Bio-Dot microfiltration system (BIO-RAD) was readied containing a nitrocellulose membrane. 100 µL fractions were collected directly into the Bio-Dot microfiltration system. After applying vacuum to affix polypeptides on the membrane surface, the membrane was stained with Ponceau S. Quantification of polypeptide levels in fractions was determined using National Institutes of Health's Image J public domain shareware. Additional characterization showed polypeptide staining was linearly responsive to amount loaded (data not shown).

CAT-SKL. The recombinant protein biologic was expressed and purified as previously described (Young et al., 2008). It was biotinylated as described in (Terlecky, 2002) to track entry into primary rat cortical/hippocampal neurons. Equal numbers of plated neurons were treated or not with 100 nM biotinylated CAT-SKL for 0, 1, 2, and 24 hours,

and harvested in PBS. Proteins were separated by SDS-PAGE, and transferred to a nitrocellulose membrane. The membrane was blocked with 5% nonfat dry milk and biotinylated CAT-SKL was visualized with streptavidin alkaline-phosphatase (1:1000). Anti-β-actin antibodies (1:10000) were used to identify β-actin which served as a loading control. These antibodies were developed by the nitro-blue tetrazolium chloride and 5-bromo-4-chloro-3'-indolyphosphate p-toluidine salt (NBT/BCIP) 1-Step Solution (Thermo Scientific).

Catalase staining in neurons. Neurons were plated onto poly-D-lysine coated coverslips as described above and fixed for 10 minutes in 3.7% paraformaldehyde and permeablized with 0.1% Triton X-100. Sites that non-specifically bind to antibodies were blocked with 5% normal goat serum for 15 minutes. Cells were then incubated with rabbit anti-catalase antibodies (1:100) for 1 hour, washed with 0.01% Tween-20 in phosphate buffered saline, and incubated with goat anti-rabbit Alexafluor 546 antibodies (1:15000) for 1 hour. Neurons were then mounted with ProLong®Gold antifade reagent with 4',6-diamidino-2-phenylindole (Invitrogen). Microscopic analysis was performed using the Zeiss ApoTome Imaging system from the Microscopy, Imaging and Cytometry Resources Core Facility (MICR), at the Wayne State University School of Medicine.

Catalase enzymatic activity and immunoreactivity. Equal numbers of plated neurons were treated or not with 1 μM CAT-SKL for 24 hours. Cells were then washed 3 times and harvested in PBS. Protein concentrations were measured using the Bradford Reagent (ThermoScientific). Catalase enzymatic activity was determined by its ability to decompose H_2O_2 as previously described (Koepke et al., 2008; Price et al., 2009). Here, equal protein concentrations of neuronal cultured lysates were added to a

final concentration of 1 mg/mL bovine serum albumin, 0.02 M imidazole, 0.2% Triton-X, and 0.06% H_2O_2 in phosphate buffered saline. Samples were incubated for 15 minutes at room temperature and a titanium oxysulfate stop solution was applied. Absorbance units at 405 nm were measured on a microplate reader. For western blots, equal amounts of protein were separated by SDS-PAGE, transferred to nitrocellulose, blocked and probed with anti-catalase antibodies (1:4000) and anti-β-actin antibodies (1:10000).

Cell viability measurements. Rat cortical/hippocampal neurons were plated on a 96-well plate in equal numbers (~100,000 cells) per well. Cells were then pretreated with CAT-SKL (1 μM) for 24 hours or the peroxisome proliferator Wy-14,643 (100 μM) (Sigma-Aldrich) for 48 hours and then challenged with ADDLs (0.1, 1, and 10 μM) for 24 hours. Cellular viability was determined by measuring metabolic activity using the water soluble tetrazolium dye (WST-1); ELISA based assay kit (Millipore). Absorbance of samples was measured in a microplate reader at 420 nm, with a reference wavelength of 600 nm.

H_2O_2 measurements. H_2O_2 was measured using the Amplex® Red (10-acetyl-3,7-dihydroxyphenoxazine) Hydrogen Peroxide/Peroxidase Assay Kit (Molecular Probes®, Inc.). Rat cortical/hippocampal neurons were plated on to 96-well plates in equal numbers and pretreated with an unrelated control peptide (1 μM), CAT-SKL (1 μM), and/or Wy-14,643 (100 μM) for 24 hours following ADDL treatment (1 μM) for an additional 24 hours. Neurons were washed two times with Hank's balanced salt solution and treated with the Amplex reagent following the manufacturer's protocol. Fluorescence units were analyzed by a microplate reader using excitation and emission wavelengths of 530 and 590 nm, respectively.

Fluorescence microscopy. Primary rat cortical/hippocampal neurons were plated on coated 2 cm^2 glass coverslips following the manufacturer's protocol (BrainBits®). All drug applications were performed blindly. After 7 days of differentiation, neurons were treated with the following concentrations: ADDL (1 μM), CAT-SKL (1 μM), Wy-14,643 (100 μM). Slides were washed three times with Hank's balanced salt solution between treatments, and then fixed and stained with the appropriate antibodies. Primary and secondary antibodies employed include: anti-MAP-2 (1:800) (Millipore) coupled with AlexaFluor 488 goat anti-mouse (1:500) (Life Technologies); and anti-PMP70 (1:500) (abcam®) coupled with AlexaFluor 546 goat anti-rabbit (1:15000) (Invitrogen). Microscopic analysis was performed using the Leica TCS SP2 confocal microscope located in the Department of Anatomy and Cell Biology's microscope facility at the Wayne State University School of Medicine, and Zeiss ApoTome Imaging System from MICR, also at the Wayne State University.

Mitochondrial assays. For mitochondrial ROS and membrane potential assays, neurons were grown and maintained as described above except that coverslips were pre-coated with 100 μg/mL poly-D-lysine. Neurons were 1) pre-treated with 1 μM CAT-SKL for 24 hours, and post-treated with 1 μM ADDL for an additional 24 hours, or 2) pre-treated with 1 μM ADDL for 24 hours and then post-treated with 1 μM CAT-SKL for an additional 24 hours. Mitochondrial ROS production was determined by using MitoTracker® Red CM-H_2XRos (Invitrogen). Medium containing 200 nM of the Mitotracker probe was incubated with neurons for 20 minutes at 37°C, 5% CO_2, and washed with Hank's balanced salt solution. Mitochondrial membrane potential was determined using the JC-1 mitochondrial potential sensor (Invitrogen). Depolarized

mitochondria appear as diffuse green structures. Medium containing 2 µg/mL of the JC-1 dye was incubated with the neurons for 20 minutes, and washed with Hank's balanced salt solution. Cells from both treatment protocols were imaged using the Zeiss ApoTome Imaging system from the MICR.

DNA microarray analysis. Cells were maintained and treated as described above, washed twice and harvested in PBS (2 plates per condition). Total RNA was isolated from cell pellets using an RNeasy Midi Kit from Qiagen. Quantity and quality of all mRNA samples was determined by analysis with the NanoDrop 1000, Agilent Bioanalyzer and the Agilent RNA 6000 Nano Kit (Agilent Technologies). Whole-genome expression was measured by a 2-color microarray approach using Agilent SurePrint G3 Rat GE 8X60K arrays (Agilent Technologies) at the Applied Genomics Technology Center Core, Wayne State University. Feature analysis and data extraction was performed using Agilent Feature Extraction software version 11.5.1.1, where for matched biological replicates the log10 expression ratios are CAT-SKL-treated (cy5-labeled) relative to control vehicle-treated sample (cy3-labeled). P values and ratios of detection for Agilent probes (background subtracted and lowess normalized) were averaged for sample replicates. A threshold of significance for ADDL, ADDL→CATSKL and CAT-SKL was set at p<=.01 and a threshold of significance for CATSKL→ADDL was set at p<=.001. The two filters were used to yield relatively similarly sized sets of significant annotated transcripts for each treatment that would be applicable to downstream pathway analysis. Duplicate significant probes were gene-averaged. Systems and pathway-level analysis for enrichment and biological meaning from resulting data was accomplished using Ingenuity Systems software (Redwood City,

CA). MIAME compliant data sets were uploaded to the Gene Expression Omnibus (GEO) website, and are available through accession number GSE55369.

GST quantification. GSTπ expression was quantified by western blot analysis using Image J software. Cells were washed with Hank's balanced salt solution and harvested into cell lysis buffer (Cell Signaling). Protein quantification was made using the Bradford reagent (ThermoScientific). For western blots, equal amounts of protein were loaded to SDS-PAGE, transferred to a nitrocellulose membrane, and blocked with 5% non-fat milk. Antibodies utilized included anti-GSTπ (MBL International Corporation) (1:1000) coupled with goat anti-rabbit-HRP antibodies (1:5000); and anti-β-actin antibodies (1:10000) coupled with goat anti-mouse-AP antibodies (1:5000).

Statistical analysis. Where appropriate, statistical analysis was performed in GraphPad Prism version 5.0 using one-way analysis of variance (ANOVA). When ANOVA indicated significant treatment effects, means were separated using Tukey's Multiple Comparison Test.

Appendix Chapter 4
Supplementary figure a 4.1A

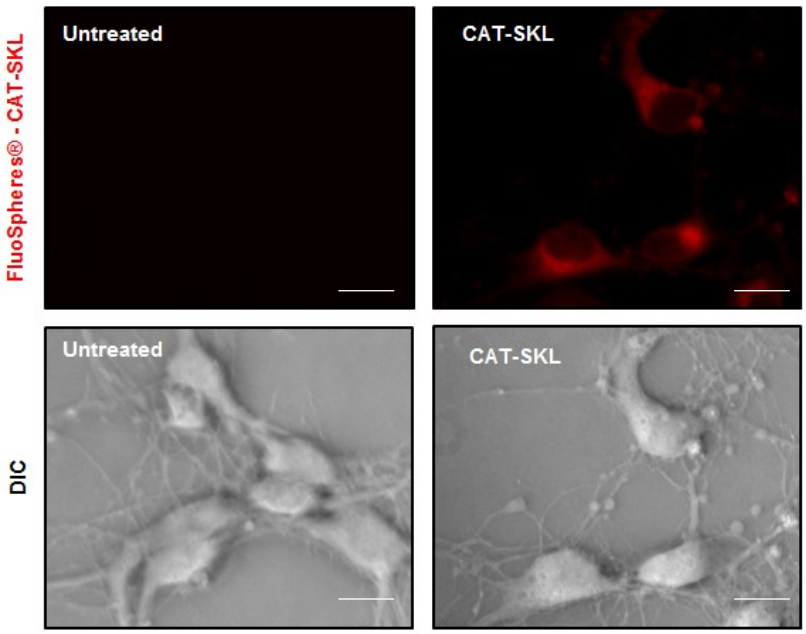

Supplementary figure a 4.1B

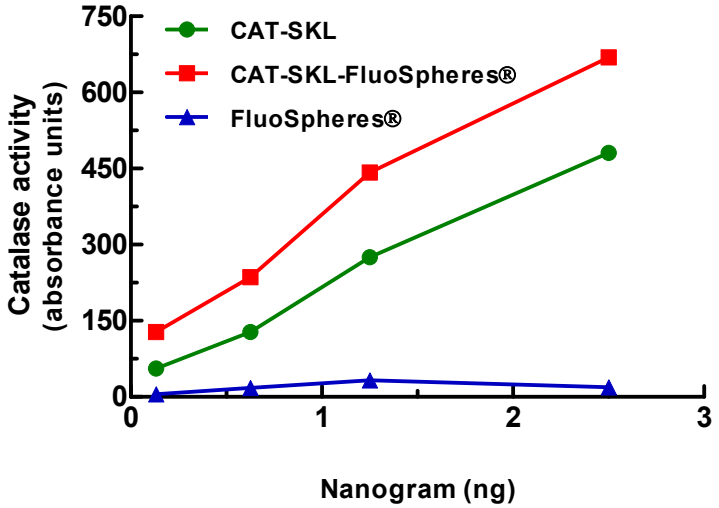

Supplementary figure a4.1. CAT-SKL-FluoSpheres®. (A) CAT-SKL-FluoSpheres® (0.1 μM) was added or not to cortical/hippocampal neurons for 24 hours. DIC = differential interference contrast microscopic image. (B) CAT-SKL-FluoSpheres® are enzymatically active similar to the unmodified CAT-SKL molecule. FluoSpheres® themselves were not able to metabolize H_2O_2. Scale bar = 20 μm.

Supplementary table a4.1. List of genes identified by microarray analysis with significant changes in gene expression. A threshold of significance for ADDL, ADDL→CATSKL and CAT-SKL was set at p<=.01 and a threshold of significance for CATSKL→ADDL was set at p<=.001.

CATSKL, CATSKL + ADDL, ADDL (79)	CATSKL (425)	CATSKL_p-value	CATSKL_LogRatio(Base10)	CATSKL+ADDL (336)	CATSKL+ADDL_p-value	CATSKL+ADDL_LogRatio(Base10)	ADDL+CATSKL (135)	ADDL+CATSKL_p-value	ADDL+CATSKL_LogRatio(Base10)	ADDL (430)	ADDL_p-value	ADDL_LogRatio (Base 10)
ACADL	4930571K23Rik	7.40E-03	-0.004	A2M	1.23E-08	0.437	ABRA	3.30E-03	0.395	1700020N15Rik/Gm6812	8.88E-03	0.062
ADAMTS9	AADAT	1.01E-03	0.389	AADAT	1.55E-04	0.676	ACSM3	3.58E-03	0.041	A2M	2.78E-05	0.301
APOC1	ACACA	3.80E-03	-0.209	ABHD3	3.20E-04	0.256	ADAMTS15	5.34E-03	0.398	ABHD14B	9.28E-03	0.018
APOE	ACADL	4.80E-03	0.242	ACACA	5.83E-05	-0.288	ADRA1D	2.88E-03	0.224	ACADL	9.61E-04	0.234
ARX	ADAM23	5.80E-03	-0.192	ACADL	1.96E-05	0.285	AEBP1	1.13E-03	0.348	Acot1	7.81E-03	0.212
ASIC4	ADAMTS9	4.84E-03	0.326	ACSS1	8.16E-05	0.264	AIF1	8.30E-04	0.242	ACSS1	1.04E-04	0.257
BTBD17	ADCYAP1R1	6.50E-03	0.382	ADAMTS9	1.99E-07	0.582	AMY2A	1.06E-04	0.26	ADAMTS1	1.33E-03	-0.21
C10orf54	AGPS	9.46E-03	-0.222	ADM	2.62E-05	0.284	ANXA3	2.67E-03	0.26	ADAMTS9	6.06E-04	0.418
C1QL1	AIF1	2.45E-08	0.415	AGT	6.22E-09	0.428	APOC2	4.98E-03	-0.304	ADCYAP1	6.14E-03	-0.174
CDCA7L	ALS2CR8	5.48E-03	-0.288	AJUBA	9.92E-04	0.296	Apol3/LOC681351	4.86E-03	0.261	ADM	5.90E-04	0.284
CDK14	ANGPTL4	2.68E-03	0.347	ALDH1L1	9.64E-05	0.266	AREG/AREGB	6.22E-03	0.002	AFP	2.05E-03	-0.217
CDK2	ANKLE2	6.75E-03	-0.32	AMPD3	1.54E-04	0.257	ARG1	4.04E-04	0.32	AGPAT9	4.31E-06	-0.37
CENPT	ANKRD26	3.75E-03	-0.395	ANGPTL4	1.69E-04	0.3	ASB15	9.74E-03	0.262	AGRP	2.19E-03	-0.233

CATSKL, CATSKL + ADDL, ADDL (79)	CATSKL (425)	CATSKL_p-value	CATSKL_LogRatio(Base10)	CATSKL+ADDL (336)	CATSKL+ADDL_p-value	CATSKL+ADDL_LogRatio(Base10)	ADDL+CATSKL (135)	ADDL+CATSKL_p-value	ADDL+CATSKL_LogRatio(Base10)	ADDL (430)	ADDL_p-value	ADDL_LogRatio (Base 10)
CHD2	ANKRD66	6.44E-04	-0.259	ANKLE2	4.94E-04	-0.254	ASB2	9.16E-03	-0.166	AGT	2.12E-04	0.416
CHST7	APAF1	5.70E-03	-0.18	ANXA1	8.11E-04	0.272	BHLHE40	4.63E-03	-0.214	AGTR1	2.18E-04	-0.456
CSF1	APOC1	4.69E-05	0.384	AOX1	5.72E-06	0.554	C3	3.40E-03	0.332	ALDH1L1	3.48E-04	0.258
CSPG4	APOD	2.65E-03	0.312	APLN	1.37E-04	0.285	C7	6.89E-06	0.345	ANGPT1	1.91E-03	0.252
CTSH	APOE	2.45E-04	0.403	APOC1	8.01E-08	0.42	CA8	8.80E-03	0.169	ANKRD33B	4.54E-04	-0.275
CYP2J2	APPL2	8.65E-03	0.184	APOD	7.62E-07	0.418	CALCR	8.43E-03	-0.156	APLN	3.67E-03	0.25
CYP4F8	ARG1	2.32E-04	0.408	APOE	9.91E-10	0.455	CAV1	1.02E-04	0.446	APOA2	4.84E-03	0.263
EFS	ARHGAP11A	2.10E-03	0.26	APPL2	6.27E-04	0.281	CCL25	3.53E-03	-0.2	APOC1	6.40E-05	0.365
ENTPD2	ARHGAP18	6.95E-03	0.252	AQP4	2.40E-08	0.399	CCL3L1/CCL3L3	5.48E-13	0.667	APOE	5.75E-06	0.41
FABP7	ARX	1.94E-03	0.319	ARG1	4.30E-04	0.263	CDC14A	8.38E-03	0.236	AQP4	1.90E-04	0.358
FAM89A	ASF1B	5.66E-03	0.566	ARHGAP18	4.94E-04	0.236	Cdca7	5.74E-03	0.258	ARC	4.32E-03	-0.191
FRAS1	ASIC4	1.52E-03	0.215	ARHGEF19	5.70E-04	0.318	CHDH	4.52E-03	-0.196	ARHGAP24	5.42E-06	-0.344
GJA1	ATM	6.61E-03	-0.654	ARX	6.79E-09	0.439	CHRDL1	2.16E-03	0.32	ARHGEF19	6.95E-05	0.475
GPR37L1	AXIN2	9.59E-03	-0.264	ASF1B	3.61E-04	0.402	CKMT2	8.69E-03	-0.54	ARHGEF9	9.98E-03	-0.221
GSTA2	AXL	7.94E-04	0.026	ASIC4	1.41E-04	0.26	CNKSR1	9.19E-03	-0.196	ARL4D	1.04E-03	-0.227

CATSKL, CATSKL + ADDL, ADDL (79)	CATSKL (425)	CATSKL_p-value	CATSKL_LogRatio(Base10)	CATSKL+ADDL (336)	CATSKL+ADDL_p-value	CATSKL+ADDL_LogRatio(Base10)	ADDL+CATSKL (135)	ADDL+CATSKL_p-value	ADDL+CATSKL_LogRatio(Base10)	ADDL (430)	ADDL_p-value	ADDL_LogRatio (Base 10)
Gstt3	BTBD17	1.29E-04	0.266	ASPM	3.60E-05	0.278	CNR1	8.44E-03	0.17	ARPP21	1.45E-04	-0.252
IGF1	C10orf54	1.32E-03	0.288	ATP1A2	5.70E-08	0.386	COL1A1	3.34E-08	0.835	ARRDC2	5.10E-03	-0.024
ITGB5	C1QL1	1.32E-04	0.346	BCAN	1.38E-06	0.335	CORT	1.14E-03	0.226	ARX	5.86E-06	0.308
JAM2	C3	1.26E-10	0.595	BCAS1	4.36E-10	0.47	CRH	5.98E-05	0.276	ASIC4	5.18E-03	0.188
KANK1	C5	7.73E-03	-0.238	BDH2	2.95E-04	0.351	Cxcl12	7.19E-04	0.275	ASPG	9.88E-03	0.417
MCM3	C7	3.05E-05	0.336	BMP4	1.65E-05	0.554	CXCL2	5.32E-03	0.678	ASPM	2.35E-03	0.224
MDFIC	CA8	7.72E-03	0.192	BMP7	3.16E-05	0.298	CYBA	5.60E-03	0.19	ATP1A2	3.54E-06	0.387
MEIS1	CACNG5	6.06E-04	-0.23	BTBD17	1.03E-05	0.305	Cyp2d22	7.60E-04	0.262	BCAN	5.01E-04	0.269
MGST1	CALCA	3.96E-03	0.323	C10orf54	1.15E-06	0.338	DAB2	3.64E-03	-0.013	BCAS1	1.58E-03	0.218
MLC1	CAPN13	2.60E-03	-0.242	C1QL1	6.17E-04	0.284	DICER1	6.90E-03	0.355	BIRC5	1.21E-03	0.222
MSX1	CAV1	4.06E-08	0.494	C3	2.76E-05	0.358	DUXA	2.08E-03	-0.217	BMP3	3.88E-03	-0.242
MYO6	CCDC125	5.36E-03	-0.362	C4orf50	6.10E-06	-0.526	EGR2	5.64E-03	0.18	BTBD17	6.01E-05	0.285
NCAPH	CCDC175	3.85E-03	-0.327	C7	1.24E-04	0.258	ELK4	3.70E-03	-0.013	C10orf54	3.39E-03	0.201
NDRG2	CCDC8	8.87E-03	0.174	CARTPT	4.28E-04	0.229	EMR1	4.56E-10	0.596	C11orf95	3.66E-03	-0.306
NFE2L2	CCL3L1/CCL3L3	7.34E-10	0.53	CASP6	4.99E-04	0.418	Entpd4	9.62E-03	-0.404	C1QL1	5.78E-03	0.249

CATSKL, CATSKL + ADDL, ADDL (79)	CATSKL (425)	CATSKL_p-value	CATSKL_LogRatio(Base10)	CATSKL+ADDL (336)	CATSKL+ADDL_p-value	CATSKL+ADDL_LogRatio(Base10)	ADDL+CATSKL (135)	ADDL+CATSKL_p-value	ADDL+CATSKL_LogRatio(Base10)	ADDL (430)	ADDL_p-value	ADDL_LogRatio (Base 10)
NTRK2	CCNB2	8.04E-03	0.203	CAV1	2.76E-05	0.325	F5	5.72E-03	-0.418	C3	2.10E-03	0.283
NXPH1	Cd163l1	7.50E-03	-0.368	CAV2	1.93E-04	0.469	Fam60a	4.46E-03	-0.207	C4orf50	6.58E-03	-0.262
PDPN	CD1D	7.39E-03	0.55	CBS	4.86E-05	0.273	FASLG	2.31E-04	0.341	C5	9.42E-03	-0.231
PLD1	CD2AP	3.75E-03	-0.222	CCL3L1/CCL3L3	8.66E-08	0.501	FBXO36	3.16E-03	0.304	C7	1.75E-05	0.31
PLEKHD1	CD55	2.08E-04	0.516	CCNA2	5.77E-07	0.353	FOXO4	8.51E-03	-0.248	CAND2	3.75E-03	0.192
PPIC	CD99L2	6.15E-03	-0.18	CCNB1	5.52E-04	0.254	GFAP	7.31E-03	-0.092	CAPN5	8.36E-03	-0.264
PRODH	CDC14A	2.85E-03	-0.686	CCNB1IP1	3.70E-05	-0.454	GPC3	1.27E-03	-0.286	CASP12	3.24E-03	-0.232
RGCC	Cdca7	1.20E-03	0.317	CDCA3	2.16E-06	0.33	Gpr165	6.66E-03	-0.104	CBFA2T2	5.55E-03	-0.315
RREB1	CDCA7L	5.88E-03	0.182	Cdca7	5.21E-05	0.317	GPR18	2.49E-03	-0.1	CBS	5.14E-04	0.238
RRM2	CDK14	1.87E-03	-0.284	CDCA7L	5.24E-06	0.316	GPR50	3.40E-03	0.617	CBX6	1.40E-03	-0.21
S100A16	CDK2	1.54E-03	0.279	CDHR1	1.49E-12	0.578	GRAMD3	4.81E-03	0.186	CCDC8	5.90E-03	0.206
S100B	CENPT	7.95E-03	0.236	CDK1	6.82E-06	0.306	Gsta3	1.30E-03	0.336	CCL3L1/CCL3L3	2.15E-03	-0.283
S1PR1	CEP72	9.51E-03	0.292	CDK14	1.25E-04	-0.268	GTF3C3	6.64E-03	-0.089	CCNA2	4.23E-03	0.266
SALL1	CERS6	8.81E-03	-0.218	CDK2	5.21E-05	0.314	HLA-B	9.06E-03	0.226	CD302	7.32E-03	0.184
SALL3	Ces1f/Cesl 1	9.90E-04	-0.517	CDKN1C	3.68E-09	0.434	HMOX1	5.99E-05	0.268	CDC20	9.14E-03	0.172

CATSKL, CATSKL + ADDL, ADDL (79)	CATSKL (425)	CATSKL_p-value	CATSKL_LogRatio(Base10)	CATSKL+ADDL (336)	CATSKL+ADDL_p-value	CATSKL+ADDL_LogRatio(Base10)	ADDL+CATSKL (135)	ADDL+CATSKL_p-value	ADDL+CATSKL_LogRatio(Base10)	ADDL (430)	ADDL_p-value	ADDL_LogRatio (Base 10)
SCRG1	CHD2	3.39E-03	-0.253	CDKN2C	4.65E-04	0.268	HMX3	1.31E-03	-0.36	CDCA2	5.90E-03	0.397
SDC4	CHIA	5.58E-03	0.227	CENPQ	8.25E-04	0.25	HOXB13	3.68E-03	-0.342	CDCA3	3.98E-04	0.274
SEPP1	CHST7	7.70E-03	0.186	CENPT	9.47E-06	0.33	HTR2B	6.10E-03	0.021	Cdca7	1.27E-03	0.27
8-Sep	CKS2	8.92E-03	0.186	CERS6	7.46E-04	-0.222	HTRA1	2.46E-03	0.322	CDCA7L	3.42E-03	0.254
SERINC5	CMYA5	3.32E-03	0.215	Ces1f/Cesl1	9.65E-05	-0.365	Ifitm6	7.02E-03	-0.233	CDHR1	9.65E-15	0.686
SLC1A3	CNNM1	7.31E-03	-0.204	CHD2	3.46E-05	-0.276	IL1A	4.64E-03	0.359	CDK1	5.85E-03	0.209
SLC32A1	CNOT6L	9.19E-03	-0.211	CHST7	1.02E-04	0.274	IL1B	6.15E-05	1.007	CDK14	3.64E-03	-0.198
SMPDL3A	COL14A1	9.74E-03	0.2	CKAP2	6.33E-05	0.265	KIF11	2.13E-04	0.293	CDK2	2.28E-03	0.239
SOX10	COL1A1	2.15E-03	-0.009	CKS2	2.36E-04	0.256	KIF18B	1.29E-03	0.292	CDKN1C	1.42E-03	0.206
SPARCL1	CORT	2.37E-05	0.329	CMTM5	7.53E-05	0.27	KLF2	2.45E-04	0.25	CDT1	6.26E-03	-0.108
SPP1	CPEB4	9.43E-03	-0.207	CNP	4.59E-04	0.251	KRIT1	4.89E-03	0.183	CENPT	5.36E-04	0.296
TCF7L2	CPT1A	9.40E-03	0.314	COL16A1	9.78E-04	0.22	LDHC	3.57E-03	0.24	CH25H	2.95E-04	-0.268
TIMELESS	CRH	2.45E-07	0.382	CORT	3.93E-08	0.394	LFNG	1.88E-03	0.266	CHD2	6.33E-03	-0.176
TMEM100	CRTAP	8.74E-03	-0.168	CPEB4	9.19E-04	-0.229	LILRA6	9.31E-03	-0.264	CHST7	2.38E-03	0.203
TOP2A	CRYAB	6.50E-03	-0.028	CPT1A	5.94E-05	0.291	LOC304903	3.19E-03	0.306	CIDEA	1.90E-05	-0.299

CATSKL, CATSKL + ADDL, ADDL (79)	CATSKL (425)	CATSKL_p-value	CATSKL_LogRatio(Base10)	CATSKL+ADDL (336)	CATSKL+ADDL_p-value	CATSKL+ADDL_LogRatio(Base10)	ADDL+CATSKL (135)	ADDL+CATSKL_p-value	ADDL+CATSKL_LogRatio(Base10)	ADDL (430)	ADDL_p-value	ADDL_LogRatio (Base 10)
TXNIP	CSF1	3.98E-04	0.342	CPT2	2.56E-04	0.31	LOC682360	6.01E-03	-0.246	CLDN5	6.86E-03	-0.381
UBE2T	CSPG4	4.83E-03	0.302	CRH	7.26E-05	0.28	LOC685608 (includes others)	5.82E-03	-0.44	CLIC1	4.36E-03	-0.21
VAMP8	CTDSPL2	3.35E-03	-0.264	CROT	7.30E-04	0.233	LOC688793 (includes others)	2.27E-03	-0.272	CMTM5	2.63E-03	0.254
VCAM1	CTGF	3.95E-03	0.198	CSF1	1.39E-06	0.43	LOC691670	8.12E-03	-0.574	CMYA5	1.15E-03	0.284
WDR16	CTSH	1.04E-06	0.518	CSPG4	2.21E-06	0.388	LPL	2.45E-03	0.032	COL16A1	9.95E-03	0.185
ZCCHC24	Cxcl12	9.14E-03	0.194	CTNND1	7.55E-04	-0.242	LRG1	1.47E-03	-0.564	COL6A1	5.48E-03	-0.192
	CXCL16	9.20E-03	0.283	CTSH	3.88E-09	0.495	MAGEB3	7.65E-04	-0.324	CORIN	1.99E-03	-0.587
	CYBA	6.65E-05	0.365	Cxcl12	3.75E-04	0.357	MARC1	4.03E-04	-0.307	CPT2	6.02E-03	0.228
	CYP2J2	1.70E-03	0.424	CXCL14	2.40E-06	0.322	MAS1	5.67E-03	0.182	CREM	4.63E-03	-0.196
	Cyp2t4	9.12E-03	0.388	CYBA	3.74E-07	0.363	Mbp	1.17E-06	-0.361	CRH	4.53E-04	0.231
	Cyp4a14	2.56E-04	-0.27	CYP2J2	1.36E-05	0.394	MGAT4C	1.62E-03	-0.349	CRHR1	1.55E-03	-0.26
	Cyp4f16/Gm9705	3.46E-03	0.231	CYP4F12	7.55E-05	0.477	MMP13	6.34E-04	0.489	CROT	1.41E-04	0.261
	CYP4F2	2.90E-03	-0.231	CYP4F8	1.71E-04	0.607	MORC2	4.80E-03	0.25	CRYAB	3.05E-04	-0.256
	CYP4F8	6.05E-03	0.658	CYP7B1	5.49E-09	0.432	MRPL50	4.99E-04	0.338	CSF1	7.36E-04	0.277
	CYTIP	5.84E-03	0.272	DDIT4L	2.79E-06	0.364	MS4A8B	8.06E-03	-0.236	CSF3	6.22E-03	0.193

CATSKL, CATSKL + ADDL, ADDL (79)	CATSKL (425)	CATSKL_p-value	CATSKL_LogRatio(Base10)	CATSKL+ADDL (336)	CATSKL+ADDL_p-value	CATSKL+ADDL_LogRatio(Base10)	ADDL+CATSKL (135)	ADDL+CATSKL_p-value	ADDL+CATSKL_LogRatio(Base10)	ADDL (430)	ADDL_p-value	ADDL_LogRatio (Base 10)
	DCAF17	8.46E-03	-0.186	DECR1	3.80E-06	0.322	MTF1	8.81E-03	0.174	CSPG4	6.15E-03	0.273
	DCC	3.88E-03	-0.187	DHRS4	7.00E-04	0.33	MYH1	1.34E-04	0.398	CSRNP1	2.12E-03	-0.24
	DCLK3	9.69E-03	0.183	DLGAP5	3.08E-04	0.24	MYH8	2.60E-03	0.248	CTSH	1.27E-03	0.362
	DDC	3.22E-05	0.421	DMRT3	2.28E-04	0.294	MYLK	6.44E-03	-0.302	Cxcl12	8.72E-04	0.272
	DEGS2	6.32E-03	-0.083	DPYSL3	9.83E-04	-0.212	MYO10	6.77E-03	-0.034	CXCL14	7.55E-03	0.252
	DEPDC1B	4.93E-03	0.359	ECI1	2.71E-04	0.276	NCEH1	5.16E-03	0.188	CXCR4	2.92E-03	0.263
	DLK1	3.50E-04	-0.238	EDEM3	3.42E-04	-0.294	NOS1AP	1.71E-03	-0.398	CXorf57	3.57E-04	-0.257
	DLX5	9.88E-03	0.188	EDNRB	5.10E-06	0.297	NPL	2.29E-04	0.278	CYB5R1	7.38E-03	0.2
	DPP4	5.89E-03	0.358	EFS	1.96E-05	0.332	NRARP	6.96E-05	0.272	CYBA	3.32E-05	0.308
	DUXA	4.86E-03	-0.261	EMR1	8.63E-05	0.312	NRL	7.02E-04	-0.622	Cyp11b1/Cyp11b3	1.71E-03	-0.23
	EARS2	3.32E-03	-0.282	ENPP2	4.93E-05	0.328	Oacyl	4.69E-03	0.252	CYP2J2	7.00E-04	0.452
	ECE1	7.88E-03	-0.25	ENTPD2	1.05E-10	0.502	OAS2	3.94E-03	-0.199	Cyp3a62	5.40E-03	-0.22
	EFS	8.30E-04	0.284	EPB41L2	3.76E-05	0.386	OLFML2A	4.38E-03	0.444	CYP4F12	5.00E-03	0.401
	EIF2AK2	4.99E-03	-0.365	EPHA3	2.55E-04	-0.241	Olfr124	2.96E-03	0.032	CYP4F8	9.71E-03	0.506
	EIF2C4	9.71E-03	-0.19	ERBB2	1.71E-05	0.36	Olfr212/Olfr213	8.08E-03	0.33	CYP7B1	1.93E-04	0.32

CATSKL, CATSKL + ADDL, ADDL (79)	CATSKL (425)	CATSKL_p-value	CATSKL_LogRatio(Base10)	CATSKL+ADDL (336)	CATSKL+ADDL_p-value	CATSKL+ADDL_LogRatio(Base10)	ADDL+CATSKL (135)	ADDL+CATSKL_p-value	ADDL+CATSKL_LogRatio(Base10)	ADDL (430)	ADDL_p-value	ADDL_LogRatio (Base 10)
	EMP1	9.58E-03	-0.046	F3	1.93E-04	0.246	OR6C68	3.45E-03	0.3	Dclk1	6.58E-03	-0.177
	EMR1	3.50E-09	0.53	FABP7	1.03E-09	0.452	PAX3	4.64E-03	-0.192	DDIT4L	3.59E-03	0.324
	ENPP1	4.94E-03	-0.202	FAM181B	1.49E-06	0.35	PCOLCE2	7.46E-03	0.635	DDR2	1.26E-03	0.214
	ENPP2	3.23E-04	0.3	FAM64A	3.40E-05	0.281	PDE4B	1.76E-03	-0.218	DECR1	1.66E-03	0.211
	ENTPD2	2.11E-04	0.387	FAM89A	9.75E-09	0.453	PDGFB	7.92E-03	0.035	DEGS2	1.90E-03	-0.34
	ERC1	2.98E-03	-0.205	FANCL	1.06E-04	0.28	PDGFRA	4.33E-04	0.29	DEPDC1	6.63E-03	0.328
	ERC2	3.73E-04	-0.262	FGFRL1	2.00E-04	0.254	PDYN	2.19E-03	0.208	DIRAS2	8.58E-04	-0.225
	ERG	2.77E-03	-0.331	FKBP10	1.48E-04	0.454	PENK	6.59E-03	0.172	DOCK7	1.71E-04	-0.37
	FABP7	1.04E-03	0.356	Fmn2	3.70E-04	-0.237	PPFIBP2	7.59E-03	-0.081	DRD2	1.33E-03	-0.209
	FAM71A	4.00E-03	0.364	FMO1	8.68E-07	0.401	PRC1	6.50E-03	0.238	DUSP1	4.24E-03	-0.19
	FAM89A	3.10E-07	0.444	Folh1	9.20E-05	0.6	PREX2	8.40E-03	0.217	ECI1	3.98E-03	0.189
	FANCL	1.09E-03	0.226	FOXE1	3.48E-04	-0.232	PRSS8	6.46E-03	-0.209	EDNRB	2.11E-05	0.31
	FCER1G	1.27E-07	0.44	FRAS1	5.38E-04	-0.23	PTHLH	3.91E-03	0.202	EFS	3.41E-05	0.296
	Fcrls	6.15E-03	0.287	FRZB	7.92E-06	0.418	PTPN13	9.88E-05	0.284	EGFR	6.74E-03	0.186
	FGF21	4.96E-03	0.406	FZD2	1.51E-04	0.3	PTPN6	1.80E-03	0.216	EGR2	1.36E-03	-0.248

CATSKL, CATSKL + ADDL, ADDL (79)	CATSKL (425)	CATSKL_p-value	CATSKL_LogRatio(Base10)	CATSKL+ADDL (336)	CATSKL+ADDL_p-value	CATSKL+ADDL_LogRatio(Base10)	ADDL+CATSKL (135)	ADDL+CATSKL_p-value	ADDL+CATSKL_LogRatio(Base10)	ADDL (430)	ADDL_p-value	ADDL_LogRatio (Base 10)
	FGF5	4.20E-03	-0.005	G0S2	2.81E-04	0.238	Pvr	9.86E-03	0.164	EGR4	3.74E-03	-0.189
	FIBIN	9.03E-04	0.298	GAD1	9.62E-04	0.214	RAB1B	4.04E-03	-0.187	ELMOD2	9.71E-03	0.016
	Fmn2	6.68E-03	-0.175	GADD45G	5.82E-04	-0.222	RAC2	1.93E-05	0.334	EMP1	2.52E-06	-0.322
	FMO1	1.09E-04	0.414	GAL3ST1	1.84E-04	0.312	RGD1562977	2.61E-03	-0.254	EMP2	2.36E-03	0.214
	FMR1	1.96E-03	-0.211	GAMT	7.75E-04	0.217	ROBO1	9.70E-03	-0.166	ENTPD2	4.10E-03	0.391
	FOXA2	8.41E-03	0.556	GAREML	4.83E-04	0.386	SHCBP1	6.61E-03	0.244	EPHA3	9.04E-03	-0.166
	FRAS1	5.83E-03	-0.215	GATM	5.01E-05	0.272	SLAMF9	1.72E-04	0.72	ESPL1	3.76E-04	0.25
	FZD2	4.59E-05	0.372	Gbp2	2.28E-08	0.838	SLC11A1	8.04E-03	0.326	ETV4	2.66E-03	-0.38
	G6PC	4.36E-03	0.02	GFAP	2.45E-04	0.292	SLC12A1	8.70E-03	-0.028	EVI2A	3.74E-03	-0.185
	GAREML	2.26E-04	0.482	GJA1	2.86E-11	0.525	SP110	6.87E-03	0.218	F12	2.70E-03	-0.199
	GAS2	7.24E-03	0.182	Gpm6b	4.14E-06	0.318	ST3GAL1	6.08E-03	0.198	F2	8.42E-03	-0.206
	Gbp2	1.16E-04	0.59	GPR37L1	6.16E-06	0.313	TAGLN2	2.36E-03	0.388	FABP7	7.65E-06	0.367
	GDAP1	7.56E-03	-0.223	GRAMD3	2.71E-07	0.369	VIPR2	7.03E-03	-0.032	FAM150B	2.62E-06	-0.322
	GINS1	6.74E-03	0.199	GSDMD	6.96E-06	0.382	Vmn1r52	6.72E-04	0.229	FAM181B	5.29E-03	0.23
	GJA1	4.64E-05	0.404	GSTA2	2.50E-05	0.33	Vom2r9	7.96E-03	-0.395	Fam187a	8.66E-03	-0.047

CATSKL, CATSKL + ADDL, ADDL (79)	CATSKL (425)	CATSKL_p-value	CATSKL_LogRatio(Base10)	CATSKL+ADDL (336)	CATSKL+ADDL_p-value	CATSKL+ADDL_LogRatio(Base10)	ADDL+CATSKL (135)	ADDL+CATSKL_p-value	ADDL+CATSKL_LogRatio(Base10)	ADDL (430)	ADDL_p-value	ADDL_LogRatio (Base 10)
	Gm4944	1.08E-03	0.308	GSTA3	2.51E-07	0.408	WNT16	6.06E-03	-0.177	FAM89A	2.63E-03	0.302
	GPR183	1.41E-03	-0.172	Gsta3	3.80E-12	0.588	ZNF385A	3.70E-04	-0.319	FASLG	8.76E-04	-0.003
	GPR37L1	8.30E-03	0.304	Gstt3	8.35E-05	0.279				FBXO36	9.18E-04	0.195
	GPR63	5.22E-03	-0.24	GUCY1A2	9.53E-04	-0.216				FCER1G	7.05E-05	0.38
	GRAMD3	3.69E-04	0.338	GULP1	7.41E-04	0.246				Fcrls	1.48E-05	0.351
	GRHL2	3.31E-03	-0.405	H2afv	7.56E-04	0.218				FIGF	4.35E-03	-0.19
	GRIK1	4.29E-03	0.192	HCN4	9.60E-04	-0.228				FOSL1	3.15E-06	-0.366
	GRIK4	3.44E-03	0.24	HES5	1.97E-04	0.406				FOSL2	3.92E-03	-0.188
	GSTA2	2.14E-03	0.248	HMOX1	1.75E-04	0.25				FOXA2	4.79E-03	0.533
	GSTA3	1.50E-03	0.326	HSPB8	9.66E-04	0.276				FRAS1	2.84E-04	-0.255
	Gsta3	2.25E-05	0.465	HTR1B	2.79E-04	-0.349				G0S2	6.15E-03	0.286
	Gstt3	1.25E-03	0.36	HTRA1	6.25E-06	0.354				GADD45G	1.33E-04	-0.28
	GUCY1A2	5.98E-04	-0.259	ID1	7.76E-06	0.422				GAL	9.05E-05	-0.272
	GULP1	2.79E-03	0.204	IFI44	1.62E-04	0.397				GALNT7	7.81E-03	-0.363
	H19	7.66E-03	-0.153	IGF1	7.24E-05	0.266				GALR1	2.22E-03	-0.416

CATSKL, CATSKL + ADDL, ADDL (79)	CATSKL (425)	CATSKL_p-value	CATSKL_LogRatio(Base10)	CATSKL+ADDL (336)	CATSKL+ADDL_p-value	CATSKL+ADDL_LogRatio(Base10)	ADDL+CATSKL (135)	ADDL+CATSKL_p-value	ADDL+CATSKL_LogRatio(Base10)	ADDL (430)	ADDL_p-value	ADDL_LogRatio (Base 10)
	HDAC4	7.19E-03	-0.182	IGSF1	3.07E-06	0.366				GAMT	5.20E-03	0.19
	Hdgfl1	4.99E-03	0.396	IGSF11	2.84E-06	0.33				GBP5	6.46E-03	0.27
	Hist1h1d	1.30E-03	-0.21	INHBA	5.70E-04	-0.224				GCNT1	2.25E-03	-0.225
	Hist2h4 (includes others)	9.62E-03	-0.232	IQGAP1	1.32E-04	-0.272				GFAP	4.40E-03	0.342
	HLA-B	3.20E-03	0.229	IRX1	2.98E-07	0.454				GFRA1	3.12E-03	-0.193
	HMG20A	4.56E-03	-0.184	ISG20	3.70E-04	-0.236				GFRA2	1.72E-03	-0.237
	HMOX1	6.38E-05	0.276	ITGB5	1.61E-06	0.37				GJA1	1.43E-05	0.379
	HOXA13	9.38E-03	-0.206	JAM2	2.46E-07	0.368				GPKOW	5.38E-03	-0.194
	Hspa1l	5.91E-04	0.442	KANK1	1.31E-06	0.421				Gpm6b	6.97E-04	0.257
	ID1	6.65E-04	0.282	KCNE1L	1.55E-05	0.302				GPR22	7.70E-03	-0.242
	IGF1	4.38E-03	0.284	KIAA0101	3.11E-06	0.338				GPR37L1	3.72E-04	0.318
	IGSF1	6.55E-03	0.262	KIF11	1.27E-07	0.422				GPRC5A	6.95E-05	-0.282
	IL11RA	1.35E-04	0.292	KIF18B	2.15E-08	0.43				GPSM1	6.08E-03	-0.176
	IL24	2.69E-03	0.241	KNSTRN	5.55E-06	0.314				GRAMD3	4.87E-05	0.359
	IQGAP1	7.15E-04	-0.3	LAPTM4B	5.92E-04	0.269				GRID1	6.66E-03	-0.02

CATSKL, CATSKL + ADDL, ADDL (79)	CATSKL (425)	CATSKL_p-value	CATSKL_LogRatio(Base10)	CATSKL+ADDL (336)	CATSKL+ADDL_p-value	CATSKL+ADDL_LogRatio(Base10)	ADDL+CATSKL (135)	ADDL+CATSKL_p-value	ADDL+CATSKL_LogRatio(Base10)	ADDL (430)	ADDL_p-value	ADDL_LogRatio (Base 10)
	IRS1	6.10E-03	-0.256	LIMS2	6.49E-04	0.674				GRIN1	1.98E-03	-0.218
	ISG20	1.15E-03	-0.214	LNPEP	7.28E-04	-0.237				GRM1	5.30E-04	0.292
	ITGB5	4.49E-05	0.405	LOC100359805 (includes others)	2.70E-04	-0.259				GRP	5.65E-03	0.286
	ITIH3	2.06E-03	0.357	LOC100361411 (includes others)	5.78E-04	-0.229				GRTP1	5.46E-03	0.214
	JAM2	2.52E-03	0.249	LOC100363229	9.92E-04	-0.212				GSTA2	5.50E-04	0.324
	KANK1	5.96E-06	0.368	LOC500013	1.30E-06	0.361				Gsta3	2.13E-06	0.488
	KBTBD10	1.17E-03	-0.013	LOC683470	2.20E-05	0.284				Gstm6	7.47E-03	0.458
	KCTD16	1.08E-03	-0.22	LOC684327	1.84E-05	0.314				Gstt3	2.39E-03	0.306
	KIAA0232	4.25E-04	-0.269	LOC686101	1.84E-06	-0.453				GUCA2B	8.91E-03	-0.18
	KIF11	3.35E-04	0.264	LPGAT1	7.95E-05	-0.261				GXYLT1	2.64E-03	0.199
	KIF16B	6.41E-03	0.194	LRRC7	9.75E-04	-0.212				H2afv	3.13E-03	0.188
	KIF18B	1.78E-03	0.27	LTBR	2.75E-04	0.272				Hdgfl1	4.50E-03	0.415
	KIF20B	4.17E-03	0.028	MAG	1.80E-04	0.806				HMGA1	2.40E-03	-0.224
	KIFC1	1.76E-03	0.24	Mbp	2.75E-05	0.286				HMOX1	2.29E-04	0.3
	KRT18	7.50E-03	-0.179	MCM3	1.55E-04	0.258				HRH4	9.97E-04	0.235

CATSKL, CATSKL + ADDL, ADDL (79)	CATSKL (425)	CATSKL_p-value	CATSKL_LogRatio(Base10)	CATSKL+ADDL (336)	CATSKL+ADDL_p-value	CATSKL+ADDL_LogRatio(Base10)	ADDL+CATSKL (135)	ADDL+CATSKL_p-value	ADDL+CATSKL_LogRatio(Base10)	ADDL (430)	ADDL_p-value	ADDL_LogRatio (Base 10)
	KRTAP10-1	1.76E-03	0.228	Mcpt8	3.05E-04	-0.276				HTR1B	1.22E-03	-0.41
	KRTAP4-3	4.66E-03	0.296	MDFIC	7.50E-06	0.32				HTR2C	7.06E-03	-0.174
	LASP1	9.10E-03	-0.19	MEIS1	6.12E-06	0.308				HTRA1	3.34E-04	0.359
	LCORL	8.77E-03	-0.248	METRN	4.64E-04	0.232				Iba57/LOC100363222	1.06E-03	0.249
	LIMD1	8.07E-03	0.275	MFGE8	7.60E-04	0.227				IER5	1.81E-03	-0.252
	LOC100359536 (includes others)	3.72E-03	-0.221	MGMT	6.09E-04	0.242				Ifitm6	6.31E-03	-0.238
	LOC100359630 (includes others)	7.84E-03	-0.174	MGP	5.02E-04	0.226				IGF1	8.26E-05	0.277
	LOC100359805 (includes others)	1.27E-03	-0.249	MGST1	3.98E-10	0.648				IGFBP2	5.00E-03	0.204
	LOC100363229	8.53E-04	-0.245	MLC1	2.16E-07	0.362				IGSF11	2.27E-03	0.254
	LOC100363421	8.18E-03	-0.168	MMP14	1.15E-06	0.345				IL6R	3.32E-03	-0.192
	LOC100365120	8.93E-03	-0.166	MMP2	5.62E-07	0.38				INHBA	1.06E-05	-0.298
	LOC259246 (includes others)	5.95E-03	0.424	MN1	5.74E-04	-0.227				IQUB	2.73E-03	-0.244
	LOC286992	8.78E-03	-0.56	MSX1	5.79E-08	0.507				IRS1	4.02E-03	-0.204

CATSKL, CATSKL + ADDL, ADDL (79)	CATSKL (425)	CATSKL_p-value	CATSKL_LogRatio(Base10)	CATSKL+ADDL (336)	CATSKL+ADDL_p-value	CATSKL+ADDL_LogRatio(Base10)	ADDL+CATSKL (135)	ADDL+CATSKL_p-value	ADDL+CATSKL_LogRatio(Base10)	ADDL (430)	ADDL_p-value	ADDL_LogRatio (Base 10)
	LOC291480	9.41E-03	-0.227	MYBL2	3.88E-04	0.238				IRX1	4.51E-03	0.363
	LOC317070 (includes others)	1.58E-03	-0.228	MYH1	2.77E-10	0.551				ISM1	7.33E-03	-0.17
	LOC367363 (includes others)	9.82E-05	-0.26	MYH8	1.17E-05	0.305				ITGA8	3.95E-05	-0.334
	LOC378467	3.66E-03	0.272	MYO6	1.54E-04	0.284				ITGB5	7.75E-07	0.364
	LOC500846	6.65E-04	-0.24	MYO9A	1.92E-04	-0.277				ITGBL1	5.50E-03	-0.004
	LOC680207	8.61E-03	-0.168	NCAPH	5.78E-04	0.228				JAM2	7.77E-05	0.302
	LOC683430	7.94E-03	0.468	NDE1	8.40E-05	0.268				KANK1	1.23E-03	0.298
	LOC684439	7.29E-03	0.246	NDRG2	7.68E-09	0.419				KCNAB1	6.42E-03	-0.248
	LOC686298	7.57E-04	0.242	NEDD1	4.70E-04	0.468				KCNC2	6.04E-03	-0.214
	LOC687062	7.49E-03	-0.192	NFE2L2	7.28E-09	0.43				KCTD4	3.19E-03	-0.2
	LOC689701 (includes others)	4.00E-03	-0.27	NIM1	3.44E-04	0.24				KCTD8	3.02E-03	-0.195
	LOC691047	2.32E-04	-0.131	NKAIN4	1.58E-04	0.252				KIAA0101	2.06E-03	0.242
	LOC691169	4.76E-03	-0.244	NOTCH1	4.73E-06	0.312				KIF11	1.80E-04	0.302
	LOC691495	4.61E-03	-0.236	NPAT	9.13E-04	-0.248				KIF18B	2.51E-04	0.287

CATSKL, CATSKL + ADDL, ADDL (79)	CATSKL (425)	CATSKL_p-value	CATSKL_LogRatio(Base10)	CATSKL+ADDL (336)	CATSKL+ADDL_p-value	CATSKL+ADDL_LogRatio(Base10)	ADDL+CATSKL (135)	ADDL+CATSKL_p-value	ADDL+CATSKL_LogRatio(Base10)	ADDL (430)	ADDL_p-value	ADDL_LogRatio (Base 10)
	LPGAT1	4.30E-03	-0.23	NQO1	7.02E-06	0.332				KIF27	7.12E-03	0.355
	LPPR5	9.14E-03	-0.174	NR3C1	9.88E-04	0.244				KIFC1	1.48E-03	0.218
	LRRC7	3.83E-03	-0.215	NRARP	9.08E-07	0.355				KNSTRN	9.59E-05	0.296
	LRRIQ3	9.36E-03	-0.488	NRIP1	5.66E-04	-0.228				LDLR	8.26E-03	-0.189
	LYPD8	6.59E-03	-0.214	NTRK2	1.06E-07	0.391				LHX6	2.83E-03	0.209
	MAGEB3	9.65E-04	-0.228	NUSAP1	2.42E-04	0.256				LOC259246 (includes others)	5.07E-03	0.503
	MAGEB6	3.56E-03	-0.314	NXPH1	3.00E-06	0.364				LOC367363 (includes others)	3.87E-03	0.013
	MAOB	4.43E-03	0.286	OAF	3.58E-05	0.296				LOC378467	6.84E-03	0.012
	MAP3K3	2.89E-03	0.098	Oas3	3.65E-04	0.286				LOC500013	1.10E-03	0.275
	MARCH3	6.86E-03	0.194	OLFML1	7.98E-04	0.302				LOC683470	1.46E-04	0.254
	MBNL1	5.40E-03	-0.209	OLFML3	1.82E-04	0.257				LOC684327	2.80E-03	0.282
	Mbp	5.64E-04	-0.022	OLIG1	8.34E-06	0.302				LOC684998	2.32E-03	-0.195
	MC4R	5.55E-03	0.21	OLIG2	2.36E-04	0.24				LOC686101	3.31E-03	-0.075
	MCM3	5.53E-03	0.204	PAPSS2	1.14E-05	0.798				LOC688387	9.23E-03	-0.647
	Mcpt8	6.38E-03	-0.223	PBK	4.30E-07	0.465				LOXL1	2.79E-03	0.374

CATSKL, CATSKL + ADDL, ADDL (79)	CATSKL (425)	CATSKL_p-value	CATSKL_LogRatio(Base10)	CATSKL+ADDL (336)	CATSKL+ADDL_p-value	CATSKL+ADDL_LogRatio(Base10)	ADDL+CATSKL (135)	ADDL+CATSKL_p-value	ADDL+CATSKL_LogRatio(Base10)	ADDL (430)	ADDL_p-value	ADDL_LogRatio (Base 10)
	MCU	7.08E-03	-0.211	PDGFRA	1.54E-10	0.491				LRRTM4	5.39E-03	0.113
	MDFIC	3.01E-04	0.26	PDPN	6.56E-10	0.47				LTB4R2	6.90E-03	0.631
	MED21	6.44E-03	-0.262	PDS5A	2.98E-04	-0.314				LTBR	3.79E-03	0.261
	MEIS1	7.68E-03	0.191	PIK3CA	2.88E-04	-0.3				LUM	5.57E-04	-0.362
	METRN	3.26E-03	0.232	PLA2G16	2.62E-08	0.416				LYNX1	6.90E-03	-0.176
	MGST1	1.98E-04	0.618	PLCD1	5.03E-04	0.359				MAML1	1.71E-03	-0.302
	MIB1	1.08E-03	-0.217	PLD1	1.33E-06	0.346				MAN1A1	8.64E-03	-0.18
	MLC1	5.95E-03	0.282	PLEKHB1	2.25E-06	0.337				MCM3	7.14E-03	0.186
	MMP13	9.71E-04	0.639	PLEKHD1	4.45E-07	0.376				MCOLN3	9.77E-03	-0.176
	MPC1L	5.38E-03	0.205	PLP1	2.59E-04	0.256				MCU	6.90E-03	-0.208
	Mrgprb13/ Mrgprb8	7.81E-03	-0.622	PLXNB3	2.79E-04	0.858				MDFIC	8.15E-03	0.243
	MSX1	1.70E-03	0.418	PMEL	2.84E-04	0.376				MEIS1	7.57E-05	0.272
	MTMR10	2.47E-03	0.286	PMP2	4.64E-05	0.838				MEPE	5.26E-03	-0.187
	Muc2	5.12E-04	-0.237	PNLIP	1.17E-04	0.602				MGST1	9.06E-04	0.355
	MX1	9.97E-03	-0.166	PNP	2.16E-04	0.242				MGST2	4.52E-03	-0.208

CATSKL, CATSKL + ADDL, ADDL (79)	CATSKL (425)	CATSKL_p-value	CATSKL_LogRatio(Base10)	CATSKL+ADDL (336)	CATSKL+ADDL_p-value	CATSKL+ADDL_LogRatio(Base10)	ADDL+CATSKL (135)	ADDL+CATSKL_p-value	ADDL+CATSKL_LogRatio(Base10)	ADDL (430)	ADDL_p-value	ADDL_LogRatio (Base 10)
	MYH1	4.71E-06	0.542	PON2	1.12E-06	0.343				MLC1	1.37E-03	0.279
	MYH8	1.86E-04	0.25	PPAP2B	4.66E-04	0.269				MMD2	8.86E-03	0.22
	MYLK	2.16E-03	-0.29	PPIC	5.55E-06	0.325				MMP12	6.23E-05	-0.728
	MYO6	9.72E-03	0.215	PPM1K	7.00E-04	-0.25				MMP14	2.74E-04	0.335
	N4BP2L1	1.10E-03	-0.251	PRC1	3.56E-06	0.318				MMP17	6.21E-03	-0.312
	NAAA	6.06E-03	0.229	PRKACB	2.39E-04	-0.248				MMS22L	2.02E-03	0.213
	NCAPH	6.98E-03	0.186	PRKAR2A	2.64E-04	-0.244				MORN5	4.30E-03	-0.278
	NDRG2	1.11E-03	0.336	PRODH	7.76E-07	0.396				MRE11A	5.14E-03	0.32
	NEDD1	9.85E-03	0.357	PTPN13	5.22E-06	0.351				MSX1	2.64E-03	0.316
	NFE2L2	2.39E-03	0.305	PTTG1	6.12E-05	0.266				MT1H	5.62E-03	0.176
	NOD1	1.44E-03	0.227	PYROXD2	4.67E-04	0.287				MTMR12	3.06E-03	-0.334
	NOS1	2.69E-03	-0.349	QKI	1.56E-04	0.257				MUSTN1	1.96E-04	-0.246
	NOS1AP	6.98E-03	-0.304	RABGAP1	4.25E-04	-0.234				MXRA8	2.41E-03	0.25
	NOV	2.85E-03	0.232	RAC2	5.81E-07	0.393				MYBL2	4.20E-03	0.25
	NPY	3.07E-03	0.242	RAD51	5.90E-04	0.228				MYD88	6.63E-03	0.176

CATSKL, CATSKL + ADDL, ADDL (79)	CATSKL (425)	CATSKL_p-value	CATSKL_LogRatio(Base10)	CATSKL+ADDL (336)	CATSKL+ADDL_p-value	CATSKL+ADDL_LogRatio(Base10)	ADDL+CATSKL (135)	ADDL+CATSKL_p-value	ADDL+CATSKL_LogRatio(Base10)	ADDL (430)	ADDL_p-value	ADDL_LogRatio (Base 10)
	NR4A3	8.05E-04	-0.242	RASSF3	2.75E-04	0.284				MYLK	3.58E-03	-0.275
	NRARP	1.05E-03	0.342	RASSF4	1.85E-04	0.358				MYO6	3.66E-04	0.24
	NRXN1	9.78E-03	-0.176	RGCC	1.85E-06	0.333				NAB1	2.66E-03	-0.234
	NTRK2	5.75E-03	0.314	RGD1311564	3.11E-05	-0.386				NAPRT1	7.52E-03	0.19
	NUDT7	2.74E-03	0.065	RREB1	9.05E-07	-0.472				NCAPH	2.54E-03	0.201
	NXPH1	4.11E-03	0.373	RRM2	8.80E-05	0.518				NDE1	7.94E-04	0.255
	OAS2	3.64E-03	-0.234	S100A1	2.60E-05	0.282				NDRG2	5.65E-06	0.408
	Oas3	9.80E-03	0.202	S100A16	8.93E-07	0.346				NES	1.55E-03	0.221
	Olfr1043	5.32E-03	0.192	S100A4	3.43E-06	0.416				NFE2L2	2.30E-03	0.324
	Olfr1154 (includes others)	5.67E-03	0.186	S100B	2.34E-07	0.866				NGFR	7.73E-03	0.217
	Olfr1229	7.92E-03	0.153	S1PR1	6.57E-07	0.345				NMBR	2.08E-05	-0.312
	Olfr1262	3.56E-03	-0.318	SALL1	2.22E-05	0.353				NMU	7.84E-04	-0.248
	Olfr1347	2.72E-03	0.177	SALL3	1.37E-04	0.278				NOD1	1.60E-03	0.22
	Olfr456	3.53E-03	-0.305	SAMD9	4.11E-04	0.248				NOTCH1	6.52E-03	0.206
	Olfr490	7.75E-03	-0.019	SAMD9L	6.28E-06	0.31				NPAS4	2.66E-04	-0.254

CATSKL, CATSKL + ADDL, ADDL (79)	CATSKL (425)	CATSKL_p-value	CATSKL_LogRatio(Base10)	CATSKL+ADDL (336)	CATSKL+ADDL_p-value	CATSKL+ADDL_LogRatio(Base10)	ADDL+CATSKL (135)	ADDL+CATSKL_p-value	ADDL+CATSKL_LogRatio(Base10)	ADDL (430)	ADDL_p-value	ADDL_LogRatio (Base 10)
	Olfr559	6.84E-03	-0.236	SCRG1	7.22E-10	0.471				NQO1	4.70E-03	0.04
	Olfr597/Olfr598	5.34E-03	-0.508	SDC4	2.24E-09	0.452				NR3C1	8.41E-03	0.239
	Olr875/Olr876	2.91E-03	0.278	SELENBP1	5.02E-04	0.362				NRAP	4.93E-03	-0.212
	OPN1SW	1.67E-03	0.467	SEMA3E	2.18E-04	-0.275				NRARP	8.20E-03	0.3
	OPN4	5.66E-03	-0.178	SEPP1	1.04E-07	0.388				NRN1	9.66E-03	-0.167
	OR10X1	8.78E-03	-0.348	SEPT8	2.61E-06	0.322				NSD1	2.48E-03	-0.276
	OR1F1	5.76E-03	0.333	SERINC5	3.29E-05	0.302				NT5DC2	7.48E-03	0.178
	OR2T1	8.54E-03	-0.42	SFRP2	2.13E-06	0.372				NTRK2	5.91E-05	0.315
	OR4K5	9.02E-03	-0.316	SHCBP1	1.66E-05	0.392				NUP98	3.53E-03	-0.224
	PAPSS2	8.10E-05	0.824	SHOC2	3.04E-04	-0.236				NXPH1	1.09E-04	0.255
	PAX3	1.38E-03	-0.233	SHPK	9.96E-04	0.243				OLFML3	7.74E-03	0.17
	PCDHGA11	6.16E-03	-0.236	SIK1	2.68E-04	-0.238				Olfr1043	1.44E-03	0.222
	PDGFRA	1.51E-08	0.495	SLC13A3	5.59E-07	0.354				Olfr1154 (includes others)	5.95E-03	0.193
	PDPN	2.09E-05	0.399	SLC15A2	2.03E-06	0.576				Olfr1179	4.52E-03	-0.015
	PDS5A	5.40E-04	-0.244	SLC1A3	1.55E-07	0.372				Olfr1232	8.76E-03	0.618

CATSKL, CATSKL + ADDL, ADDL (79)	CATSKL (425)	CATSKL_p-value	CATSKL_LogRatio(Base10)	CATSKL+ADDL (336)	CATSKL+ADDL_p-value	CATSKL+ADDL_LogRatio(Base10)	ADDL+CATSKL (135)	ADDL+CATSKL_p-value	ADDL+CATSKL_LogRatio(Base10)	ADDL (430)	ADDL_p-value	ADDL_LogRatio (Base 10)
	PDZD8	2.99E-03	-0.214	SLC32A1	2.24E-04	0.242				Olfr159	9.74E-03	-0.276
	PHC3	2.26E-03	-0.298	SLC35D3	1.45E-04	0.288				Olfr397	6.00E-03	0.228
	PIK3CA	8.18E-04	-0.338	SLC38A3	2.38E-06	0.358				Olfr589	4.82E-03	0.275
	PIWIL2	3.80E-04	0.304	SLC38A7	3.59E-04	-0.232				OLIG1	3.28E-05	0.281
	PLAG1	7.56E-04	-0.219	SLC44A1	2.14E-04	0.534				OLIG2	1.07E-03	0.225
	PLAUR	9.74E-03	0.21	SLC6A1	3.34E-06	0.316				OR2D2	3.66E-03	0.21
	PLCD1	3.34E-03	0.322	SLC7A10	4.08E-04	0.304				OR8B12	1.35E-03	0.42
	PLD1	1.67E-03	0.249	SLCO1C1	2.38E-05	0.319				OSBPL5	8.49E-03	-0.202
	PLEKHD1	6.85E-03	0.289	SLK	5.39E-04	-0.256				OTOR	6.94E-03	0.209
	PLEKHG1	7.32E-03	-0.004	SMPDL3A	2.02E-04	0.41				PAX3	1.81E-03	0.238
	PLLP	6.89E-03	0.274	SOX10	2.85E-05	0.298				PCGF5	6.74E-03	-0.185
	PMEL	1.19E-05	0.393	SOX2	3.84E-05	0.284				PCSK6	9.02E-03	0.172
	PNMAL1	3.30E-03	-0.21	SOX8	1.01E-05	0.303				PDE12	6.38E-03	-0.253
	PNO1	8.60E-03	0.167	SP110	9.57E-04	0.246				Pde4dl1	6.33E-04	-0.273
	POGK	9.28E-03	-0.047	SPAG5	1.10E-04	0.281				PDGFB	4.39E-03	-0.488

CATSKL, CATSKL + ADDL, ADDL (79)	CATSKL (425)	CATSKL_p-value	CATSKL_LogRatio(Base10)	CATSKL+ADDL (336)	CATSKL+ADDL_p-value	CATSKL+ADDL_LogRatio(Base10)	ADDL+CATSKL (135)	ADDL+CATSKL_p-value	ADDL+CATSKL_LogRatio(Base10)	ADDL (430)	ADDL_p-value	ADDL_LogRatio (Base 10)
	PPAP2B	9.80E-04	0.301	SPARC	9.32E-04	0.214				PDGFRA	6.60E-05	0.38
	PPIC	2.39E-03	0.243	SPARCL1	1.30E-07	0.379				PDGFRB	1.31E-04	0.706
	PRC1	8.22E-03	0.215	SPC25	2.65E-04	0.246				PDPN	3.25E-05	0.386
	PRIMA1	7.31E-03	0.311	SPP1	3.82E-05	0.406				PERP	8.52E-03	-0.171
	PRKACB	3.88E-03	-0.26	STAT1	4.34E-04	0.234				PKIB	2.54E-03	0.2
	PRKAR2A	4.38E-03	-0.328	SUCLG2	8.98E-07	0.35				PLA2G16	2.11E-03	0.31
	PRKCD	2.08E-03	0.218	Syna	3.38E-04	-0.26				PLCB4	8.46E-04	0.25
	PRM2	1.05E-03	-0.222	TACC1	1.61E-04	-0.284				PLD1	3.34E-03	0.241
	PRODH	2.14E-04	0.382	TCF7L2	6.64E-12	0.558				PLEKHD1	2.04E-03	0.332
	PRSS23	6.07E-03	0.211	TEAD2	8.31E-05	0.29				PLOD1	5.83E-03	0.179
	Prss32	7.86E-03	0.01	TFAP2E	5.95E-05	0.311				PNMA3	3.36E-03	-0.26
	PTPN13	5.43E-03	0.225	TIMELESS	5.16E-04	0.28				PNOC	8.54E-04	-0.218
	PTPN6	8.00E-03	0.238	TLE6	6.54E-04	0.238				PON2	7.47E-04	0.26
	PYROXD2	3.08E-04	0.327	TLR6	2.58E-05	0.404				POU1F1	6.88E-03	0.196
	RAB13	1.89E-03	0.248	TMBIM1	3.31E-09	0.456				POU4F3	6.53E-04	-0.288

CATSKL, CATSKL + ADDL, ADDL (79)	CATSKL (425)	CATSKL_p-value	CATSKL_LogRatio(Base10)	CATSKL+ADDL (336)	CATSKL+ADDL_p-value	CATSKL+ADDL_LogRatio(Base10)	ADDL+CATSKL (135)	ADDL+CATSKL_p-value	ADDL+CATSKL_LogRatio(Base10)	ADDL (430)	ADDL_p-value	ADDL_LogRatio (Base 10)
	RAC2	7.05E-09	0.502	TMEM100	1.11E-07	0.392				PPIC	1.96E-04	0.288
	RAMP3	8.44E-03	0.174	TMEM178B	3.44E-04	-0.237				PPM1L	6.80E-03	-0.202
	RANBP2	2.22E-03	0.052	TMEM229A	4.89E-04	0.246				PPP1R3C	2.34E-03	0.245
	RAPGEF6	2.28E-03	0.046	TNS1	4.65E-06	0.318				PRC1	2.63E-03	0.284
	RFX5	1.84E-04	-0.255	TNS3	1.64E-06	0.328				PRODH	3.52E-04	0.361
	RGCC	6.35E-04	0.332	TOP2A	1.25E-08	0.422				PRSS27	5.33E-03	-0.249
	RIMS2	3.44E-03	-0.207	TPX2	2.00E-05	0.375				PTPN13	7.61E-05	0.311
	RLBP1	3.12E-03	0.234	TRAF3IP2	7.91E-05	0.312				PTPN22	4.90E-03	-0.072
	RNF141	8.82E-04	-0.234	TRIL	1.58E-09	0.448				PYGL	6.52E-03	0.246
	RPGRIP1L	3.14E-03	-0.252	TRIM47	3.19E-05	0.306				QKI	4.81E-03	0.209
	RREB1	4.48E-04	-0.32	TSPAN12	6.42E-04	0.224				RAB20	5.00E-03	-0.182
	RRM2	3.51E-04	0.547	TTK	1.86E-05	0.32				RAD51AP1	9.21E-03	0.169
	S100A16	8.15E-03	0.282	TXNIP	9.40E-05	0.332				REM2	1.73E-03	-0.226
	S100B	3.09E-03	0.614	UBE2T	4.03E-05	0.354				RETN	8.76E-03	0.209
	S1PR1	3.96E-04	0.298	UNC13A	1.44E-04	-0.25				RGCC	3.22E-03	0.289

CATSKL, CATSKL + ADDL, ADDL (79)	CATSKL (425)	CATSKL_p-value	CATSKL_LogRatio(Base10)	CATSKL+ADDL (336)	CATSKL+ADDL_p-value	CATSKL+ADDL_LogRatio(Base10)	ADDL+CATSKL (135)	ADDL+CATSKL_p-value	ADDL+CATSKL_LogRatio(Base10)	ADDL (430)	ADDL_p-value	ADDL_LogRatio (Base 10)
	SALL1	2.79E-03	0.04	VAMP8	4.10E-04	0.342				RGS2	7.89E-03	-0.168
	SALL3	9.61E-03	0.202	VCAM1	2.72E-10	0.477				RRAD	5.27E-03	-0.188
	SAMD9	1.40E-03	0.271	VEGFA	9.64E-04	-0.284				RREB1	1.65E-04	-0.379
	SCN8A	6.08E-03	-0.182	WDR16	1.64E-06	0.361				RRM2	5.14E-05	0.29
	SCRG1	1.41E-05	0.393	WIPF1	7.74E-04	0.254				S100A1	1.40E-03	0.271
	SDC4	1.11E-03	0.374	WNT6	1.44E-04	-0.254				S100A16	2.66E-04	0.31
	SELENBP1	3.77E-03	0.314	XPO6	8.74E-04	-0.276				S100B	4.19E-04	0.324
	SEMA3D	5.81E-03	-0.166	ZBTB38	9.54E-04	-0.226				S1PR1	8.95E-03	0.227
	SEMA5B	8.99E-03	0.217	ZC3H13	4.48E-05	-0.276				SALL1	2.87E-05	0.43
	SEPP1	9.10E-03	0.274	ZCCHC24	2.08E-07	0.464				SALL3	5.00E-04	0.316
	SEPT8	2.18E-03	0.248	ZNF23	4.66E-04	-0.231				SAMD9L	2.53E-04	0.258
	SERINC5	6.21E-03	0.227							SARDH	3.59E-03	0.222
	SFRP2	3.39E-05	0.342							SCRG1	5.80E-04	0.328
	SFRP4	7.22E-03	0.302							SDC4	1.72E-03	0.316
	SHCBP1	6.92E-03	0.194							SEC16B	1.82E-03	-0.213

CATSKL, CATSKL + ADDL, ADDL (79)	CATSKL (425)	CATSKL_p-value	CATSKL_LogRatio(Base10)	CATSKL+ADDL (336)	CATSKL+ADDL_p-value	CATSKL+ADDL_LogRatio(Base10)	ADDL+CATSKL (135)	ADDL+CATSKL_p-value	ADDL+CATSKL_LogRatio(Base10)	ADDL (430)	ADDL_p-value	ADDL_LogRatio (Base 10)
	SKA1	4.58E-04	0.386							SEMA3E	1.93E-03	-0.248
	SLAMF9	2.39E-05	0.816							SEMA7A	6.93E-04	-0.22
	SLC11A1	5.60E-03	0.483							SEPP1	1.38E-04	0.308
	SLC12A1	9.56E-03	-0.192							SEPT8	5.97E-04	0.24
	SLC13A3	3.56E-04	0.35							SERINC5	2.72E-03	0.194
	SLC15A2	1.83E-03	0.453							SERPINB2	4.77E-06	-0.511
	SLC16A8	9.60E-03	-0.194							SERPINH1	4.26E-03	0.22
	SLC18A1	1.18E-03	-0.218							SERTAD1	2.24E-03	-0.2
	SLC1A3	8.60E-03	0.284							SH3BP4	6.64E-03	0.18
	SLC20A2	6.54E-03	0.188							SH3BP5L	4.40E-03	-0.312
	SLC25A18	3.50E-03	0.219							SHANK2	6.61E-03	-0.283
	SLC30A3	6.41E-03	0.196							SIK1	5.71E-03	-0.224
	SLC32A1	8.11E-03	0.219							SLAMF9	8.98E-03	0.528
	SLC35D3	2.24E-03	0.266							SLC1A2	6.75E-03	0.229
	SLC39A14	3.04E-03	-0.196							SLC1A3	2.05E-04	0.321

CATSKL, CATSKL + ADDL, ADDL (79)	CATSKL (425)	CATSKL_p-value	CATSKL_LogRatio(Base10)	CATSKL+ADDL (336)	CATSKL+ADDL_p-value	CATSKL+ADDL_LogRatio(Base10)	ADDL+CATSKL (135)	ADDL+CATSKL_p-value	ADDL+CATSKL_LogRatio(Base10)	ADDL (430)	ADDL_p-value	ADDL_LogRatio (Base 10)
	Slc7a12	1.08E-03	-0.216							SLC22A3	6.01E-03	0.257
	SLC8A1	4.29E-04	-0.238							SLC27A5	6.15E-04	0.355
	SLC9A3R1	1.04E-03	0.258							SLC32A1	1.26E-04	0.252
	SLCO1C1	7.95E-03	0.27							SLC35G2	1.34E-03	0.212
	SLK	7.40E-03	-0.256							SLC38A3	6.30E-03	0.208
	SMPDL3A	8.85E-04	0.324							SLC40A1	3.36E-04	-0.242
	SOX10	8.40E-04	0.318							SLC6A1	4.36E-04	0.274
	SP110	6.04E-04	0.258							SLC7A10	8.70E-03	0.27
	Spag11a	4.89E-04	-0.262							SLC7A9	9.28E-04	0.361
	SPARCL1	4.62E-03	0.393							SLCO4C1	1.23E-03	-0.403
	SPN	9.69E-03	0.447							SMPDL3A	9.30E-04	0.334
	SPP1	3.09E-04	-0.182							SNX15	3.34E-03	-0.103
	SRSF1	9.73E-03	0.165							SOX10	3.37E-03	0.211
	SSH2	1.01E-03	-0.228							SOX2	2.65E-03	0.205
	Ssty1 (includes others)	8.15E-03	-0.292							SOX8	8.61E-04	0.228

CATSKL, CATSKL + ADDL, ADDL (79)	CATSKL (425)	CATSKL_p-value	CATSKL_LogRatio(Base10)	CATSKL+ADDL (336)	CATSKL+ADDL_p-value	CATSKL+ADDL_LogRatio(Base10)	ADDL+CATSKL (135)	ADDL+CATSKL_p-value	ADDL+CATSKL_LogRatio(Base10)	ADDL (430)	ADDL_p-value	ADDL_LogRatio (Base 10)
	ST8SIA4	5.22E-03	-0.3							SP110	1.68E-03	0.326
	STOX2	7.38E-03	-0.188							SPAG7	5.36E-03	0.206
	Sult2a2	1.82E-03	0.662							SPARC	1.66E-04	0.288
	SUSD3	8.60E-03	-0.181							SPARCL1	6.20E-05	0.356
	SYCP2	4.48E-03	-0.214							Spata31d1d	6.77E-03	-0.233
	TAGLN2	6.34E-03	0.357							SPINT1	9.40E-03	-0.188
	TANC2	6.16E-03	-0.192							SPP1	1.20E-04	0.502
	TAS2R10	9.89E-05	-0.694							SS18	9.46E-03	0.176
	TAS2R20	4.82E-03	-0.2							ST14	4.20E-03	0.301
	TBC1D5	8.36E-03	-0.192							ST6GALNAC3	9.23E-04	0.004
	TBR1	6.70E-03	0.198							ST8SIA1	5.40E-03	-0.202
	TCF7L2	2.05E-04	0.357							STARD5	9.68E-03	-0.284
	TCTEX1D1	5.31E-03	0.092							STAT1	4.36E-04	0.234
	TGIF2	2.11E-03	0.394							SUCLG2	3.19E-03	0.226
	TGM4	4.30E-03	-0.082							SUCO	4.42E-03	-0.192

CATSKL, CATSKL + ADDL, ADDL (79)	CATSKL (425)	CATSKL_p-value	CATSKL_LogRatio(Base10)	CATSKL+ADDL (336)	CATSKL+ADDL_p-value	CATSKL+ADDL_LogRatio(Base10)	ADDL+CATSKL (135)	ADDL+CATSKL_p-value	ADDL+CATSKL_LogRatio(Base10)	ADDL (430)	ADDL_p-value	ADDL_LogRatio (Base 10)
	TIMELESS	1.69E-03	0.246							SULF2	4.50E-03	0.187
	TLR6	4.64E-05	0.401							SYN3	2.78E-03	-0.252
	TMEM100	5.20E-04	0.344							SYNGR2	9.84E-03	0.014
	TMEM176B	7.02E-04	0.324							SYT10	1.95E-03	-0.225
	TMEM178B	7.72E-03	-0.212							TAC1	2.64E-03	-0.195
	TMEM229A	2.01E-03	0.252							TCF15	4.48E-03	0.213
	TMEM52B	1.18E-06	-0.372							TCF7L2	5.40E-04	0.34
	TNC	2.12E-04	0.25							TEAD2	7.61E-04	0.238
	TNRC6B	7.43E-03	-0.211							TFAP2E	3.60E-07	0.42
	TOP2A	3.38E-03	0.254							TGFBI	4.66E-03	-0.318
	Trib2	7.43E-03	0.193							THBS2	7.17E-04	-0.27
	TRIM47	2.35E-03	0.224							TIMELESS	9.28E-03	0.222
	TSNAXIP1	5.70E-03	-0.338							TIMP4	2.33E-05	0.356
	TSPAN12	6.52E-03	0.217							TM4SF1	6.22E-03	-0.222
	TTC36	2.41E-03	-0.218							TMC5	7.42E-03	0.287

CATSKL, CATSKL + ADDL, ADDL (79)	CATSKL (425)	CATSKL_p-value	CATSKL_LogRatio(Base10)	CATSKL+ADDL (336)	CATSKL+ADDL_p-value	CATSKL+ADDL_LogRatio(Base10)	ADDL+CATSKL (135)	ADDL+CATSKL_p-value	ADDL+CATSKL_LogRatio(Base10)	ADDL (430)	ADDL_p-value	ADDL_LogRatio (Base 10)
	TTK	3.66E-04	0.259							TMEM100	3.84E-04	0.284
	TUBA1A	6.92E-03	0.215							TMEM200A	8.68E-03	-0.186
	TWIST1	1.76E-03	0.282							TMEM243	9.61E-03	0.185
	TXLNB	7.72E-03	0.198							TMOD1	1.10E-03	-0.225
	TXNIP	5.95E-06	0.338							TNFRSF11B	1.40E-03	-0.284
	UBE2T	7.34E-05	0.326							TNFRSF12A	6.41E-03	-0.174
	UNC13A	3.19E-03	-0.236							TNS1	7.19E-03	0.217
	UNCX	2.30E-04	-0.244							TNS3	1.96E-03	0.2
	VAMP8	5.08E-06	0.46							TOP2A	4.54E-03	0.242
	VCAM1	4.83E-05	0.416							TRIL	1.17E-04	0.368
	VEGFA	2.95E-03	-0.226							TSPAN9	8.54E-03	-0.18
	Vof16	6.51E-04	-0.291							TUBA1A	2.92E-03	0.195
	Vom2r48	4.59E-03	0.24							TXNIP	3.16E-07	0.464
	Vom2r9	1.94E-03	-0.34							UAP1	2.33E-03	-0.209
	WAPAL	5.41E-03	-0.202							UBE2T	1.67E-03	0.27

CATSKL, CATSKL + ADDL, ADDL (79)	CATSKL (425)	CATSKL_p-value	CATSKL_LogRatio(Base10)	CATSKL+ADDL (336)	CATSKL+ADDL_p-value	CATSKL+ADDL_LogRatio(Base10)	ADDL+CATSKL (135)	ADDL+CATSKL_p-value	ADDL+CATSKL_LogRatio(Base10)	ADDL (430)	ADDL_p-value	ADDL_LogRatio (Base 10)
	WDR16	4.35E-04	0.334							UCN	1.25E-03	-0.208
	WIPF1	3.10E-03	0.236							UGT1A6	5.28E-03	0.194
	Wnk1	5.29E-03	-0.32							USP53	9.06E-03	-0.171
	WNT16	3.44E-03	-0.188							UTP15	7.42E-03	-0.224
	WNT6	2.04E-06	-0.332							UTP20	2.06E-03	-0.267
	ZBTB38	2.50E-03	-0.208							VAMP8	6.85E-03	0.741
	ZC3H13	1.81E-03	-0.214							VCAM1	1.68E-05	0.413
	ZCCHC24	1.02E-04	0.376							VCL	3.78E-03	-0.215
	ZNF445	8.10E-03	-0.181							Vcsa1/Vcsa2	4.62E-04	-0.311
	ZNF624	8.30E-03	-0.295							WDR16	9.37E-04	0.24
										ZBTB3	2.00E-03	-0.149
										ZCCHC24	6.20E-03	0.313
										ZFHX4	3.16E-03	-0.352
										Zim1	9.58E-03	-0.202
										ZNF219	7.15E-03	-0.003

4.6 References

Brewer GJ (2010) Why vitamin E therapy fails for treatment of Alzheimer's disease. *Journal of Alzheimer's disease : JAD* **19**:27-30.

Brewer GJ and Price PJ (1996) Viable cultured neurons in ambient carbon dioxide and hibernation storage for a month. *Neuroreport* **7**:1509-1512.

Brewer GJ, Torricelli JR, Evege EK and Price PJ (1993) Optimized survival of hippocampal neurons in B27-supplemented Neurobasal, a new serum-free medium combination. *Journal of neuroscience research* **35**:567-576.

Chance B (1948) The enzyme-substrate compounds of catalase and peroxides. *Nature* **161**:914-917.

Cimini A, Benedetti E, D'Angelo B, Cristiano L, Falone S, Di Loreto S, Amicarelli F and Ceru MP (2009) Neuronal response of peroxisomal and peroxisome-related proteins to chronic and acute Abeta injury. *Current Alzheimer research* **6**:238-251.

Droge W (2002) Free radicals in the physiological control of cell function. *Physiological reviews* **82**:47-95.

Fanelli F, Sepe S, D'Amelio M, Bernardi C, Cristiano L, Cimini A, Cecconi F, Ceru MP and Moreno S (2013) Age-dependent roles of peroxisomes in the hippocampus of a transgenic mouse model of Alzheimer's disease. *Molecular neurodegeneration* **8**:8.

Garcia-Escudero V, Martin-Maestro, P., Perry, G., and Avila, J. (2013) Deconstructing Mitochondrial Dysfunction in Alzheimer Disease. *Oxidative Medicine and Cellular Longevity* **2013**:13.

Giordano CR, Mueller KL, Terlecky LJ, Krentz KA, Bollig-Fischer A, Terlecky SR and Boerner JL (2012) A targeted enzyme approach to sensitization of tyrosine kinase inhibitor-resistant breast cancer cells. *Experimental Cell Research* **318**:2014-2021.

Giordano CR and Terlecky SR (2012) Peroxisomes, cell senescence, and rates of aging. *Biochimica et biophysica acta* **1822**:1358-1362.

Hirai K, Aliev G, Nunomura A, Fujioka H, Russell RL, Atwood CS, Johnson AB, Kress Y, Vinters HV, Tabaton M, Shimohama S, Cash AD, Siedlak SL, Harris PLR, Jones PK, Petersen RB, Perry G and Smith MA (2001) Mitochondrial Abnormalities in Alzheimer's Disease. *The Journal of Neuroscience* **21**:3017-3023.

Holtzman DM, Mandelkow E and Selkoe DJ (2012) Alzheimer disease in 2020. *Cold Spring Harbor perspectives in medicine* **2**.

Hsieh H-L and Yang C-M (2013) Role of Redox Signaling in Neuroinflammation and Neurodegenerative Diseases. *BioMed Research International* **2013**:18.

Huang Y and Mucke L (2012) Alzheimer mechanisms and therapeutic strategies. *Cell* **148**:1204-1222.

Huybrechts SJ, Van Veldhoven PP, Brees C, Mannaerts GP, Los GV and Fransen M (2009) Peroxisome dynamics in cultured mammalian cells. *Traffic (Copenhagen, Denmark)* **10**:1722-1733.

Inestrosa NC, Carvajal FJ, Zolezzi JM, Tapia-Rojas C, Serrano F, Karmelic D, Toledo EM, Toro A, Toro J and Santos MJ (2013) Peroxisome proliferators reduce spatial memory impairment, synaptic failure, and neurodegeneration in brains of

a double transgenic mice model of Alzheimer's disease. *Journal of Alzheimer's disease : JAD* **33**:941-959.

Ivashchenko O, Van Veldhoven PP, Brees C, Ho YS, Terlecky SR and Fransen M (2011) Intraperoxisomal redox balance in mammalian cells: oxidative stress and interorganellar cross-talk. *Molecular biology of the cell* **22**:1440-1451.

Klein WL (2002) Aβ toxicity in Alzheimer's disease: globular oligomers (ADDLs) as new vaccine and drug targets. *Neurochemistry International* **41**:345-352.

Koepke JI, Nakrieko KA, Wood CS, Boucher KK, Terlecky LJ, Walton PA and Terlecky SR (2007) Restoration of peroxisomal catalase import in a model of human cellular aging. *Traffic (Copenhagen, Denmark)* **8**:1590-1600.

Koepke JI, Wood CS, Terlecky LJ, Walton PA and Terlecky SR (2008) Progeric effects of catalase inactivation in human cells. *Toxicology and applied pharmacology* **232**:99-108.

Kou J, Kovacs GG, Hoftberger R, Kulik W, Brodde A, Forss-Petter S, Honigschnabl S, Gleiss A, Brugger B, Wanders R, Just W, Budka H, Jungwirth S, Fischer P and Berger J (2011) Peroxisomal alterations in Alzheimer's disease. *Acta neuropathologica* **122**:271-283.

Legakis JE, Koepke JI, Jedeszko C, Barlaskar F, Terlecky LJ, Edwards HJ, Walton PA and Terlecky SR (2002) Peroxisome senescence in human fibroblasts. *Molecular biology of the cell* **13**:4243-4255.

Lovell MA, Xie C and Markesbery WR (1998) Decreased glutathione transferase activity in brain and ventricular fluid in Alzheimer's disease. *Neurology* **51**:1562-1566.

Lue LF, Kuo YM, Roher AE, Brachova L, Shen Y, Sue L, Beach T, Kurth JH, Rydel RE and Rogers J (1999) Soluble amyloid beta peptide concentration as a predictor of synaptic change in Alzheimer's disease. *The American journal of pathology* **155**:853-862.

McLean CA, Cherny RA, Fraser FW, Fuller SJ, Smith MJ, Beyreuther K, Bush AI and Masters CL (1999) Soluble pool of Abeta amyloid as a determinant of severity of neurodegeneration in Alzheimer's disease. *Annals of neurology* **46**:860-866.

Persson T, Popescu BO and Cedazo-Minguez A (2014) Oxidative Stress in Alzheimer's Disease: Why Did Antioxidant Therapy Fail? *Oxidative Medicine and Cellular Longevity* **2014**:11.

Petersen RC, Thomas RG, Grundman M, Bennett D, Doody R, Ferris S, Galasko D, Jin S, Kaye J, Levey A, Pfeiffer E, Sano M, van Dyck CH and Thal LJ (2005) Vitamin E and donepezil for the treatment of mild cognitive impairment. *The New England journal of medicine* **352**:2379-2388.

Polidori MC and Nelles G (2013) Antioxidant Clinical Trials in Mild Cognitive Impairment and Alzheimer's Disease - Challenges and Perspectives. *Current pharmaceutical design*.

Price M, Terlecky SR and Kessel D (2009) A role for hydrogen peroxide in the pro-apoptotic effects of photodynamic therapy. *Photochemistry and photobiology* **85**:1491-1496.

Santos MJ, Quintanilla RA, Toro A, Grandy R, Dinamarca MC, Godoy JA and Inestrosa NC (2005) Peroxisomal proliferation protects from beta-amyloid neurodegeneration. *The Journal of biological chemistry* **280**:41057-41068.

Saraiva MJ, Magalhaes J, Ferreira N and Almeida MR (2012) Transthyretin deposition in familial amyloidotic polyneuropathy. *Current medicinal chemistry* **19**:2304-2311.

Selkoe DJ (2011) Alzheimer's disease. *Cold Spring Harbor perspectives in biology* **3**.

Terlecky SR (2002) In vitro analysis of peroxisomal protein import. *Current protocols in cell biology / editorial board, Juan S Bonifacino [et al]* **Chapter 11**:Unit 11 15.

Undyala V, Terlecky SR and Vander Heide RS (2011) Targeted intracellular catalase delivery protects neonatal rat myocytes from hypoxia-reoxygenation and ischemia-reperfusion injury. *Cardiovascular pathology : the official journal of the Society for Cardiovascular Pathology* **20**:272-280.

Vainshtein BK, Melik-Adamyan WR, Barynin VV, Vagin AA and Grebenko AI (1981) Three-dimensional structure of the enzyme catalase. *Nature* **293**:411-412.

Walton PA and Pizzitelli M (2012) Effects of peroxisomal catalase inhibition on mitochondrial function. *Frontiers in physiology* **3**:108.

Wang B, Van Veldhoven PP, Brees C, Rubio N, Nordgren M, Apanasets O, Kunze M, Baes M, Agostinis P and Fransen M (2013) Mitochondria are targets for peroxisome-derived oxidative stress in cultured mammalian cells. *Free radical biology & medicine* **65**:882-894.

Wang J, Dickson DW, Trojanowski JQ and Lee VM (1999) The levels of soluble versus insoluble brain Abeta distinguish Alzheimer's disease from normal and pathologic aging. *Experimental neurology* **158**:328-337.

Watson J (2013) Oxidants, antioxidants and the current incurability of metastatic cancers. *Open biology* **3**:120144.

Wood CS, Koepke JI, Teng H, Boucher KK, Katz S, Chang P, Terlecky LJ, Papanayotou I, Walton PA and Terlecky SR (2006) Hypocatalasemic fibroblasts accumulate hydrogen peroxide and display age-associated pathologies. *Traffic (Copenhagen, Denmark)* **7**:97-107.

Xie H, Guan J, Borrelli LA, Xu J, Serrano-Pozo A and Bacskai BJ (2013) Mitochondrial alterations near amyloid plaques in an Alzheimer's disease mouse model. *The Journal of neuroscience : the official journal of the Society for Neuroscience* **33**:17042-17051.

Young CN, Koepke JI, Terlecky LJ, Borkin MS, Boyd Savoy L and Terlecky SR (2008) Reactive oxygen species in tumor necrosis factor-alpha-activated primary human keratinocytes: implications for psoriasis and inflammatory skin disease. *The Journal of investigative dermatology* **128**:2606-2614.

CHAPTER 5: Conclusions

Published: Terlecky, SR, Terlecky LJ, and **Giordano CR**. Peroxsiomes, Oxidative stress, and Inflammaton. (2012) *World J of Biol Chem* **3**: 93-97.

5.1 Abstract

Peroxisomes are intracellular organelles mediating a wide variety of biosynthetic and biodegradative reactions. Included among these are the metabolism of hydrogen peroxide and other reactive species, molecules whose levels help define the oxidative state of cells. Loss of oxidative equilibrium in cells of tissues and organs potentiates inflammatory responses which can ultimately trigger human disease. In summary there is significant evidence for connections between peroxisome function, oxidative stress, and inflammation in the context of human health and degenerative disease.

5.2 Oxidative stress, inflammation, and degenerative disease

The peroxisome's handling of hydrogen peroxide, a reactive oxygen species produced by oxidative reactions occurs within the organelle. Under most conditions, hydrogen peroxide is produced and immediately processed by the organelle's resident marker enzyme, catalase. However, conditions exist in which the balance of hydrogen peroxide production is upset, and the potentially toxic metabolite accumulates. Another pivotal function carried out by peroxisomes is the ability of the organelle to break down the arachidonic acid derivatives known as eicosanoids. Eicosanoids are critically important signaling molecules which exert tremendous control over inflammatory reactions.

Among the arachidonic acid derivatives under consideration here are prostaglandins, thromboxanes, leukotrienes, and prostacyclins. These compounds elicit broad ranging inflammatory reactions depending on concentration and location. The important point is that through their ability to be metabolized by peroxisomes - organelle function is linked to the inflammatory response. Lastly, docosahexaenoic acids, peroxisomally produced omega-3 fatty acids, are the pivotal precursors of resolvins ("resolution-phase interaction products"), maresins ("macrophage mediator in resolving inflammation"), and protectins (formerly called "neuroprotectins") (Ariel et al., 2007, Das, 2010, Serhan et al., 2008). These molecules possess potent anti-inflammatory, inflammatory resolving, and immunoregulatory activities.

Oxidative stress and inflammation are inextricably tied processes. Chronic inflammation is associated with elevated ROS levels; anti-inflammatory cascades are linked to diminished ROS concentrations. And the converse is true - elevated oxidative stress triggers inflammation, whereas redox balance inhibits the cellular response. Thus, oxidative stress and inflammation may be seen as both causes and consequences of cellular pathology. We suggest here that through the peroxisome's role in cellular redox balance, as well as its ability to synthesize various anti-inflammatory molecules and degrade pro-inflammatory mediators, the organelle is part of a critical network controlling cell function and organismal well-being (Figure 5.1). What is surprising is that these vital roles for the organelle have been unappreciated for so long.

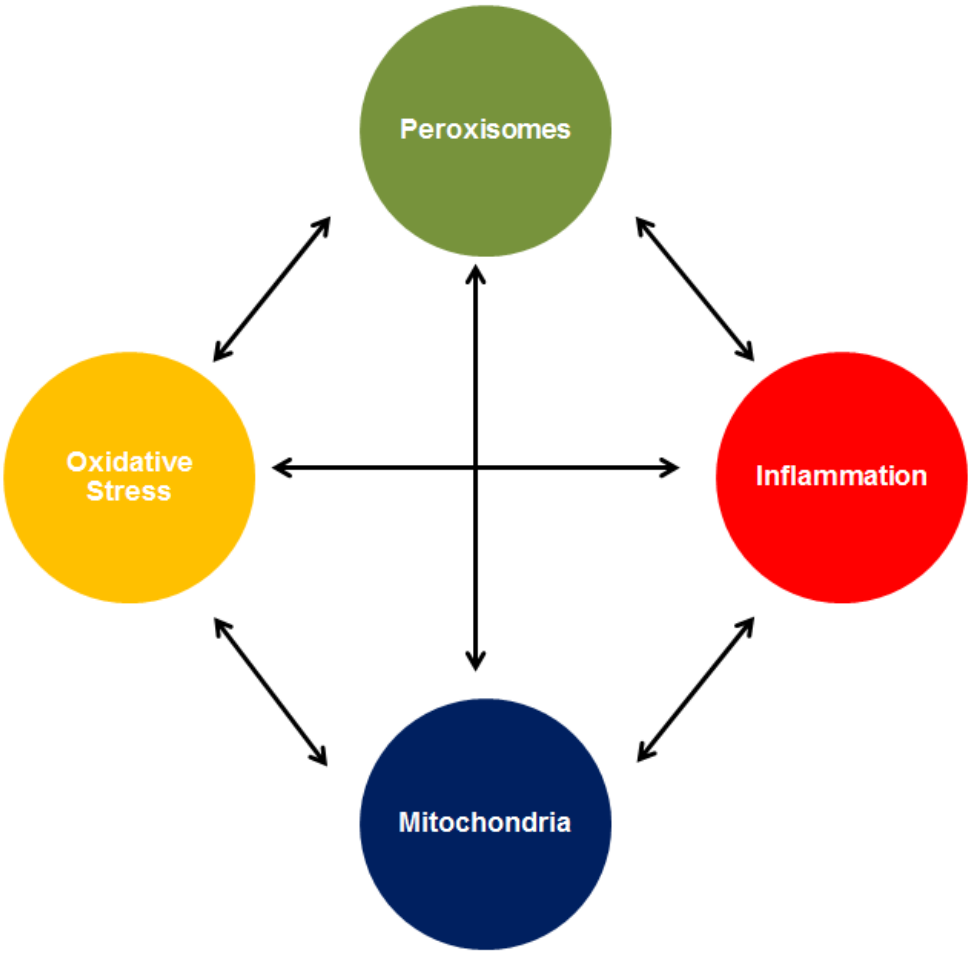

Figure 5.1. Emergent connections between peroxisomes and cellular metabolism. Image appears in *World J Biol Chem*. 2012 by Terlecky, SR, Terlecky LJ, and Giordano, CR.

It has been previously argued that peroxisomes function as important communication centers - integrating signals from various sources to alter their own metabolism as well as that of other organelles, and to initiate or inhibit cellular aging programs (Titorenko and Terlecky, 2011). A major redox-based interplay exists between peroxisomes and mitochondria, a relationship that warrants additional analysis. Several reports indicate that altering peroxisomal redox balance triggers oxidative stress in mitochondria - resulting in ROS production, diminished membrane potential, and compromised organelle function (Koepke et al., 2008; Ivashchenko et al., 2011). Obviously, the cellular consequences of diminished mitochondrial function are profound. However, restoring peroxisomal redox balance - for example by supplementing (peroxisomal) catalase, renews mitochondria (Koepke et al., 2007). Mitochondria repolarize and aging cells delay appearance of senescence markers. Increasing oxidative stress in peroxisomes is “progeric” on cells; eliminating the stress revives them.

As summarized in Chapter 1 this approach of targeted antioxidant prophylaxis has also been successful in disease models. For example, in a human cell model for psoriasis, catalase supplementation reduces expression of the inflammatory cytokine, TNF-α, that is thought to be a major initiator of the chronic inflammation seen in psoriatic tissue (Young et al., 2008). Similarly, in *in vitro* (Undyala et al., 2011) and *in vivo* (Terlecky, unpublished) models of ischemia-reperfusion (heart attack), damage to cardiomyocytes and cardiac tissue is dramatically inhibited. Enhancing peroxisomal catalase also reduces inflammatory cytokine production in appropriately challenged human fibroblasts (Terlecky, unpublished). The work presented in this dissertation

describes, (i) a breast cancer model where the drug sensitizes otherwise resistant human breast cancer cells to the TKI, gefitinib (Chapter 2) (Giordano et al., 2012), (ii) a diabetic retinopathy model, where CAT-SKL significantly reverses compromised retinal function (Chapter 3), and (iii) a rat cell model of Alzheimer's disease, where β-amyloid peptide-induced neuronal toxicity is significantly reduced (Chapter 4). The evidence is mounting - peroxisome redox balance is a major determinant of cell stress and the presence or absence of cell pathology. Perhaps it is not surprising then that epidemiological studies suggest a very strong link exists between diminishing cellular catalase levels and the onset of degenerative disease.

5.2 Conclusions

The treatment of human degenerative disease requires, in our view, a distance from the reductionist and extremely focused approaches long applied by the scientific and medical communities. Rather, we suggest a broader attack, targeting oxidative stress, chronic inflammation, and the resultant pro-aging programs initiated in cells and tissues (Figure 5.2). There are many ways to approach this - the direction focused on here is the peroxisome. The organelle plays a key role in controlling inflammation and maintaining oxidative balance in cells. By targeting peroxisomes -perhaps a number of devastating diseases could be more effectively treated or prevented. We suggest enhancing peroxisome function and maintaining the organelle's redox balance by all means possible. Mitochondrial integrity/activity will be maintained or enhanced, oxidative stress will be reduced, inflammation will be held in check, and cellular pathology will be all but eliminated. Oxidative stress and resultant damage to intracellular constituents is critical to the development of disease. This analysis of a

potentially powerful therapeutic has further established the peroxisome as a major site of cellular ROS regulation and critical metabolic control involved in the protection against a number of degenerative diseases.

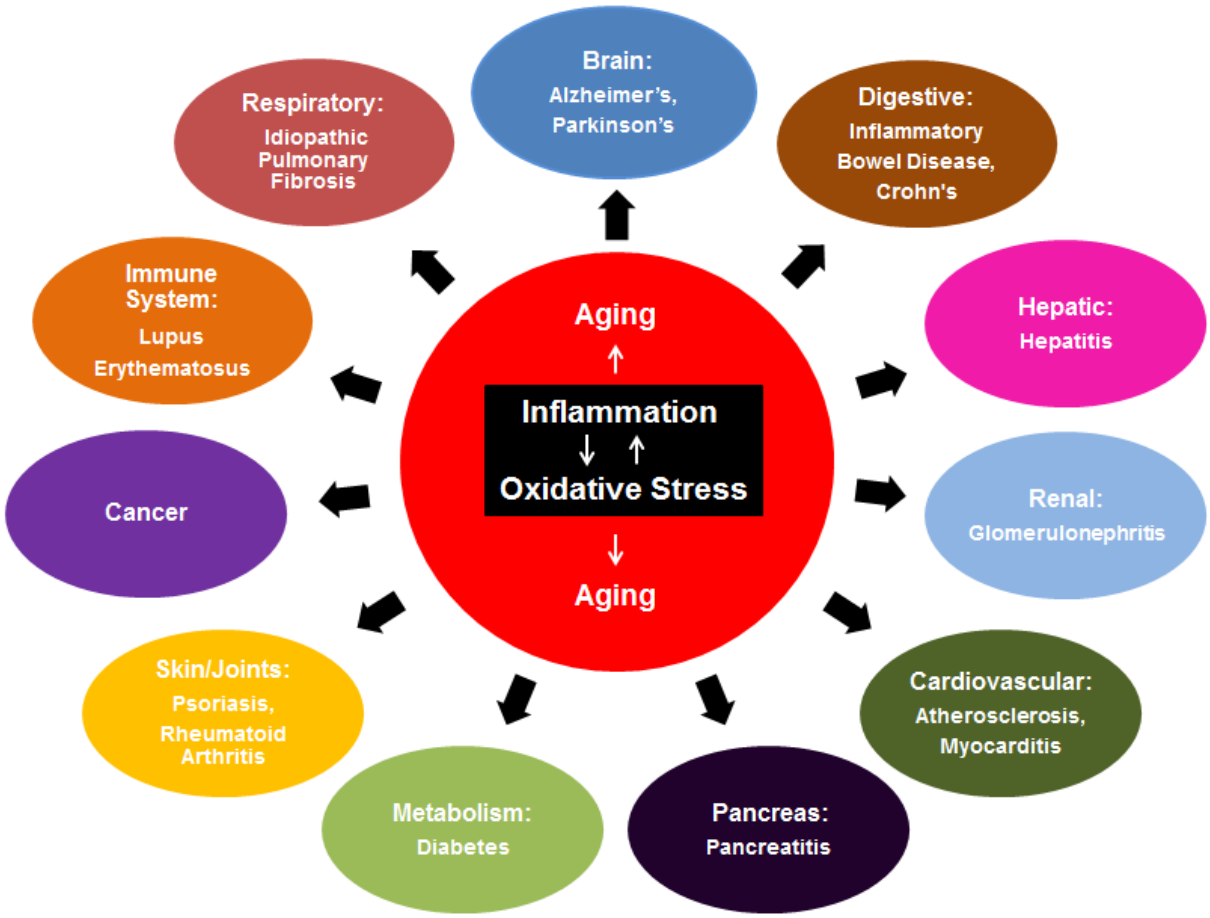

Figure 5.2. Inflammation, oxidative stress, and aging as driving forces of human disease. Listed here are human diseases in which the emergent connections displayed in Figure 1, most importantly oxidative stress and inflammation, are thought to trigger a pro-aging program in cells and initiate or progress pathology. Image appears in *World J Biol Chem*. 2012 by Terlecky, SR, Terlecky LJ, and Giordano, CR.

5.3 References

Ariel A, Serhan CN (2007) Resolvins and protectins in the termination program of acute inflammation. *TRENDS in Immunology* **28**:176-183.

Das UN (2010) Lipoxins, resolivns, protectins, maresins, and nitrolipids: connecting lipids, inflammation, and cardiovascular disease risk. *Curr Cardio Risk Rep* **4**:24-31.

Giordano CR, Mueller KL, Terlecky LJ, Krentz KA, Bollig-Fischer A, Terlecky SR and Boerner JL (2012) A targeted enzyme approach to sensitization of tyrosine kinase inhibitor-resistant breast cancer cells. *Experimental Cell Research* **318**:2014-2021.

Ivashchenko O, Van Veldhoven PP, Brees C, Ho YS, Terlecky SR and Fransen M (2011) Intraperoxisomal redox balance in mammalian cells: oxidative stress and interorganellar cross-talk. *Molecular biology of the cell* **22**:1440-1451.

Koepke JI, Nakrieko KA, Wood CS, Boucher KK, Terlecky LJ, Walton PA and Terlecky SR (2007) Restoration of peroxisomal catalase import in a model of human cellular aging. *Traffic (Copenhagen, Denmark)* **8**:1590-1600.

Koepke JI, Wood CS, Terlecky LJ, Walton PA and Terlecky SR (2008) Progeric effects of catalase inactivation in human cells. *Toxicology and applied pharmacology* **232**:99-108.

Serhan CN, Yang R, Martinod K, Kasuga K, Pillai PS, Porter TE, Oh SF, Spite M (2008) Maresins: novel macrophage mediators with potent antiinflammatory and proresoliving actions. *The Journal of Experimental Medicine* **26**:15-23.

Titorenko VI and Terlecky SR (2011) Peroxisome metabolism and cellular aging. *Traffic (Copenhagen, Denmark)* **12**:252-259.

Undyala V, Terlecky SR and Vander Heide RS (2011) Targeted intracellular catalase delivery protects neonatal rat myocytes from hypoxia-reoxygenation and ischemia-reperfusion injury. *Cardiovascular pathology : the official journal of the Society for Cardiovascular Pathology* **20**:272-280.

Young CN, Koepke JI, Terlecky LJ, Borkin MS, Boyd Savoy L and Terlecky SR (2008) Reactive oxygen species in tumor necrosis factor-alpha-activated primary human keratinocytes: implications for psoriasis and inflammatory skin disease. *The Journal of investigative dermatology* **128**:2606-2614.

ABSTRACT

EFFECTS OF ALTERING THE PEROXISOMAL REDOX STATE IN MODELS OF DEGENERATIVE DISEASE

by

COURTNEY R. GIORDANO

August 2014

Advisor: Dr. Stanley R. Terlecky

Major: Pharmacology

Degree: Doctor of Philosophy

Peroxisomes are important regulators of cellular redox balance and function as a signaling platform to regulate anti-aging metabolic and communication networks. In addition the organelle has emerged as a major player in maintaining cellular ROS at an optimal level. At such levels, these ROS are involved in initiation of signaling cascades and that produce an array of anti-aging and disease processes. However, as cells age over time, ROS amass within the peroxisome and elsewhere in the cell. This leads to an imbalance in oxidative homeostasis and results in compromised signaling networks. The goal of this dissertation was to treat disease cell models with a targeted antioxidant approach to help elucidate its biological effects and the extent to which reprograming the cellular redox environment contributes to cellular homeostasis.

There have been many studies involving antioxidant therapies; however, for the most part, these approaches have not been successful. We would argue this is due to their non-selective, non-targeted natures. In contrast, we have chosen to examine a selective and carefully targeted antioxidant – CAT-SKL. It is our contention that this molecule efficiently and safely targets oxidative stress, chronic inflammation, and resultant pro-aging and pro-disease pathways initiated in cells. CAT-SKL is designed to enter cells by virtue of a cell penetrating peptide. Once inside, presumably mediated by an endocytic event, it is directed to the peroxisome via its peroxisomal targeting signal, SKL, and metabolizes H_2O_2 within the organelle and elsewhere in the cell.

In conditions where H_2O_2 and related ROS are unchecked, their accumulation leads to a pro-aging cascade and the onset of disease. Maintaining cellular redox balance and degrading pro-inflammatory mediators within the peroxisome is essential for normal cellular function. By specifically targeting this organelle and restoring peroxisomal catalase in a number of disease cells, CAT-SKL may represent a major therapeutic advance. This enzyme has provided important results with respect to several major disease models. In a breast cancer model the drug sensitizes otherwise resistant human breast cancer cells to the TKI, gefitinib; in a diabetic retinopathy model, CAT-SKL significantly reverses compromised retinal function; and in a rat cell model of Alzheimer's disease, β-amyloid peptide-induced neuronal toxicity is significantly reduced.

AUTOBIOGRAPHICAL STATEMENT

COURTNEY R. GIORDANO

EDUCATION

WAYNE STATE UNIVERSITY
School of Medicine, Detroit, MI

- **Doctor of Philosophy**: Pharmacology
  2010-2014
- **Basic Medical Sciences Master's Program**
  Enrolled 2009-2010

MICHGAN STATE UNIVERSITY
College of Natural Sciences

- **Bachelor of Science:** Human Biology
  2004-2008

PUBLICATIONS

Terlecky SR, Terlecky LJ, and **Giordano CR.** (2012) Peroxisomes, oxidative stress, and inflammation. *World Journal of Biological Chemistry* **20123**:93-97.

Giordano CR, and Terlecky SR. (2012) Peroxisomes, cell senescence, and rates of aging. *Biochimica et Biophysica Acta* **1822**:1358-1362.

Giordano CR, Mueller KL, Terlecky LJ, Krentz KA, Bollig-Fischer A, Terlecky SR and Boerner JL. (2012) A targeted enzyme approach to sensitization of tyrosine kinase inhibitor-resistant breast cancer cells. *Experimental Cell Research* **318**: 2014-2021.

Giordano CR, Terlecky LJ, Bollig-Fischer A, Walton PA, and Terlecky SR. (2014) Amylloid-beta neuroprotection mediated by a targeted antioxidant. *Scientific Reports* **4**:4983.

Giordano CR, Roberts R, Krentz KA, Bissig D, Talreja D, Kumar A, Terlecky SR, and Berkowitz BA. (2014) Towards Peroxisomes-targeted therapy for diabetic retinopathy. Manuscript in preparation.

Giordano CR, Walton PA, and Terlecky SR. (2014) Catalase: function as a compartmentalized antioxidant enzyme. Manuscript in preparation.

Wijesinghe P, Kruger A, **Giordano CR**, Boerner JL, Terlecky SR, Ruden D, Dyson G, and Bollig-Fischer A. (2014) Fine-mapping 5-hydroxymethyl-cytosine in breast cancer reveals a path to activating NOTCH. Manuscript in preparation.

Nell HJ, Wang L, **Giordano CR**, Terlecky SR, Walton PA, Cechetto DF, and Whitehead SN. The targeted antioxidant, CAT-SKL, reduces amyloid-beta toxicity in rat brain. Manuscript in preparation.